Fall 2018

Investigation of proppant static settling velocity in hydraulic fractures using viscoelastic linear gel

Vismay Manishbhai Shah

Department:

INVESTIGATION OF PROPPANT STATIC SETTLING VELOCITY IN HYDRAULIC FRACTURES USING VISCOELASTIC LINEAR GEL

By

VISMAY MANISHBHAI SHAH

A THESIS

Presented to the faculty of the Graduate School of the

MISSOURI UNIVERSITY OF SCIENCE AND TECHNOLOGY

In Partial Fulfilment of the Requirements for the Degree

MASTER OF SCIENCE IN PETROLEUM ENGINEERING

2018

Approved by:

Dr. Abdulmohsin Imqam, Advisor
Dr. Shari Dunn-Norman
Prof Larry Britt

ABSTRACT

Few studies have quantified proppant transport in static conditions using actual proppant and validated previously established correlation. The objective of this study is to investigate the rheological properties of the linear gel, and determine the effect of size, shape and specific gravity of the proppant, fracture walls and rheological properties of the fluid on the proppant settling velocity in static condition and validate the previously established correlation.

Shear viscosity and dynamic frequency sweep tests were performed to investigate the viscous and viscoelastic behaviour of the HPG linear gel with five different concentrations. Proppant settling experiments were conducted with different proppant types and sizes with two different setups, one with a large diameter transparent cylinder and another with a parallel plexiglass plate model which imposes wall effects. Parameters used during the experiments were inserted into previously established correlation and the calculated settling values were compared with the experimental ones to identify the best suitable correlation.

HPG linear gel behaved as non-Newtonian shear thinning fluid and showed very little elasticity for the angular frequency from 1 to 100 rad/sec. With increasing shear thinning behaviour of the linear gel it was found that the effect of proppant size, specific gravity and fracture walls got more pronounced. With increasing diameter and specific gravity of the proppant, the effect of viscosity of the unbounded fluid on the settling velocity decreased; however, it remained constant in the case of confined fracturing fluid. The correlation provided by Swanson (1967) and Liu and Sharma (2005) were identified as best suitable correlations based on this study for unbounded fracturing fluid and confined fracturing fluid respectively.

ACKNOWLEDGEMENTS

I would like to express my gratitude towards my advisor Dr. Abdulmohsin Imqam for providing me the opportunity of the research and exploring that potential and capability in me which I never knew I possessed. Thank you for helping me to push my limits every single day and having faith in me.

A special thanks to committee members, Dr. Shari Dunn-Norman for always being friendly and open to discuss any problem and Professor Larry for helping to direct the path of the research and sparing all the possible time from his busy schedule.

I am forever grateful to my parents for their lifelong advises, and moral and financial support. During these two years, they became the reason for me to become successful in future.

Especially I would like to thank Priyesh and Shail who were no less than my family here and thanks to all my other friends from the research group who always encouraged me to achieve whatever I dreamed of.

I would like to thank Dr. Feys, Daniel, and Margarita for their special training and help to use rheometer throughout my research.

TABLE OF CONTENTS

Page

LIST OF ILLUSTRATIONS

Page

LIST OF TABLES

Page

NOMENCLATURE

Symbol	Description
g	Gravitational constant, 980 cm/s^2
ρ_f	Fluid density, gm/cm^3
ρ_p	Particle density, gm/cm^3
d_p	Particle diameter, cm
μ	Fluid viscosity, poise
μ_0	Zero shear viscosity, poise
ν	Dynamic viscosity, gm / cm*sec
α, β	Boundary layer coefficient
F_b	Buoyant force, $gm*cm/s^2$
F_d	Drag force, $gm*cm/s^2$
F_{Dv}	Viscous drag force, $gm*cm/s^2$
F_{Dp}	Pressure drag force, $gm*cm/s^2$
F_g	Gravity force, $gm*cm/s^2$
V_s	Terminal settling velocity, cm/sec
C_D	Drag coefficient
C_{Dv}	Viscous drag coefficient
C_{Dp}	Pressure drag coefficient
A	Characteristic area of the particle, cm^2
N_{re}	Particle Reynolds number
τ	Shear stress, Pa
γ	Shear rate, sec^{-1}

K	Flow consistency index, Pa*sec^n
n	Flow behaviour index
Φ	Sphericity of the particle
Φ_{II}	Lengthwise sphericity
$\Phi_{\perp}$	Crosswise sphericity
G’	Storage modulus/Elastic modulus, Pa
G”	Loss modulus/Viscous modulus, Pa
CMC	Carboxymethyl cellulose
PAA	Polyacrylamide
PEO	Polyethylene oxide
HEC	Hydroxyethyl cellulose
HPG	Hydroxypropyl guar
CMHPG	Carboxymethyl hydroxypropyl guar
HPAM	Hydrated polyacrylamide
pptg	Pounds per thousand gallon

1. INTRODUCTION

1.1. STATEMENT AND SIGNIFICANCE OF THE PROBLEM

Hydraulic fracturing has been proved one of the most useful technique for stimulating the well and it is continuously being improved since its first application in 1947 at Hugoton gas field in limestone formation. Now the implementation of this technique is not only restricted to conventional formations such as limestone and sandstone but also to unconventional formations such shale and tight sand (Barati and Liang, 2014). Figure 1.1 shows the hydraulic fractures generated in real conditions with arbitrary geometries.

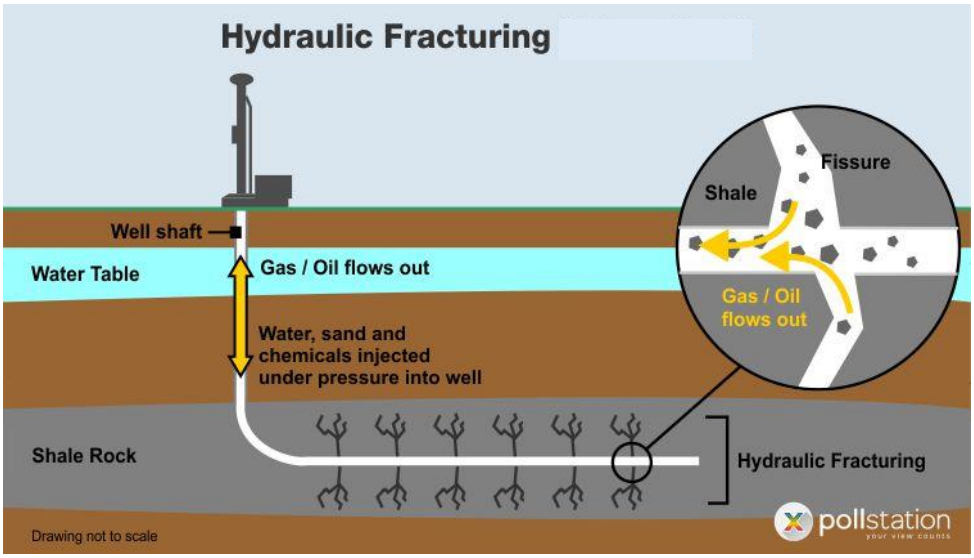

Figure 1.1. Hydraulically fractured formation

To attain highest productivity from hydraulically fractured wells, achieving long propped fracture length and high fracture conductivity is of vital importance. Both of these parameters rely on how effectively proppants are settled inside the fractures.

Figure 1.2 clearly demonstrates the huge increment in the cumulative production of gas and oil with increasing fracture half-length and fracture conductivity (from case 1 to case 4) respectively. There are two important stages where the settling has to be understood properly. 1) During the process of fracturing. 2) During the closure of fracture when pumping is stopped.

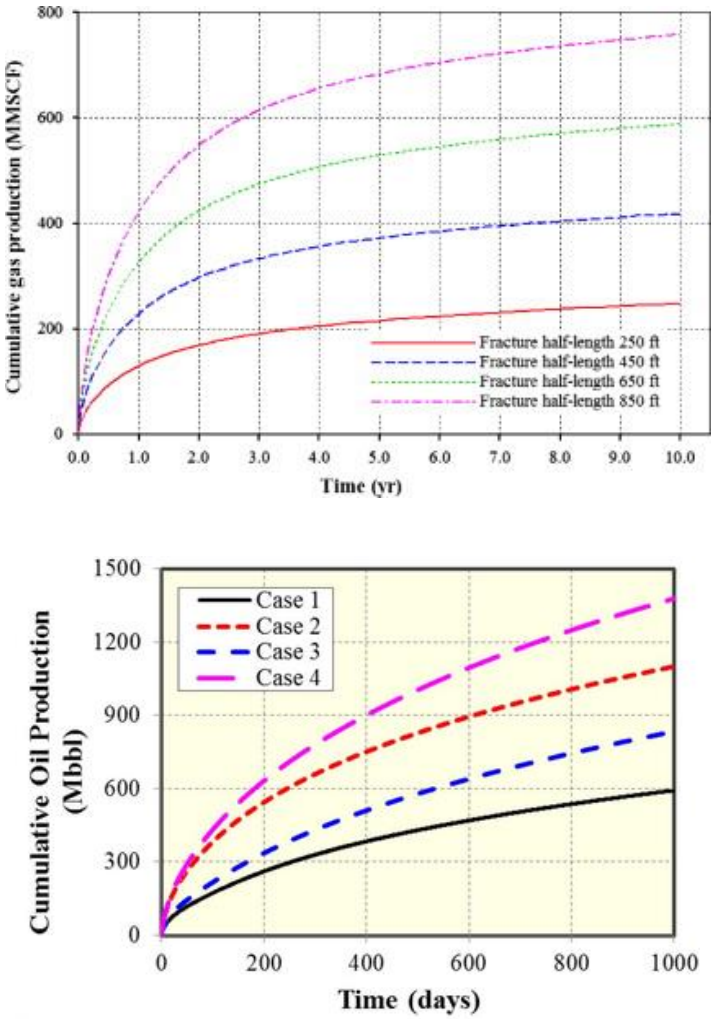

Figure 1.2. Effect of fracture half-length and conductivity on production
[Fracture half length: Yu et al. (2014), Fracture conductivity: Yu et al. (2017)]

Novotny (1977) showed that the knowledge of proppant settling during closure of the fracture is necessary and has to be considered while designing the fracturing

operation to achieve the anticipated stimulation ratio. Once pumping is stopped, the fluid inside the fracture will get stagnant and proppant will start settling until the fracture closes. Taking this scenario into the account, it is important to understand the settling behaviour of proppant with static conditions as well.

In the past several years intensive research has taken place related to proppant settling with static conditions. Different fracture setups have been used and different techniques have been implemented to understand the settling behaviour. Because of the irregular shape of the actual proppant, complex rheological properties of fracturing fluid, and the difficulty in replicating the real fracture conditions in the laboratory, the issue has not been resolved completely. Different correlations have been established with number of assumptions and limitations which always require more data to get more accurate results.

1.2. EXPECTED IMPACTS AND CONTRIBUTION

Analysis of the experimental findings and validation of some of the previously established correlations will improve the understanding of the settling behaviour of the proppant in the static conditions. The effect of physical properties of the proppant such as size and specific gravity, rheological properties of the fluid such as viscosity and elasticity, and effect of the fracture walls on the settling velocity is analysed critically to get a clear understanding about the individual role of each parameter behind the settling of a proppant particle. As intensive research has already taken place in this area, this research would add some valuable information to the past researches and would direct the path for the future research work to be done.

1.3. OBJECTIVE

The objective of this study is to determine the settling velocity of actual proppant particle using linear gel and water with two different fracture setups; one including the fracture wall effect and another without any wall effect, to understand the effect of proppant's size and specific gravity, rheological properties of the linear gel and effect of fracture walls on the settling velocity of the proppant in the static conditions. Then the experimental results were compared with the previously established correlations and the best suitable correlation was opted out based on our study.

1.4. SCOPE OF THIS STUDY

This study is divided in three tasks: 1) Investigation of the rheological properties of the linear gel using different concentrations of hydroxypropyl guar. 2) Determining

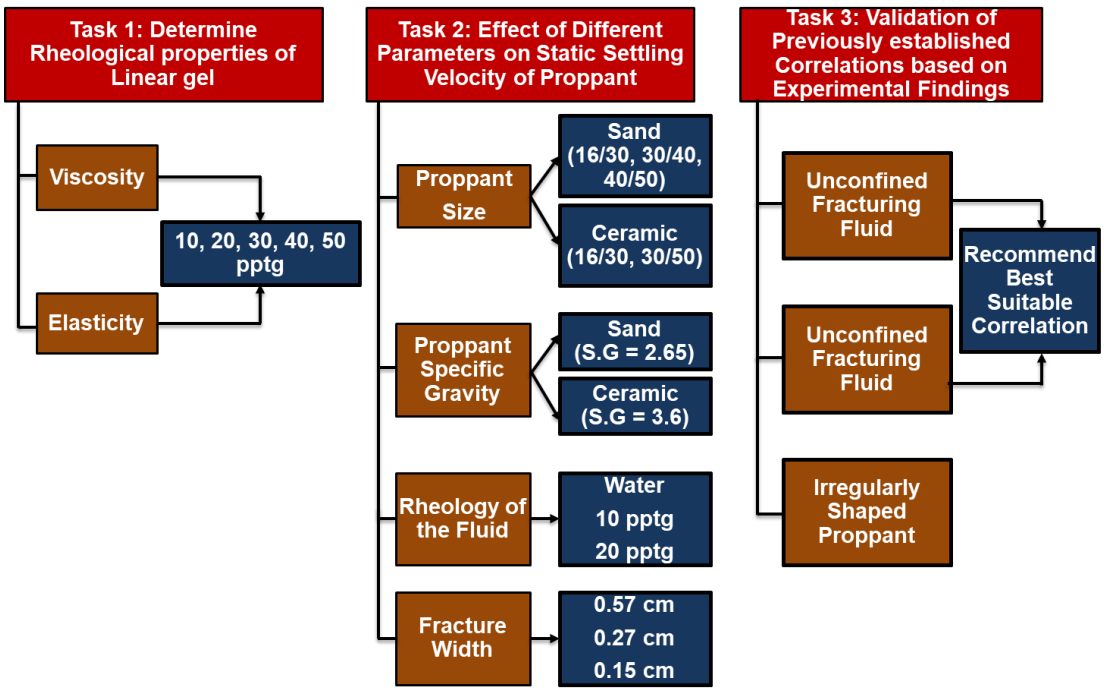

Figure 1.3. Research scope

the settling velocity of two different types of proppant with the different sizes with water and linear gel using two different setups and analysing the effects of different parameters on the settling velocity. One setup is used to avoid any wall effects on the settling velocity which replicates the settling behaviour of that proppant which is at the centre of the fracture and another setup generates wall effects which replicates the settling of the proppant while in contact with the fracture walls. 3) Validation of the previously established correlations using experimental results and suggesting the best suitable correlations under specific conditions.

2. BACKGROUND AND EXISTING TECHNOLOGY

2.1. REAL FIELD HYDRAULIC FRACTURING OPERATION

Hydraulic fracturing is the operation during which the fracturing fluid is injected downhole with high pressure sufficient enough to break down the target formation and propagate a fracture. Figure 2.1 shows the surface facilities used during the hydraulic fracturing operation. The propping agents; known as proppants, are mixed with the fracturing fluid which go inside the fracture(s) and keep the fracture(s) open at the time when pumping is stopped and the in situ stresses have started forcing the fractures to get closed. There are three or four different stages of the fracturing operation depending upon the condition of the well.

Stage 1 (Pre flush): The mixture of water and acid is circulated in the borehole to remove the debris and provide a clean environment to the fracturing fluid allowing the access to the formation efficiently.

Stage 2 (Pad): The viscous fracturing fluid; also known as pad, is injected with sufficient high pressure to create the fractures inside the formation.

Stage 3 (Proppant Slurry): In this stage same composition of the fracturing fluid as in stage 2 is used. Only the proppants are the additional solid particles which are mixed with the fracturing fluid. The fracturing fluid carries these particles from surface to downhole and inside the fractures. As soon as the pumping is stopped the fractures start closing immediately due to in situ stresses and at that time theses proppants will help to keep the fractures open and increase the permeability of the formation which can be observed from Figure 2.2.

Stage 4 (Flush): Clean fluid is circulated in the borehole to displace the proppant slurry through the perforations.

Figure 2.1. Surface facilities of hydraulic fracturing operation

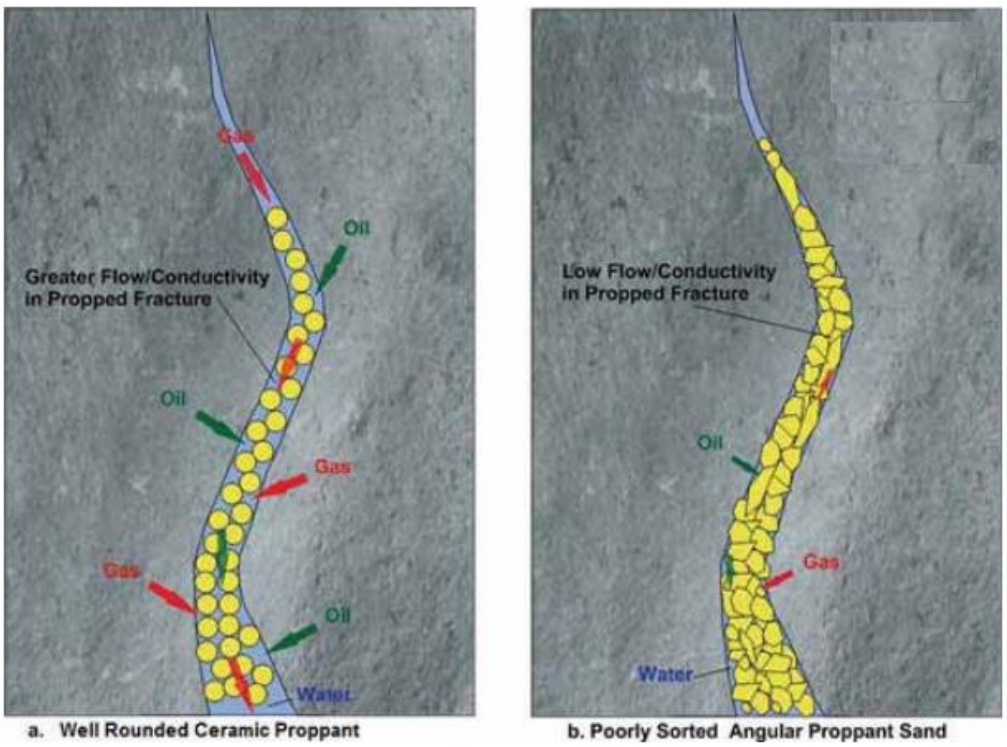

Figure 2.2. Settling behaviour of proppants after fracture closure

2.2. FRACTURING FLUIDS

The success of hydraulic fracturing operation in terms of achieving the anticipated production rate depends on several factors such as fracture geometry, fracture orientation, propped fracture length, fracture conductivity, leak off characteristics of the fluid inside the formation and proppant placement inside the fractures. From all these parameters the only parameters which can be controlled precisely from the surface are rheological properties of the fracturing fluid and the most appropriate proppant for the operation. These fracturing fluids are categorized based on the base fluid used to prepare it.

Conventional fracturing fluids include water based and polymer containing fluids, hydrocarbon based fluids, energized fluids and foam whereas unconventional fracturing fluids are categorized as viscoelastic surfactant fluids, methanol containing fluids, liquid CO2 based fluids and liquefied petroleum gas based fluids. Unconventional fracturing fluid can be identified as a non-polymer containing fluids (Gupta, 2009). Unconventional fracturing fluids are out of the scope this study but details can be found in (Gupta, 2009). In conventional fracturing fluids, slick water, linear gel and crosslinked fluids are discussed in detail with their composition, rheological properties, advantages, disadvantages and applicability.

2.2.1. Slick Water. Slick water has been most widely used fracturing fluid especially in unconventional reservoirs. In 2004, more than 30% of the stimulation treatments in North America were performed with slick water as a fracturing fluid (Schien, 2005). The primary components of this fracturing fluid are sand and water (>98%). Other additives are mixed to solve different issues like reducing the friction, corrosion, bacterial growth etc. Unlike the polymer solutions, viscosity of the slick water is very low because the only chemical which can substantially increase the

viscosity is used in very low amount to reduce the friction while injecting the fluid downhole. Hence the amount of proppant which can be injected using slick water per gallon is very low (maximum 2.5 ppg) (Palisch et al., 2010) because of the less proppant carrying capacity and the fracture width created will be narrow as well from which very less amount of proppant can go inside the fracture. Due to lack of viscosity this fracturing fluid faces two major issues 1) Usage of high volume of water to inject sufficient amount of proppant 2) Usage of high pump rate to overcome the friction losses and to ensure that sufficient amount of proppant reach to the tip of the fracture. The pump rates used in the field goes as high as 120 bbl/min (Kaufman et al., 2008) and volume of water injected can go up to one million barrel (Al- Muntasheri, 2014).

The major benefits of using slick water as a fracturing fluid are reduced gel damage as very low concentrations of polymer are used as a friction reducer, less cost, high stimulated reservoir volume and better fracture containment (Mohanty et al., 2012). The fracture length will be very long and reservoir-wellbore connectivity may be better because of the potential complex fracture network created by slick water (Gandossi, 2013).

2.2.2. Linear Gel. Back in 1953 the bio polymers such as guar and cellulose were used as fluid thickeners in acid fracturing treatment (Hurst, 1953). Since then guar is one of the most widely used polymer in the fracturing fluid which contains a long chain of polysaccharide with side chains of galactose and has high molecular weight (Jennings, 1996). Weaver et al. (2002) reported the average molecular weight of guar as 2-4 million Dalton approximately. The chemical structure of guar is shown in the Figure 2.3(a) below (Al-Muntasheri, 2014). It is usually used in the form of dry powder that swells when mixed with an aqueous solution and form a viscous gel (Gandossi, 2013). The viscosity attained using these linear polymers is around 35–50 cp at shear

rates of 40 to 500 sec^{-1} (Al-Muntasheri, 2014). This viscosity is sufficient enough to carry at least much more amount of proppant than any usual slick water will carry.

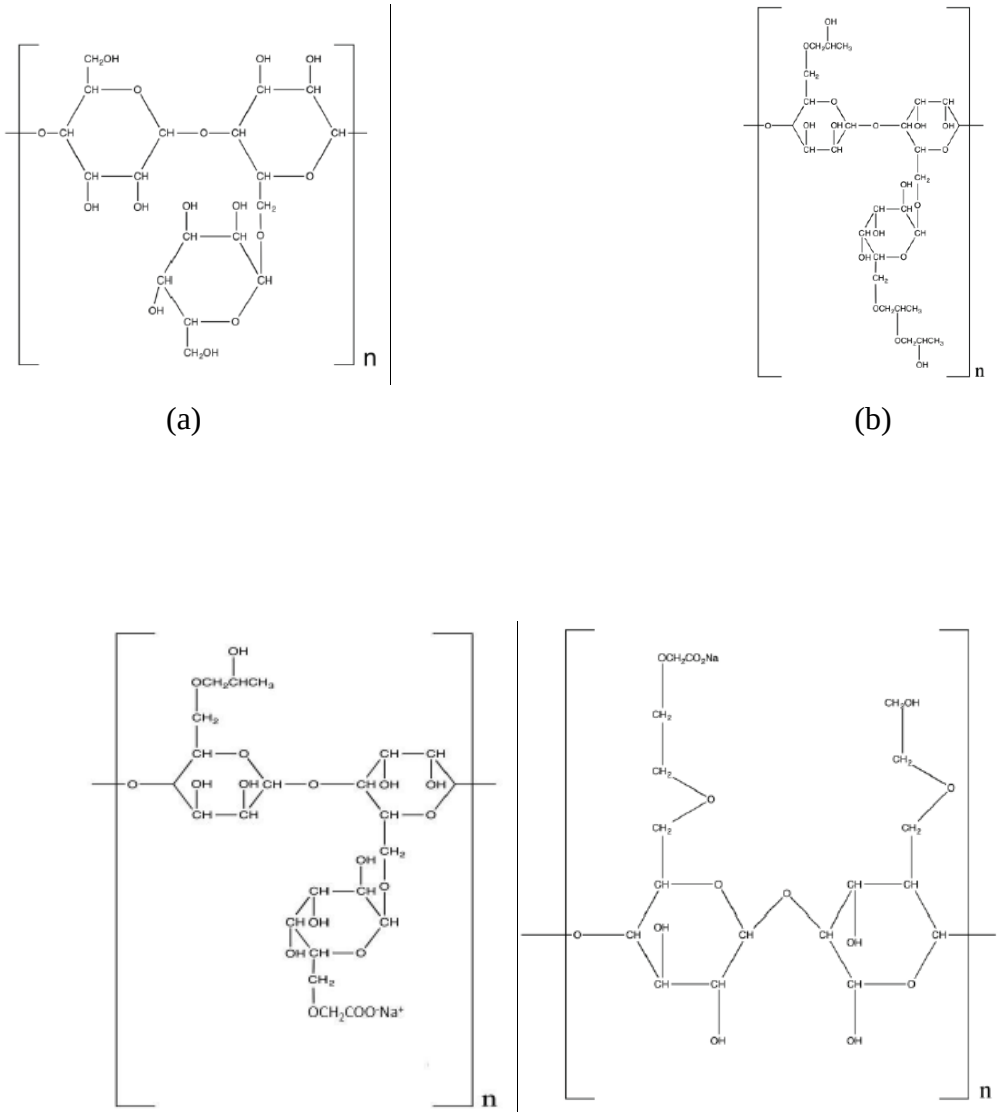

(a) (b)

(c) (d)

Figure 2.3. Chemical structure of guar and its derivatives (a) Chemical structure of guar (b) Chemical structure of Hydroxypropyl guar (c) Chemical structure of CMHPG (d) Chemical structure of CMHEC (e) Chemical structure of CMC (f) Chemical structure of HEC

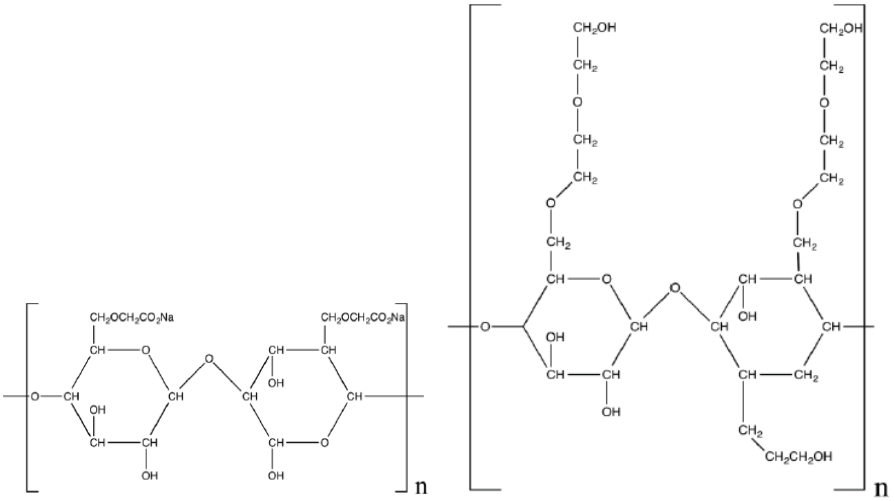

(e) (f)

Figure 2.3. Chemical structure of guar and its derivatives (a) Chemical structure of guar (b) Chemical structure of Hydroxypropyl guar (c) Chemical structure of CMHPG (d) Chemical structure of CMHEC (e) Chemical structure of CMC (f) Chemical structure of HEC (Cont.)

Thermal stability of guar at temperatures higher than 180 °F was questionable. So industry developed derivatives of guar such as hydroxypropyl guar (HPG) and carboxymethylhrdroxypropyl guar (CMHPG) whereas the other forms of cellulose based polymers are carboxymethyl cellulose (CMC), hydroxyethyl cellulose (HEC) and carboxymethylhydroxyethyl cellulose (CMHEC). The chemical structures can be found in the Figure 2.3 (b), (c), (d), (e) and (f) (Ely, 1989)

This high viscous linear gels prevent fluid loss by creating a filter cake on face of the moderate permeability formation but damages the formation conductivity by leaving the polymer residue at the same time. In high permeability formation the behaviour of linear gel be completely opposite and the amount of fluid loss will be high as there won't be any mud cake created on the face of the formation (Gondassi, 2013). Guar concentration to prepare linear gel on the field is reported to be 0.12-0.96 w/w for operations (Robert and Pin, 1993). As long as clean up property of guar is concern, the

expected residue is approximately 6-10% by weight and is less for HPG which is around 2-4% by weight. (Economide et al., 2000)

2.2.3. Crosslinked Gel. Water based polymer fracturing fluids are crosslinked using one of these two major crosslinkers: Borate esters (Figure 2.4) and metallic ions such as Titanate (IV), Zirconium (IV) and Al (III). Crosslinking occurs by reacting through cis-OH pairs on the galactose side chains of guar. All the crosslinking agents have their own specifications and range of applicability in terms of pH, temperature, and the type of polymer with which they can crosslink with (Barati and Liang, 2014). Crosslinking results in substantial increase in the viscosity of the linear gel (can be more than 1000 cp) (Al- Muntasheri, 2014).

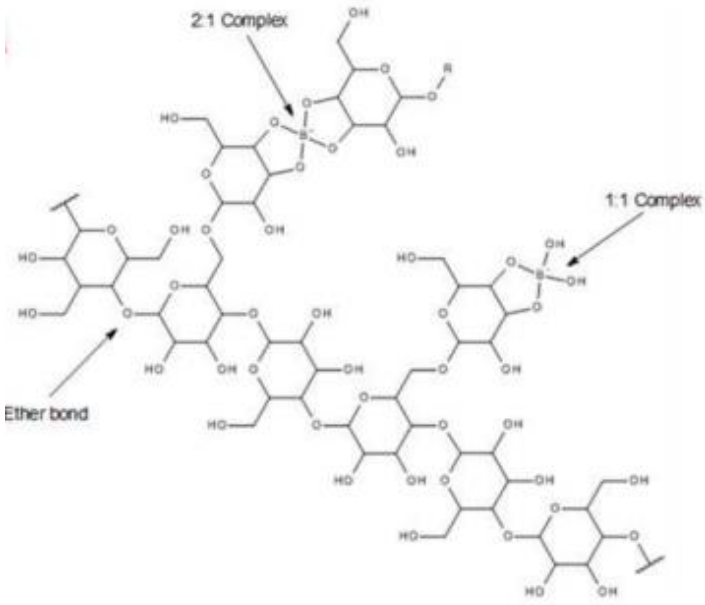

Figure 2.4. Mechanism of guar crosslinking by borate (Horton et al., 1996)

Borate has been most commonly used crosslinking agent with guar polymer solution. They are highly effective in both low and high permeability formations. As they are highly viscous they provide good proppant carrying capacity and low fluid

loss. Their rheology remains stable at temperatures up to 300 °F and they provide good clean up property as well (Halliburton 2011). Borax and boric acid (with caustic soda) with crosslinking agent concentration ranging from 0.024 – 0.09% w/w have been used on field to crosslink borate ions with guar (Economides et al. 2000). Titanium and Zirconium crosslinked fluid is mostly used when the reservoir temperature is very high where borate crosslinked fluid can't work efficiently. The reason behind the less usage of these crosslinking agents are provision of less fracture conductivity and more face damage (Figure 2.5) compare to borate crosslinked fluids (Rae and Lullo 1996).

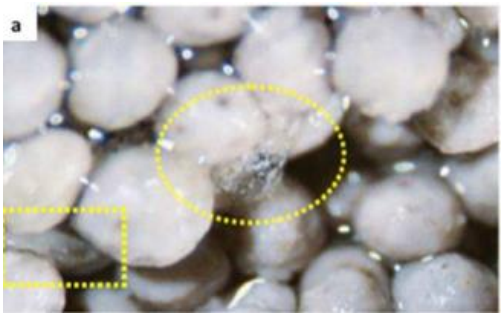

Figure 2.5. Residual gel damage by breaking crosslinked fluid (Palisch et al. 2007)

2.3. PROPPANTS

As discussed earlier, proppants are one of the two parameters which is under our control to optimally design the hydraulic fracturing operation. The success of the hydraulic fracturing process depends on how effectively proppant has been transported inside the fracture. Long propped fracture length and high fracture conductivity, both depend on proppant transport inside the fracture and their settling behaviour. And this settling or suspension of proppant inside the fractures not only depend on rheological property of the fluid but also physical properties of proppant such as size, shape and density of the proppant used.

2.3.1. Size of the Proppant. Considering the size or diameter is necessary to understand the settling phenomenon of proppant well. Proppant size is never described by an absolute value like 1 mm or 2 mm but is always described with mesh sizes and every mesh size has its own absolute value. For an example sand proppant with 16/30 mesh size means that sand proppants fall between 16 and 30 size meshes. The mesh size is basically the number of openings across one linear inch of screen. 16/30 mesh size means the size of the proppant particle falls between 590 μm and 1190 μm. In traditional fracture treatment different mesh sizes of proppant are used in combination. In the very beginning of the operation smaller proppants are injected inside the fracture and in the end larger proppants are injected so that maximum fracture conductivity can be attained near wellbore. Larger proppants provide higher conductivity (Liang et al., 2016).

Though it is very common in hybrid completion design to mix various sizes of proppant, Schmidt et al. (2014) investigated the effectiveness of this mixing experimentally. They found that higher concentration of larger size proppants have significant impact on propped fracture conductivity. They found that mixture of 40/70 sand and light weight proppant (LWC) improves the conductivity of the proppant pack regardless of concentration. They also found that the conductivity almost remains same whether high concentration of 40/80 LWC is mixed with larger size of LWC or low concentration of 40/70 LWC is mixed with larger size of LWC. Hu et al. (2014) published a data regarding the usage of different type, amount and mixture of various sizes of proppant in designing the stimulation operation in the Bakken shale play between 2011 and 2013. It was evident from the published data that by mixing the sizes of different types of proppants or same type of proppant, the production almost got doubled in 180 days' time period when we compare the production at 90 days and at

270 days. Alotaibi et al. (2015) used the same size of brown sand that is 30/70 mesh size throughout his experiment inside the slot flow model. They observed layers of varying particles with a downward slope in the slurry direction. Those layers indicated size sorting larger particles followed by smaller particles. That type of behaviour indicates that there would be layers of low and high conductivity instead of single conductivity for 30/70 mesh size which could be of significant importance in designing hydraulic fracturing operation.

2.3.2. Shape of the Proppant. Ideally the shape of the proppant should be spherical to achieve highest fracture conductivity but is never the case in reality. There are two parameters need to be evaluated to understand the shape of the proppant and those are roundness and sphericity. Krumbein et al. (1963) established a scale by which roundness and sphericity of any particle can be estimated visually. Figure 2.6 below shows how roundness and sphericity are evaluated. ISO13503-2:2006/Amd.1:2009(E) has specified requirements for roundness and sphericity of different proppants. According to them, ceramic and resin coated proppants require to have roundness and sphericity both 0.7 and greater and all other proppants need to have roundness and sphericity both 0.6 and greater.

In development of different shaped proppant other than spherical, rod shaped proppant was found to be useful one. Theoretically they provide higher conductivity due to higher porosity in their packing. McDaniel et al (2014) studied the untapped pack porosity of spherical and rod shaped particles and came up to be 37% and 48% respectively. The risk in using rod shaped proppant is its different diameter and length which might impair the conductivity and affect proppant flow back operation as well.

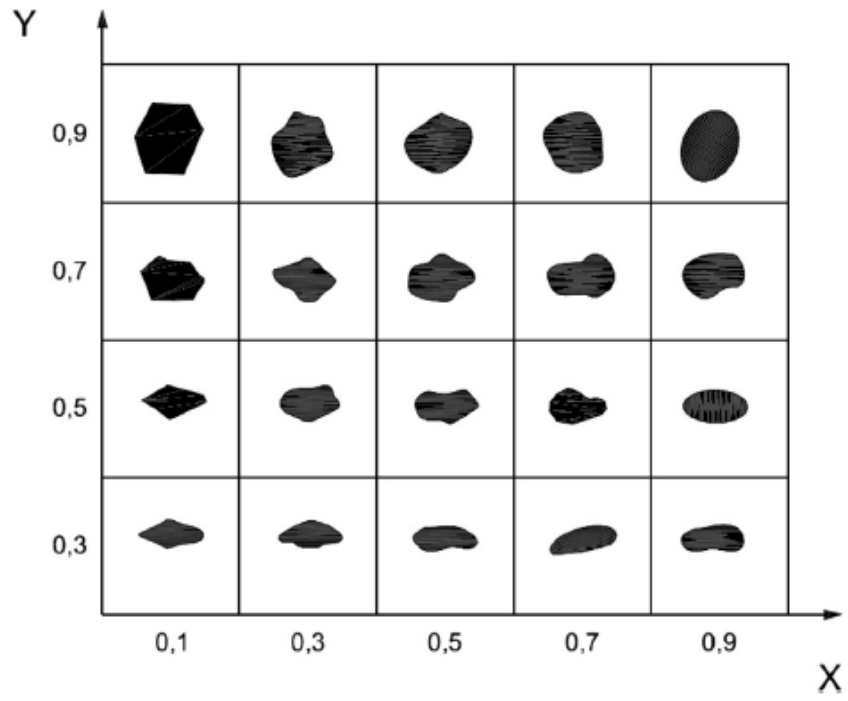

Figure 2.6. Chart for visual estimation of sphericity and roundness

Liu et al. (2015) tested different shaped proppant which induced high drag because of their shape. The proppant is designed in such a way that the center of gravity and centroid of volume do not align in a stable manner, so proppant keeps changing its orientation while falling inside the fluid. This unique proppant did show less settling time than conventional proppant but still more work has to be done in order to make it implacable on the real field.

2.3.3. Density of the Proppant. Frac sand is composed of processed and graded, high-silica content quartz sand. White sand and brown sand are two major types of sand. White sand is lighter in the colour due to few impurities whereas Brown sand is brownish because of high impurities which make it cheaper and less crush resistant even at lower stress. Figure 2.7 below shows the production of sand and gravel in USA during 2010 to 2014. The production almost exceeded more than double in four years

span. The reason behind that is rapid expansion of shale oil and gas which is highly dependent on hydraulic fracturing process (Al-Muntasheri, 2014).

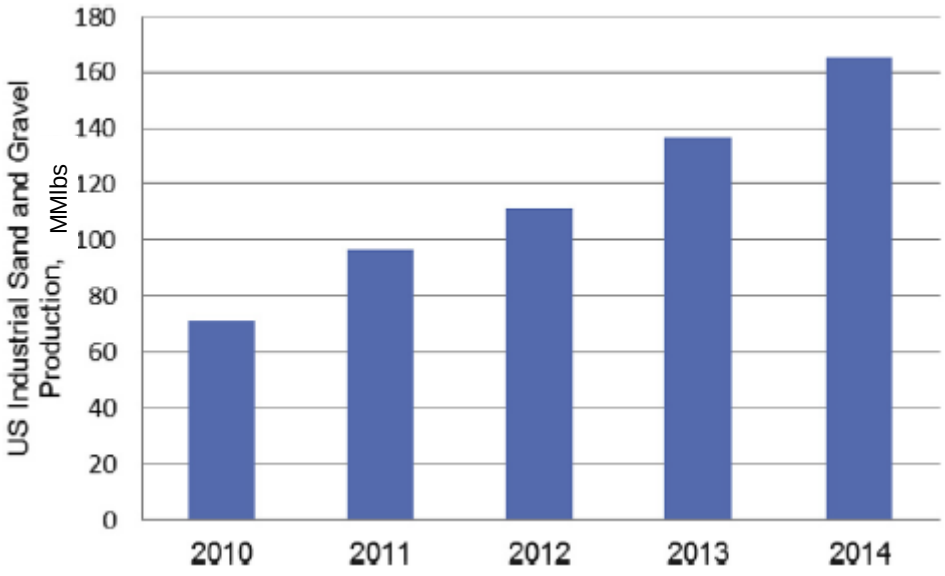

Figure 2.7. Industrial sand and silica gravel production in USA
[Data source: USGS Mineral Commodity Summaries, 2015]

Roundness and sphericity of frac sand keeps changing from company to company. Below a data sheet of physical properties of sand proppant from Preferred Sands Company has been given in Table 2.1 to get clear idea about the values. The values are around 0.7 for both the sphericity and the roundness and far away to be considered as a sphere. The values of density have significance importance in laboratory measurements of settling velocity of proppant. Here the values for densities are ranging from 2.5 to 2.7 but usually the sand with 2.65 S.G is used. The crush resistance also increases with decreasing diameter that means that larger particles can provide better conductivity but at the same time restricted application at higher stresses.

Table 2.1. Physical properties of sand proppant (www.preferredsands.com)

PROPERTIES	UNITS/METHOD	16/30		20/40		30/50		40/70		50/140	
Typical Sieve Analysis		SIEVE NO.	% RETAINED	SIEVE NO.	% RETAINED	SIEVE NO.	% RETAINED	SIEVE NO.	% RETAINED	SIEVE NO.	% RETAINED
		16	0.5	20	0.4	30	0.3	40	1.8	50	0.6
		18 20 25 30	99.4	25 30 35 40	96.3	35 40 45 50	96.6	45 50 60 70	98.3	80 100 120 140	99.3
		40	0.1	50	3.3	70	2.9	100	0.0	200	0.0
		Pan	<1	Pan	<1	Pan	<1	Pan	<1	Pan	<1
Sphericity	Krumbein	0.7		0.7		0.7		0.8		0.7	
Roundness	Krumbein	0.7		0.7		0.7		0.8		0.8	
Turbidity	NTU	9		8		34		45		10	
Mean Particle Diameter	mm	0.920		0.595		0.446		0.336		0.228	
Bulk Density	g/cc	1.48		1.51		1.51		1.51		1.50	
Bulk Density	lb/ft³	92.03		93.91		94.17		94.23		93.81	
Specific gravity	g/cc	2.50		2.51		2.70		2.61		2.50	
Crush		3K		5K		6K		8K		11K	
Closure Stress (PSI)	PSI	Conductivity (md-ft)	Permeability (Darcy)	Conductivity (md-ft)	Permeability (Darcy)	Conductivity (md-ft)	Permeability (Darcy)	Conductivity (md-ft)	Permeability (Darcy)	Conductivity (md-ft)	Permeability (Darcy)
	1000	8844	460	5869	280	3294	162	2057	101	806	41
	2000	4362	236	5205	253	2533	129	1878	101	643	33
	4000	1193	70	3020	153	1350	71	1120	65	317	17
	6000	363	22	903	49	552	29	405	25	107	6
	8000	170	11	250	14	154	8	165	11	30	2

Ceramic proppants are manufactured from sintered bauxite, kaolin, magnesium silicate or blends of bauxite and kaolin. As it is designed to perform better than sand proppant, it has got high crush resistance, more roundness and sphericity than the sand proppant which will eventually yield higher porosity and permeability. Additionally it has got high thermal stability and chemical stability which will prevent its degradation at the time of high temperature applications. Because of all the properties contained by a ceramic proppant eventually gives higher permeability both long term and shirt term, the cost of it is also very high compare to sand proppant (Al-Muntasheri, 2014). They are divided into three different categories based on their density. 1) Lightweight ceramic proppant 2) Intermediate strength ceramic proppant and 3) High strength ceramic proppant. Table 2.2 and 2.3 below show the values of different properties of

ceramic proppant for light weight and high strength has which are taken from Carboceramic and Sintexminerals companies respectively.

Table 2.2. Physical properties of CARBOLITE ceramic proppant

U.S. Mesh [mesh]	Microns	12/18	16/20	20/40	30/50	40/70
API/ISO crush test % by weight fines generated	@7,500 psi	17.9	14.0	5.2	2.5	2.0
	@10,000 psi		19.3	8.3	5.8	4.4

Roundness	0.9	Apparent specific gravity	2.71
Sphericity	0.9	Absolute volume [gal/lb]	0.044
Bulk density [lb/ft³] [g/cm³]	97 1.57	Solubility in 12/3 HCl/HF acid [% weight loss]	1.7

Table 2.3. Physical properties of SinterBall Bauxite ceramic proppant (www.sintexminerals.com)

Properties	Sieve	16/30	20/40	30/50	40/80
		% Retained			
Median Diameter	mm	0.940	0.700	0.501	0.356
Sphericity & Roundness	K&S*	0.9X0.9	0.9X0.9	0.9X0.9	0.9X0.9
Bulk Density	g/cm³	2.05	2.05	2.04	2.02
	lb/ft³	128	128	128	126
Apparent Density	g/cm³	3.59	3.59	3.59	3.64
	lb/ft³	224	224	224	228
Absolute Density	g/cm³	3.60	3.62	3.67	3.69
Absolute Volume	gal/lb	0.033	0.033	0.033	0.032
Acid Solubility	(HCl+HF), %	5.9	5.8	5.8	5.8
Crush Resistence stress psi, %fines	7.500				
	10.000				
	12.500	5.6	2.1	1.6	0.7
	15.000	-	-	1.8	1.2
	20.000				

Table 2.2 above describes the properties of CARBOLITE proppant which has almost the same bulk density and specific gravity as sand but delivers better performance in terms of providing higher conductivity. Table 2.3 above describes the properties of Sintered Bauxite High strength ceramic proppant from Sintex Company. These particles can almost be considered as spheres and provide much better crush resistance at high pressure or stresses.

One of the modified proppants is procured Resin coated proppant (RCP), developed to enhance the conductivity of frac sand. Usually frac sand gets broken into fine grains when crushed under high stresses and so this resin coating above it can keep those pieces inside the coating and prevent proppant flowback to the wellbore. The same coating can be applied on ceramic proppants and glass beads as well. Because of their sticky coating made up of polymer, one proppant can aggregate with other and stop proppant flow back as well. Because of the polymer made coating they have low softening temperatures or low degradation temperatures which is the major disadvantage of this type of proppant. The most commonly used resins to coat the proppants are epoxy resin, furan, polyesters, vinyl esters, and polyurethane. Among all these resins, epoxy resin is used most because it provides high mechanical strength and excellent heat and chemical resistance (Al-Muntasheri, 2014). As the proppant itself is not new, the physical properties such as absolute density/specific gravity and bulk density will remain same as the original proppant on which the coating is applied. There are again different types of resin coated proppants provided by different companies with different applicability range. This type of proppant provides higher crush resistance and higher conductivity compare to the original one.

2.4. PROPPANT TRANSPORT MECHANISM

This section discusses the forces acting on the proppant particle while settling in the stagnant fluid and different flow regimes based on particle Reynolds number (N_{re}). George Gabriel Stokes was the first to derive the expression for terminal settling velocity in 1851 which is known as Stokes law. According to Stokes law, when a spherical object is falling freely through the stagnant fluid (as shown in Figure 2.8), the velocity of the object keeps increasing until it reaches to a constant value where the downward acceleration (F_g) is balanced by the frictional and buoyancy forces (F_d and F_b) acting on it. This constant value of velocity is termed as terminal settling velocity of the object through that particular fluid in static conditions.

According to the Stokes law (McCabe and Smith et al., 1956), terminal settling velocity can be mathematically expressed as:

$$V_s = g*(\rho_p - \rho_f)*d_p^2 /18*\mu \quad (1)$$

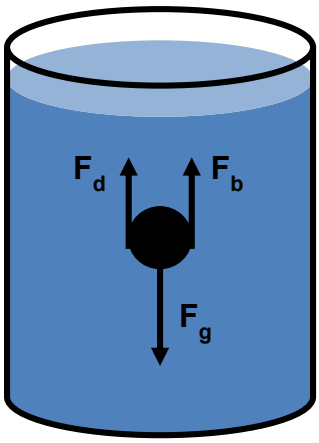

Figure 2.8. Free fall of the spherical particle inside stagnant fluid

There are two different types of drag forces acting on the particle due to its motion inside the fluid (Peden and luo, 1987). One is fluid viscous drag which can be expressed as:

$$F_{Dv} = 10^{-3}*C_{Dv}*A_p*\rho_f*v_s^2/2 \quad (2)$$

Where C_{Dv} is viscous drag coefficient and A_p is the characteristic area of the particle parallel to the direction of motion. Another drag force is the pressure drag which can be expressed as:

$$F_{Dp} = 10^{-3}*C_{Dp}*A_N*\rho_f*v_s^2/2 \quad (3)$$

Where C_{Dp} is pressure drag coefficient and A_p is the characteristic area of the particle normal to the direction of motion. Summing up the above mentioned two components of drag will give total drag force which can be expressed as:

$$F_D = 10^{-3}*C_D*A*\rho_f*v_s^2/2 \quad (4)$$

Where C_D is total drag coefficient and A is Characteristic area of the particle depends on the shape and orientation of the particle during free fall inside the fluid.

Drag coefficient can be calculated mathematically as shown below by equating the drag force (F_D) with the gravity force and buoyancy force ($F_G - F_B$) when equilibrium is reached

$$C_D* \pi*d^2* \rho_f*V_s^2/8 = (\rho_p - \rho_f)*g*\pi*d_p^3/6 \quad (5)$$

$$\therefore C_D = 4*(\rho_p - \rho_f)*g*d_p/3*\rho_f *V_s^2 \quad (6)$$

The drag coefficient of a spherical particle is unique function of the particle Reynolds number for Newtonian fluid where particle Reynolds number can be expressed as:

$$N_{re} = \rho_f*v_s*d_p/\mu \quad (7)$$

Particle Reynolds number is nothing but the ratio between inertial and viscous forces of the fluid whereas the drag coefficient can be defined as a fraction of the kinetic

energy of the velocity of the particle falling inside the fluid which is used to overcome the drag forces acting on the particle (Chien, 1994)

Drag coefficient can be closely approximated for three different regions categorized based on different particle Reynolds number and according to that equation to calculate the terminal settling velocity also changes (Novotny, 1977). The three different equations shown below are applicable to the Newtonian fluids and assuming that no fracture walls are present to hinder the particle settling velocity.

For $N_{re} \leq 2$ (Stokes law region) where $C_D = 24/ N_{re}$

$$Vs = g*(\rho_p - \rho_f)*d_p^2 / 18*\mu \quad (8)$$

For $2 < N_{re} < 500$ (Intermediate region) where $C_D = 18.5/ N_{re}^{0.6}$

$$Vs = 20.34*(\rho_p - \rho_f)^{0.71}*d_p^{1.14} / \rho_f^{0.29}*\mu^{0.43} \quad (9)$$

For $N_{re} \geq 500$ (Newton's law region) where $C_D = 0.44$

$$Vs = 1.74*\sqrt{g*(\rho_p - \rho_f)*d_p / \rho_f} \quad (10)$$

For Non-Newtonian fluids, some of the past studies used the same correlations established for Newtonian fluids except replacing the constant viscosity term with effective viscosity at apparent shear rate (Novotny, 1977; Daneshy, 1978; Hannah and Harrington, 1981; Shah, 1982; Asadi et al., 1999) to show the deviation in the values obtained using correlations and experimental results. Roodhart (1985) and Asadi et al. (2002) highlighted the importance of zero shear viscosity while determining the settling velocity in static conditions. Some of the authors tried to modify the drag coefficient in order to develop new correlation and improve the previous correlations for Non-Newtonian fluids (Acharya, 1988; Peden and luo, 1987; Chien, 1994; Cheng, 1997; Holzer and Sommerfield, 2007). All the research work mentioned above has been discussed in detail in the later sections.

3. LITERATURE REVIEW

3.1. RHEOLOGY OF THE LINEAR GEL

Most of the hydraulic fracturing treatments use gelled fluids because of their high viscosity which can create wide enough fractures that can take sufficient amount of proppant inside it. Once the pumping process is stopped, fractures will start closing and conductive channels will be created due to improper closure of the fractures caused by the proppants settled in between those fractures. The rheological properties of the fluid such as apparent viscosity, yield stress, viscoelasticity, dynamic viscosity etc. directly affect fracture fluid's performance and hence proppant carrying capacity (Harris and Morgan, 2005). Past researches have shown that consideration of viscosity alone could not accurately assess proppant transport and hence effects of elasticity on the proppant transport need to be investigated. (Acharya et al., 1976 (a); Acharya, 1986; Machac and Lecjaks, 1995; Goel et al., 2002; Harris and Morgan, 2005; Malhotra and Sharma, 2012; Hu et al., 2015; Gomma et al., 2015; Hu et al., 2015; Malhotra and Sharma, 2011; Arnipally and Kuru, 2017). Therefore, in this study efforts are made to investigate the elasticity of the linear gel and see whether it affects the settling velocity or not under specific conditions.

3.1.1. Viscosity of the Linear Gel. Viscosity is a measure of the fluid's resistance to flow. Steady shear sweep test is performed to identify the fluid's viscous characteristics in which shear stress is measured for each shear rate implemented.

Fluids are characterized as Newtonian or non-Newtonian based on the behaviour of shear stress or viscosity as a function of shear rate. In the case of Newtonian fluid, the plot between shear stress and shear rate shows a straight line which passes through the origin of the first quadrant of the Cartesian coordinate system. In

simple words, the value of viscosity remains constant for any applicable shear rate on the fluid and the examples are water (1 cp) and glycerine (780 cp). In the case of Non-Newtonian fluids, the viscosity keeps changing according to the shear rate implemented on it and the examples are polymer solutions, paint etc.

Non-Newtonian fluids are further divided in sub-classes such as shear thinning or pseudoplastic fluids, shear thickening, viscoelastic etc. The detailed description of all the different classes of non-Newtonian fluids can be found in (Chhabra, 2007). Most of the linear gels or uncrosslinked gels are considered shear thinning non-Newtonian fluid because its viscosity decreases with increasing shear rate. Most of the polymeric fluids exhibit shear thinning behaviour and the rate of decrease of viscosity with shear rate depends on factors such as type and concentration of polymer used, molecular weight distribution of polymer, type of solvent and temperature.

To characterize shear thinning non-Newtonian fluid (linear gel in this case) power law model which is also known as Ostwal-De Waele model is used in this study. This model uses power law expressions to fit the curve between shear stress vs shear rate. The equation is

$$\tau = K (\gamma)^n \tag{11}$$

or

$$\mu = K (\gamma)^{n-1} \tag{12}$$

Where τ represents shear stress (Pa), μ represents viscosity of the fluid (Pa.s), γ represents shear rate (sec^{-1}), and K and n are power law parameters which are referred as flow consistency index and flow behaviour index respectively. For Newtonian fluids value of n is equal to one and as it decreases from one, the shear thinning behaviour of the fluid increases. As linear gel is shear thinning non-Newtonian fluid, value of effective viscosity is used for calculations which is taken at values of apparent shear rate (particle shear rate caused by the movement of the sphere falling in a quiescent

fluid) between V_s/d_p and $3V_s/d_p$ (Roodhart, 1985). Intensive research has taken place where linear gel was used as a fracturing fluid and its viscous behaviour was evaluated based on two power law parameters K and n. Table 3.1 below contains the information regarding the different linear gels used by previous researchers and K and n parameters according to the concentration of the polymers used to prepare the linear gel.

Table 3.1. Viscous characteristic of various fracturing fluids

Author	**Fluids**	**Density (gm/cc)**	**K ($Pa.sec^n$)**	**n**	**Range of shear rate (sec^{-1})**
Acharya et al. 1976 (a)	CMC	1.02 (20 ℃)	0.2	0.86	1-1000
	PAA	1.008 (20 ℃)	0.127	0.65	0.1-1000
	PEO	1.0027 (20 ℃)	0.03014	0.9988	0.1-1000
	HEC	1.005 (20 ℃)	0.76	0.86	0.1-1000
	Carbopol	1.0 (20 ℃)	0.22	0.79	0.01-10
Harrington et al. 1979	Crosslinked HPG	-	2.68 – 25.47	0.543-0.425	1-100
Hannah and Harrington 1981	HEC	-	3.11-6.94	0.344-0.306	100-1022
Clark et al. 1981	HPG	-	0.00029-0.202	0.829-0.293	0-150
Shah 1982	HEC	~1.0 (26.7℃)	0.047 – 0.814	0.762-0.470	-
	HPG	~1.0 (26.7℃)	0.275-8.6	0.553-0.281	
Roodhart 1985	Guar gum	-	0.33-8.5	0.52-0.29	0.1-1000
	HEC	-	1.4-40	0.45- 0.22	

Table 3.1. Viscous characteristic of various fracturing fluids (cont.)

Kirkby and Rockefeller 1985	HPG, Xanthan gum	-	-	-	0.01-1000
Acharya 1986	CMC	~1.02 (20 ℃)	2-38.5	0.86- 0.51	1-1000
	HEC	~1.005 (20 ℃)	7.6-69.4	0.86- 0.306	
	PAA	1.150 (20 ℃)	56	0.52	
	PEO	1.003 (20 ℃)	7	0.56	
Peden and Luo 1987	CMC	1.015	0.194	0.798	5-1021
	CMC+XC	~1.00	0.1696-0.7688	0.627-0.449	
	HEC	~1.00	0.0374-3.992	0.716-0.418	
Acharya 1988	HPG (26.7 ℃)	-	0.1053-2.5424	0.6349-0.3473	1-103
	CMHPG (26.7 ℃)	-	0.4644-2.5281	0.4381-0.3532	
McMechan and Shah 1991	HPG	-	-	-	-
	HEC	-	-	-	
Machac and Lecjaks 1995	Tylose	1.00	0.515	0.898	1.5-16.2
	Natrosol	1.00	1.12	0.741	
	Kerafloc	1.00	1.62	0.356	
Asadi et al. 1999	Guar gel	-	-	-	3-600 RPM
	HPG	-	-	-	
Goel et al. 2002	Guar gel	-	-	-	0.1-1000
Kelessidis and Mpandelis 2004	CMC	1.00 (20 ℃)	0.11521-0.08492	0.7449-0.9099	5-1000
Liu and Sharma 2005	Guar gel	-	0.156-0.892	0.59-0.42	5-1022

Table 3.1. Viscous characteristic of various fracturing fluids (cont.)

Hu et al. 2015	CMHPG	-	2.75	0.62	10-100
Shahi and Kuru 2016	CMC	-	0.028-0.116	0.818-0.714	0.1-1000
Arniaplly and Kuru 2017	HPAM	~1	0.16-0.53	0.35-0.38	1-200

3.1.2. Viscoelasticity of the Linear Gel. Elasticity is basically material's ability to regain its original shape once the stress is removed from it. If the material is able to regain its perfect original shape than that material is called perfect elastic material. Viscoelastic fluid's behaviour is characterised by both the viscosity and elasticity over certain ranges of frequency implemented on it. Various techniques can be used to determine rheological properties of viscoelastic fluid which can be found in (Ferry, 1970). Measurement of primary normal stress difference vs shear rate, Stress relaxation test, Amplitude sweep test, and Dynamic frequency sweep test are commonly used tests to investigate the viscoelastic behaviour of fracturing fluids. Malhotra and Sharma (2011), Gomma et al. (2015), and Ozden et al. (2017) investigated viscoelastic behaviour of newly evolving viscoelastic surfactant fluid. Crosslinked fluids were found to possess elasticity (Acharya, 1988; Hu et al., 2015) and uncrosslinked gel or linear gel is also taken into investigation for its viscoelastic behaviour (Acharya et al., 1976 (a); Acharya, 1986; Goel et al., 2002; Gomaa et al., 2015; Hu et al., 2015; Arnapalli and Kuru, 2017)

Acharya et al. (1976 (a)) and Acharya (1986) found after investigating viscoelastic behaviour of several different linear gels that CMC is purely viscous fluid because it did not show any measurable stress difference vs shear rate implemented

whereas PAA, PEO and HEC have some elasticity as they showed some measurable stress difference. Machac and Lecjaks (1995) used three different linear gels named Tylose (mixture of water and methylcellulose), Natrosol (mixture of water and HEC), and Kerafloc (mixture of water and polyacrylamide) to investigate proppant settling velocity and wall effects. They neglected the elasticity of Tylose and Natrosol because of the low values of relaxation time around 0.132 sec and 0.358 sec respectively.

By applying different angular velocity ranged from 0.01 – 100 rad/sec on uncrosslinked gel and crosslinked guar gel, Goel et al. (2002) found that 100 pptg (1.2 wt %) linear gel prepared using guar has almost equal value of elastic modulus (G') as the crosslinked fluid prepared using 0.42% of guar and 0.72 g/l, 0.06 g/l, 0.054 g/l and 0.21 g/l borate at pH 9, 10, 11 and 9 respectively. That means that the elastic behaviour and effect of elasticity on proppant transport would be same in the case of linear gel and crosslinked gel for the specific concentrations and conditions mentioned above. Gomaa et al. (2015) used dynamic oscillatory frequency sweep test to measure the viscoelastic behaviour of 20 pptg guar polymer solution and the range of the frequency used was 0.01-10 Hz. They found that the viscous modulus (G") dominates elastic modulus (G') for all the values of frequency and the values of both the stress modulus's (G" and G') increases with frequency. For two different fluids with same power law parameters, they found that the fluid which has G'>G" behaved as semi-solid material where it deformed instead of flowing when shear stress was applied and the other fluid with G">G' flowed when shear stress was applied. Hu et al. (2015) investigated viscoelastic behaviour of 50 pptg CMHPG linear gel using oscillatory shear at strain amplitude of 10%. The frequency range used was 0.1-10 rad/sec in which they observed similar behaviour mentioned in Gomaa et al. (2015) that the viscous modulus dominated the elastic modulus for all the values of frequency and the values of both the

modulus increased with increasing frequency. Arnipalli and Kuru (2017) used three different grades of HPAM and mixed them with different concentration in such a way that from the six fluids prepared out of those combinations, three had same elastic property and three had same viscous property. They investigated relaxation time of the three fluids having same elastic property (because of same average molecular weight but different molecular weight distribution) using oscillatory frequency test where the range of frequency applied was 0.001-10 rad/sec. They quantified molecular weight distribution in the polymer solution in terms of polydispersity index. They found that as polydispersity index increases, the relaxation time increases and therefore elasticity of the solution increases.

Dynamic frequency sweep test is used in this study to investigate viscoelastic behaviour of linear gel where a range of angular frequency (1.0 rad/sec – 100 rad/sec) is implemented on the sample fluid and loss modulus (G”- viscosus modulus) and storage modulus (G’ – elastic modulus) are measured. The cross over point of G’ and G” is used to determine the relaxation time of the fluid based on which elasticity of the fluid is quantified. The procedure to obtain the relaxation time is described in detail in the later section. The relaxation time is a measure of the time at which fluid structure changes from anisotropic to isotropic (Gracssley 1974) or the time needed for any deformed material to regain its original structure (Choi 2008). Higher the relaxation time, more the elasticity of the material. The material with zero relaxation time is considered as completely inelastic fluid.

3.2. MEASUREMENT OF SETTLING VELOCITY IN UNBOUNDED FLUID

Measurement of settling velocity of single proppant particle in stagnant fluid does not replicate the actual field condition of hydraulic fracturing treatment but the

results obtained through these experiments give the basic understanding of how the proppant might actually move within the fracture in real conditions. Basically results obtained with static conditions help to develop the understanding of the complex proppant transport process inside the fractures. However, experiments performed with static conditions do replicate the condition of real field operation when the pumping is stopped and the fractures have started closing. At that time the fluid inside the fracture will be stagnant and proppant will keep settling until the fractures get completely closed. Novotny (1977) showed that consideration of proppant settling at the time of fracture closure is equally necessary to optimize the design of hydraulic fracturing to attain anticipated stimulation ratio. Wide range of research has taken place in the past to understand this complex settling phenomenon using different fracturing fluids, different fracture setups and different proppants. Correlations have been established; theoretically and empirically, between the drag coefficient and particle Reynolds number and still under extensive research in order to improve the accuracy of the calculations while comparing it with the experimental results.

Acharya et al. (1976 (a)) used glass tube of 15.24 cm diameter and 300 cm length to investigate the static settling velocity of different spherical material such as steel, glass, red acrylic and black phenolic of different diameters with different linear gels such as carboxymethyl cellulose (CMC), polyacrylamide (PAA), polyethylene oxide (PEO), hydroxyethyl cellulose (HEC) and Carbopol with different concentrations. They found that for the creepy flow regime ($N_{re}<1$), elasticity of the fluid doesn't affect the settling velocity of the particle. In the case of high Reynolds number region ($N_{re}>1$) the elasticity of the fluid was found to be responsible for decreasing drag coefficient and therefore increasing the settling velocity of the particle. Similar results were obtained in the later researches as well with different linear gels

such as HPG and carboxymethyl HPG (Acharya, 1986; Acharya, 1988; Hu et al., 2015). Even for the dynamic conditions it was pointed out that the proppant transport is governed by viscous property of the fluid and elastic forces do not show any dominance over viscosity at that low shear rates (Harris et al., 2005). Using linear gels of CMC, XC and HEC Peden and Luo 1987 showed that at $N_{re}<10$, power law fluids affect settling velocity similarly as any other Newtonian fluid but at higher particle Reynolds number ($N_{re}>10$) drag coefficient reduces and therefore the settling velocity of proppant increases. They also showed that as the shear thinning behavior of power law fluid increases, drag reduction becomes more pronounced. They also developed a generalized numerical model which can be used for both the Newtonian and non-Newtonian fluids for various shapes of proppants and all the particle flow regimes. Chien (1994) showed that in the laminar slip regime Nre<10, fluid's rheology plays very important role whereas in turbulent slip regime Nre>50 fluid's rheology plays minor role but particle's density and surface characteristics play important role in governing the proppant settling phenomenon. In contrast (Malhotra and Sharma 2011) found that elasticity causes drag reduction for particular range of K, n values and particle size when Nre is between 0.0005 and 2.63 while using polymer free, two component viscoelastic surfactant fluid.

By performing experiments with both the static and dynamic conditions Novotny (1977) concluded that settling velocity measured with static conditions are not reliable for predicting settling behaviour in a flowing fluid for $0.34 < n < 0.4$. However, for $0.8 < n < 1.0$ the proppant particle showed similar settling velocities for both the static and dynamic conditions. They also showed that at low Reynolds number ($N_{re}\leq 2$) the settling velocity of single proppant particle can be calculated using effective viscosity of non-Newtonian fluid at apparent shear rate (Vs/d_p) in the correlations

established for Newtonian fluid. Similar observations were made by Liu and Sharma (2005) for $N_{re} \leq 2$ as well as $2 < N_{re} \leq 500$. For concentrated slurry of proppant Novotny (1977) found that the correlations already established for Newtonian fluids work perfectly to predict the proppant settling rate in the non-Newtonian fluid with static conditions.

By using linear HEC gels and static conditions Hannah and Harrington (1981) showed that none of the correlations provided by (Novotny, 1977) and (Daneshy, 1978) can accurately determine the settling velocity of single proppant. They also performed dynamic tests with HEC gels using concentric cylinder assembly where inner cylinder (rotor) rotates and outer cylinder (stator) remains stationary and found that the experimental results of settling velocity of single proppant particle doesn't deviate more than 40% than the Stokes law. In their later research Harrington et al. (1979) they showed that the settling velocity of single proppant within crosslinked fluid follows similar trend obtained with Stokes law but the values were 78% lower when using 46 RPM of shear rate. They suggested to use a correction factor with the Stokes correlation and concluded that every different fluid has its own correction factor which is to be used with Stokes correlation. Clark et al. (1981) observed that after particular concentration of HPG, the static settling results show high deviation from the Stokes law. Experimental results of Alcocer et al. (1992) also showed deviation from Stokes law because of usage of non-Newtonian fluid.

Shah (1982) used plexiglass column of 213 cm long and 6.35 cm ID to investigate settling velocity of different spherical particles made up of different material such as aluminium, Teflon polymer, brass, sapphire, steel, plastic, glass and lead of different sizes ranging from 0.102 to 1.02 cm with specific gravities from 1.05 to 11.0. Linear gel of HPG and HEC were used with different concentrations to develop

empirical correlations. He suggested to plot C_D^{2-n} vs. N_{re} or $\sqrt{C_D^{2-n}}\ N_{re}^2$ vs. N_{re} for non-Newtonian fluids so that y-axis of the plot becomes independent of the settling velocity term and velocity can directly be found by knowing the particle Reynolds number (N_{re}) corresponding to C_D^{2-n} or $\sqrt{C_D^{2-n}}\ N_{re}^2$ value on y-axis. To avoid the complexity of having different curve for each value of n, he designed an equation based on regression analysis having three unknown coefficients which can be found by knowing the value of "n" of the fluid and after determining the value of those three coefficients, the value of Nre can directly be calculated without even using the plot. Then by using the equation for non-Newtonian fluids $N_{re} = D_p^n * V_s^{2-n} * \rho_f / 3^{n-1} * K$, settling velocity of the particle can be calculated. The range of applicability of the correlation which he established is from 0.281 to 1.0 for values n and 0.01 to 100 for values N_{re}. Shah (1986) provided the method to calculate the static settling velocity step by step. Later the correlation was modified using 391 data points and different effective viscosity; $\mu = K\ (2*Vs/dp)^{n-1}$, which can be found in (Shah et al. 2007). They suggested to use these correlations only when the experimental data is unable to obtain.

Roodhart (1985) introduced the concept of zero shear viscosity stating that the fluid in a stagnant condition has a high viscosity than anticipated at even very low shear rates. He used a cylindrical vessel of different diameters and different sizes of steel balls and glass balls as proppants with the linear gels of HEC and guar gum with different concentrations. He showed that the usage of conventional power law model can produce the settling velocity values smaller by an order of magnitude compared to the values calculated by extended power law model which includes zero shear viscosity. Zero shear viscosity term was introduced in the power law model as shown below:

$$1/\mu_a = 1/\mu_o + (K*\gamma^{n-1})^{-1} \qquad (13)$$

Similarly, Asadi et al. (2002) also emphasized the importance of zero shear viscosity to develop the understanding of settling phenomenon and suggested a methodology to determine the zero shear viscosity of any fracturing fluid. The methodology includes steps such as measurement of fluid's viscosity as a function of frequency at constant stress after preconditioning the fluid and then using non-linear regression software measuring the zero shear viscosity.

For the static conditions Kirkby and Rockefeller (1985) performed experiments using single proppant as well as concentrated slurry having two different sizes (20/25 Ottawa sand and 40/45 Ottawa sand) with Newtonian fluid as well as non-Newtonian fluid (includes linear and crosslinked gel both). They found that the average slurry settling velocity is way higher than the single proppant because of the formation of the clusters while using concentrated slurry. They found that the difference in the settling velocities were huge for various fluids even after having the same viscosity value at particular shear rate showing the vitality of measuring the viscosities at lower shear rates to understand the actual difference between the viscosities at static conditions. McMehen and Shah (1991) used HPG and HEC linear gel and used different concentrations of 20/40 mesh sand from 2 ppg to 15 ppg to investigate the effect of proppant concentration in static conditions. They found that when the proppant concentration is below 10 ppg the average settling rate of proppant goes higher than the single particle rate because of formation of high concentration clusters. When the concentration is higher than 10 ppg the average settling rate was found to be lower than the single particle rate because of hindered settling. Asadi et al. (1999) conducted similar type of experiments with concentrated slurry and found that the difference between the settling rates in two different linear gels was smaller than the difference between their viscosity measurements at low shear rates. Viscosity measurements

showed four fold reduction in the viscosity of 40 pptg HPG gel compare to 60 pptg HPG gel at lower shear rates whereas settling velocity showed less than four fold reduction due hindered settling occurring in both the fluids. Goel et al. (2002) showed a critical polymer concentration point above which the suspension characteristics of the solution seems much better than the solution with lower concentration of polymer than the critical one. They used uncrosslinked guar gel concentrated with 20 wt% slurry to show the above result.

Gomma et al. (2015) showed that viscosity alone cannot predict the proppant settling in the fluid using 16/40 mesh sand proppant with 4 ppg concentration in crosslink fluid. Further they concluded that the speed of settling will depend on viscosity of the fluid when G”>G’. But in case of elastic fluids where G’>G”, elasticity of the fluid will not allow the proppant to settle.

Arnipally and Kuru (2017) used six different solutions of HPAM; three having same viscous properties and other three having same elastic properties, to investigate the effect of elasticity and viscosity both separately on the static settling velocity of proppant. They used Particle Image Shadowgraph technique and spherical particles of four different sizes as proppants. By performing experiments with the fluids having same shear viscosity properties, they found that as the relaxation time of the fluid increases the settling velocity of the particle decreases. They also verified the results by comparing the experimental values with (Shah et al., 2007) correlation for visco-inelastic fluids and found that experimental values were deviating and the deviation increased as the elasticity of the fluid increased. By performing experiments with the fluids having similar elastic properties, they found that settling velocity of the particle reduced with increasing consistency index K. They also observed that the magnitude of

the increase in the settling velocity of the particle with increasing diameter was less for the fluids having higher elasticity and same shear viscosity properties.

3.3. MEASUREMENT OF SETTLING VELOCITY IN CONFINED FLUID

Clark et al. (1981) performed experiments using parallel plate model and HPG linear gel with different concentrations. Using 28-35 mesh sand proppant they found that as the fracture wall's width increases, the effect of walls on settling velocity decreases. The wall effect found to be diminishing significantly at 0.5 inch.

Machac and Lecjaks (1995) investigated the fracture wall effects using rectangular column of 80 cm height, 8 cm longer width and 1.2 cm shorter width. They used six different sizes of spheres with different densities and Glycerol as Newtonian fluid and Tylose, Natrosol and Kerafloc as non-newtonian viscoelastic fluids. They found the effect of fracture walls on the settling velocity decreasing with increasing the shear thinning behavior and elasticity of the fluid and decreasing rectangular duct aspect ratio a/b. The correlation established based on their experimental results is not only applicable to rectangular duct but also the square duct and parallel plates which is described in detail in the later section. The conditions used during experiments were $1 \geq n \geq 0.36$, $0.00014 \leq N_{re} \leq 0.5$, $0.15 \leq a/b \leq 1$.

Liu and Sharma (2005) used 40 pptg linear guar gel, water and mixture of water and glycerin to investigate effect of fracture walls on the settling velocity of proppant with static conditions. By analyzing the results obtained from the parallel plate model using different sizes and specific gravities of proppant, they found that with increasing viscosity of the fluid, the fracture wall effect gets more pronounced and reduces the settling velocity. Specifically for water they found that the fracture walls do not affect the settling velocity until the slot width is 10-20% of the particle diameter. They also

showed that with increasing the particle diameter to fracture width ratio the settling velocity reduces for both the Newtonian and non-Newtonian fluid. The empirical correlations to calculate the settling velocity with the fracture wall effects are given in Table 3.3.

Malhotra and Sharma (2012) observed that increasing shear thinning behavior of the fluid reduces the wall retardation effect. Even elasticity of the fluid retards the effects of wall and this retardation gets pronounced as the particle dimeter to fracture width ratio increases.

3.4. CORRELATIONS FROM PAST RESEARCHES

Swanson (1967) developed a correlation to calculate the settling velocity of any size of the particle directly for static conditions. The equation was based on Newton's Law where the drag coefficient or friction factor was taken as a function of the laminar boundary layer. Two different equations were established using the experimental data of previous researches and implementing the concepts of laminar boundary layer respect to the fluid flowing past a sphere. Equation (14) shown below was developed for spherical particles which can be expressed as:

$$V_s = (V_N/\alpha)*(1/(1+ (\sqrt{48}*\beta*\mu)/dp*\rho_f*V_N)) \quad (14)$$

Where $V_N = \sqrt{(4*g*dp*(\rho_p - \rho_f) / 3* \rho_f)}$ and α, β are parameters relevant to the laminar boundary layer. For this study α was taken as 1.277 and 0.942 whereas β was taken as 2.80 and 3.27 for sand and ceramic proppant respectively from Swanson (1967). Equation to calculate the settling velocity for non-spherical particle was also developed but has not been used here for this study as the parameters required to validate that equation were not determined during this study.

Acharya et al. (1976 (a)) established correlations; based on theoretical studies and their own experimental work, between drag coefficient (C_D) and N_{re} for creepy flow regime ($N_{re}<1$) which is expressed as:

$$C_D = 24*F(n)/ N_{re} \quad (15)$$

Where F(n) is function of the flow behaviour index (n) which is expressed as

$$F(n) = 3^{3n-3/2} [33n^5 – 63n^4 – 11n^3 + 97n^2 + 16n / 4n^2*(n+1)*(n+2)*(2n+1)]$$

The other correlation established was based on experimental study for the range of particle Reynolds number from 0.001 to 1000 which can be expressed as:

$$C_D = [24 F(n) / N_{re}] + [f_2(n)/N_{re}^{f_3(n)}] \quad (16)$$

Where $f_2(n) = 10.5*n – 3.5$, $f_3(n) = 0.32*n + 0.13$. Both the correlations were established based on the data of purely viscous non-Newtonian fluid. For creepy flow regime they found that the correlation works with acceptable range of errors for both the pure visco-inelastic and viscoelastic fluids whereas at higher Reynolds number the experimental values of viscoelastic fluids lied below than the values calculated based on correlation. So they concluded that elasticity reduced the drag at higher particle Reynolds number. Acharya (1986) substituted the definition of $C_D = 4*(\rho_p – \rho_f)*g*d/3*\rho_f *V_s^2$ and equation of $F(n) = 3^{3n-3/2} [33n^5 – 63n^4 – 11n^3 + 97n^2 + 16n / 4n^2*(n+1)*(n+2)*(2n+1)]$ into $C_D = 24*F(n)/ N_{re}$ and established a correlation to calculate the settling velocity of single proppant inside the stagnant fluid when $N_{re}<2$ which can be expressed as:

$$Vs = [(\rho_p – \rho_f)*g*d_p^{n+1} / 18*K*F(n)]^{1/n} \quad (17)$$

By applying similar procedure for $2<N_{re}<500$ they established correlation which can be expressed as:

$$V_s = \{(3*\rho_f/4*(\rho_p–\rho_f)*g*d)* [(24*F(n)/4*N_{re}) + f_2(n)/N_{re}^{f3(n)}]\}^{-1/2} \quad (18)$$

They found a good correlation between experimental results and correlation.

The correlations which are provided in the literature published by Novotny (1977) are for the Newtonian fluids in which the viscosity term can be replaced by effective viscosity of non-Newtonian fluid.

For $N_{re} \leq 2$ (stokes law region), $C_D = 24/ N_{re}$, settling velocity Vs will be

$$V_s = g*(\rho_p - \rho_f)*d_p^2 / 18*\mu \quad (19)$$

For $2 < N_{re} < 500$ (Intermediate region), $C_D = 18.5/ N_{re}^{0.6}$, settling velocity Vs will be

$$V_s = 20.34*(\rho_p - \rho_f)^{0.71} *d_p^{1.14}/ \rho_f^{0.29}*\mu^{0.43} \quad (20)$$

For $N_{re} \geq 500$ (Newton's law region), $C_D = 0.44$, settling velocity Vs will be

$$V_s = 1.74*\sqrt{g*(\rho_p - \rho_f)^{0.71} *d_p/ \rho_f} \quad (21)$$

For non-Newtonian fluids, effective viscosity is calculated by power-law model in which the shear rate is given by apparent shear rate expressed as V_s/d_p. So for $N_{re} \leq 2$, non-Newtonian fluid the settling velocity will be:

$$V_s = [g*(\rho_p - \rho_f)*d_p/ 18*K]^{1/n}*d_p \quad (22)$$

For $2 < N_{re} < 500$, the equation can't be solved explicitly and trial-error method should be used. Daneshy (1978) used maximum particle shear rate as $3*V_s/d_p$ and substituted in the power law equation and obtained similar type of equation just with small change. The equation for settling velocity can be expressed as:

$$V_s = [g*(\rho_p - \rho_f)*d_p/ 18*K*(3)^{n-1}]^{1/n}*d_p \quad (23)$$

Peden and Luo (1987) established a correlation to calculate the settling velocity of irregularly shaped particle based on their experimental results. The correlation can be expressed as:

$$Vs = [4/3*g*(0.001*d_s)^{(1+en)}*(\rho_p - \rho_f) / a*F_s*I_c^{e}*\rho_f^{(1-e)}*1000^{-e}]^{1/[2-e*(2-n)]} \quad (24)$$

Where d_s is the diameter of the sphere, Fs is the shape factor and Ic is the viscosity of the fluid. To calculate the shape factor the equation is Fs = 1.5-0.5* ψ (sphericity). The equations to calculate parameters a, e and sphericity of the particle can be found in their literature based on different ranges of particle Reynolds number, flow behavior index (n) and different shapes.

Chien (1994) established new correlations by collecting data of previous authors which consider the size, density, and shape of the proppant, rheology of the fluid for a wide range of particle Reynolds number from 0.001 to 10,000. The correlation between drag coefficient and particle Reynolds number can be expressed as:

$$C_D = (30/N_{re}) + (67.289/e^{5.030\psi}) \quad (25)$$

for $0.2 \leq \psi \leq 1$ and $0.001 \leq N_{re} \leq 10{,}000$

Most of the data from other authors fell in range of +/- 25% when compared with the values calculated using this correlation.

For laminar slip regime the correlation to calculate settling velocity can be expressed as:

$$Vs = 120*(\mu_e/d_p*\rho_f)*[\sqrt{1 + 0.0727*\ d_p\ *(\rho_p/\rho_f - 1)*\ (dp*\rho_f/\ \mu_e)^2 - 1}] \quad (26)$$

For turbulent slip regime the correlation to calculate the settling velocity can be expressed as:

$$V_{s(t)} = 4.410\ e^{2.515\psi}\ \sqrt{d*[(\rho_p/\rho_f) - 1]} \quad (27)$$

Where ψ is sphericity of the particle and μ_e is the effective viscosity of the fluid

Machac and Lecjaks (1995) established correlations based on their experimental results using rectangular duct keeping shorter width constant as 1.2 cm and changing the longer width from 1.2 cm until 8 cm. The fracture wall factor can be expressed as:

$$F_W = 1/[1+k_1*(d/D_E) + k_2*(d/D_E)^2] \quad (28)$$

Where $k_1 = 1.120 - 3.025n + 3.715n^2$ and $k_2 = 0.49$. They have defined different correlations for d/D_E for sphere falling in rectangular duct, parallel plates and square duct respectively in their literature. While comparing the values calculated using above correlations from experimental results, the mean deviation did not exceed 3.7% for Natrosol and 2.7% for other liquids with the maximum deviation to be 9.2%. They also compared the values of wall factors of Newtonian fluids calculated by their correlations with previously established correlations which used square duct and parallel plates to generate the wall effects and found very good agreement with them as well.

Cheng (1997) established an explicit correlation by which the static settling velocity can be calculated for natural sediment particles of irregular shapes. They extended the Stokes law for the wide range of N_{re} which is from 1 to 1000 by correlating drag coefficient (C_D) and particle Reynolds number (N_{re}) using results of several other authors. The explicit equation to calculate the settling velocity can be expressed as:

$$V_s = \nu/d_p * (\sqrt{25 + 1.2*d_p^2} - 5)^{1.5} \quad (29)$$

Where ν is dynamic viscosity of the fluid and $d_* = ((\rho_s - \rho_f)/ \rho_f * g)/ \nu^2)^{1/3}*d_p$. Average deviation was found to be 6.1% when comparing other author's data with the correlation.

Kelessidis and Mpandelis (2004) established correlation between drag coefficient and particle Reynolds number based on their experimental results and data from other authors as well. They used water, glycerol, and three different CMC linear gel as fracturing fluid whereas glass beads, lead and steel with different densities and sizes as proppants to investigate the relationship between C_D and N_{re}. Using non-linear regression analysis they established correlation for non-Newtonian fluids considering 80 different data points including their own results and results from other authors for $0.1<N_{re}<1000$. The correlation can be expressed as:

$$C_D = 24/N_{re} (1+0.1466*N_{re}^{0.378}) + (0.44/1+0.2635/N_{re}) \quad (30)$$

They established another correlation considering 148 data points which can predict the drag coefficient for both Newtonian and non-Newtonian fluids for 0.1<Nre<1000 which can be expressed as:

$$C_D = 24/N_{re} (1+0.1407*N_{re}^{0.6018}) + (0.2118/1+0.4215/N_{re}) \quad (31)$$

By mathematically calculating the standard deviations they concluded that the correlation which was established by Heider and Levespiel (1989) using only Newtonian fluid considering 408 data points should be used to predict the static settling velocity for non-Newtonian fluid as well for $Nre<2.6*10^5$ and the correlation can be expressed as:

$$C_D = 24/N_{re} (1+0.186*N_{re}^{0.6459}) + (0.4251/1+6880.95/N_{re}) \quad (32)$$

Wu and Wang (2006) reevaluated the correlation published by U.S Interagency Committee using wider range of data and correlation given by Cheng (1997) and developed a new correlation. As the shape affects the C_D - N_{re} relationship, Corey factor was used in the equation to calculate the coefficients used in the new correlation developed by Wu and Wang. Total 571 data points were used to validate this correlation and other three correlation from previous authors. The newly developed correlation by Wu and Wang (2006) showed the least deviation that is 9.1% compared to the nine formulas existing in the literature.

Shah et al. (2007) built a new model to estimate static settling velocity of single proppant for flow behavior index from 0.281 to 1 and particle Reynolds number from 0.001 to 1000 by collecting 391 data points from past researches. The correlations for coefficients used earlier in (Shah, 1982); which correlates C_D and N_{re}, were modified

considering apparent effective viscosity as K $(2Vs/dp)^{n-1}$. They found that usage of Newtonian fluid's correlation does not estimate the settling velocity within the acceptable range and so they recommended to use this correlation only when the experimental data is unable to obtain.

Helbar et al. (2009) reviewed work from several different authors from 1933 to 2007 and examined and re-evaluated 22 different correlations and developed a new correlation for sediment particles inside water. Particles sizes ranged from 0.01 mm to 100 m and all the different particles; one after other , were tested with all the selected 22 correlations and from that best suitable correlations were screened out and mean particle settling velocity was determined. Based on these values new correlation was developed which can be expressed as:

$$Vs = 0.033*(\nu/d_p)*(d_p^3*g*(s-1))/\nu^2)^{0.963} \quad (33)$$

for $D_{gr} \leq 10$

$$Vs = 0.51*(\nu/d_p)*(d_p^3*g*(s-1))/\nu^2)^{0.553} \quad (34)$$

for $D_{gr} > 10$

Where D_{gr} is effective diameter of the particle which is equal to $d_p*(g*(s-1)/\nu^2)^{1/3}$ where s = Relative density $(\rho_p - \rho_f)$. The mean relative error was 11.75% using this correlation when compare to the data published by other authors.

Holzer and Sommerfeld (2008) developed a correlation based on numerical study and data of drag coefficient and particle Reynolds number from several other authors. They introduced crosswise sphericity and lengthwise sphericity into the correlation as they considered various shapes of sediments such as spheres, cuboids, cylinders, isomeric particles, disks and plates with water as an experimental fluid. They found that the mean relative deviation to be 14.1% comparing 2061 experimental data with the correlation. The correlation can be expressed as:

$$C_D = (8 / Nre * 1/\sqrt{\Phi_{II}}) + (16 / Nre * 1/\sqrt{\Phi}) + (3 / \sqrt{Nre} * 1/ \Phi^{3/4} + 0.42100.4 (-\log \Phi)0.2*1/\Phi_{\perp} \quad (35)$$

Where Φ is sphericity of the particle, Φ_{II} is lengthwise sphericity, and $\Phi_{\perp}$ is crosswise sphericity

Shahi and Kuru (2015) developed a model only applicable to calculate the settling velocity of natural sand inside water. The important expression which they introduced was equivalent circular diameter for irregularly shaped proppant. They used 980 quartz sand particles with different sizes ranging from 0.35 mm to 1.18 mm to establish two different models; a circular model and an elliptical model, and verified those models by their own experimental results to see the suitability of the correlation. They found the average error of 7.7% using the circular model for the sieve size range of 0.19 mm – 1.22 mm whereas for the elliptical model the average error was found to be 9.2%.

Shahi and Kuru (2016) used CMC linear gel with different concentrations and investigated particle settling velocity using spherical particles of different sizes ranging from 0.5 mm to 2.0 mm. They established an empirical correlation in order to improve the correlation previously established by Shah et al. 2007. They found average error to be 9.6% using their own correlation whereas the error was found to be 14.5% for the same data using the correlation of (Shah et al. 2007).

Table 3.2, 3.3 and 3.4 below only contains that information which is useful and correlatable to this study regarding different fluids, types of proppants, fracture walls, range of particle Reynolds number and the correlations established.

Table 3.2. Different parameters used by several authors and their correlations

Author	Proppant	Fluid	(N_{re})	Correlation
Swanson 1967	Sand	-	-	$V_s = (V_N/\alpha)*(1/(1+(\sqrt{48}*\beta_p*\mu)/d*\rho*V_N))$
Acharya et al. 1976(a), Acharya 1986 and 1988	Steel, Glass, Red acrylic, Black phenolic	CMC PAA PEO HEC Carbopol	$N_{re} < 1$	$C_D = 24*F(n)/ N_{re}$
			$0.001<N_{re}< 1000$	$C_D = [24 F(n) / Nre] + [f_2(n)/Nre^{f_3(n)}]$
Novotny 1977	Sand Glass bead	Newtonian	$N_{re} <= 2$	$V_s = g*(\rho_p-\rho_l)*d^2 / 18*\mu$
			$2< N_{re} < 500$	$V_s = 20.34*(\rho_p-\rho_l)^{0.71} *d^{1.14} / \rho l^{0.29} *\mu^{0.43}$
		Non Newtonian	$N_{re} <= 2$	$V_s = (g*(\rho_p- \rho_l) * d / 18*K)^{1/n} *d$
Daneshy 1978	Sand	Newtonian	$N_{re} <= 2$	$V_s = (g*(\rho_p-\rho_l)*d^{n+1} / 18*K* 3^{n-1})^{1/n}$
Hannah and Harrington 1978	Glass beads	HEC	-	-
Harrington et al. 1979	Glass beads Sand Sinter bauxite	HPG + Metal ion	-	$V_s = \beta*g*(\rho_p-\rho_f)*d^2 / 18*\mu$
Shah 1982	Glass Steel Teflon Brass Sapphire	HPG HEC	$0.01 < N_{re} <100$	$V_s = [3^{n-1}*K*N_{re}) / d^n *\rho_f)]^{1/2-n}$
Roodhart 1985	Glass Steel	HEC Guar gum	-	$Vs = [g*(\rho_p-\rho_f)*d_p^2/18] * [1/\mu_0 + (1/K * (V_s/d_p)^{1-n})]$

Table 3.2. Different parameters used by several authors and their correlations (cont.)

Kirkby and Rockefeller 1985	Sand	HPG Xanthan gum PAM, Glycerol, HPG + Borate, Fluid A-1 Fluid A-2	-	-
Peden and Luo 1987	Sphere Disc Rectangular plates	Oil 68, CMC, HEC, Xanthan gum biopolymer	0.001-270	$\mathbf{C_D} = a/Nre^{e}$ $\mathbf{Vs} = [4/3*g*(0.001*d_s)^{(1+en)}*(\rho_p-\rho_f) / a*F_s*I_c^{e}*\rho_f^{(1-e)}*1000^{-e}]^{1/[2-e*(2-n)]}$
Acharya 1988	Steel Balls Sand	HPG CMHPG Crosslink Gel	$N_{re} <= 2$	$\mathbf{V_s} = (g*(\rho_p-\rho_l)*d^{n+1} / 18*K*F(n))^{1/n}$
			$2< N_{re} < 500$	$\mathbf{V_s} = \{(3*\rho_l/4*(\rho_p-\rho_l)*g*d)* [(24*F(n)/4*N_{re}) + f_2(n)/N_{re}^{f3(n)}]\}^{-1/2}$
McMechan and Shah 1991	Sand	HPG HEC Crosslink Gels	-	-
Alcocer et al. 1992	Ceramic	XCD	-	-
Chien 1994	-	-	$N_{re} < 10$	$Vs = 120*(\mu_e/d_p*\rho_f)*[\sqrt{1} + 0.0727* d_p *(\rho_p/\rho_f - 1)* (dp*\rho_f/ \mu_e)^2 – 1]$
			$N_{re} > 50$	$V_{s(t)} = 4.410\ e^{2.515\psi} * \sqrt{d*[(\rho_p/\rho_f) – 1]}$
Asadi et al. 1999	Sand	HPG Borate + Guar	-	-
Goel et al. 2002	Sand	Guar gel Borate + Guar	-	-

Table 3.2. Different parameters used by several authors and their correlations (cont.)

Kalessidis and Mpandelis 2004	Glass Bead Lead Steel	Water Glycerol CMC	0.1<N_{re}<1000	$C_D = 24/N_{re} (1+0.1407*N_{re}^{0.6018}) + (0.2118/1+0.4215/N_{re})$ [non-Newtonain + Newtonian]
				$C_D = 24/N_{re} (1+0.1466*N_{re}^{0.378}) + (0.44/1+0.2635/N_{re})$ [non-Newtonain]
Shah et al. 2007	-	-	0.0001< Nre< 1000	**Vs** = [(2)$^{n-1}$*K*Nre) / dn * ρf)]1/2-n
Gomma et al. Gupta 2015	Sand (4 ppg conc)	Crosslink Gel	-	-
Shahi and Kuru 2016	Glass Beads	CMC	0.0001< Nre< 1000	**Vs** = [(2)$^{n-1}$*K*Nre) / dn * ρf)]1/2-n
Arnipally and Kuru 2017	Spherical particles	HPAM	-	-

Table 3.3. Different fracture widths used by several authors and the correlations

Author	Proppant	Fracture Walls	Fluid	Correlation
Clark et al. 1981	Sand	0.32, 0.64, 0.95, 1.27 (cm)	HPG	$C_D = [(A/N_{re})^{1/n} + B^{1/n}]^n$ $V_s = \nu/d_p * (\sqrt{25} + 1.2*d_*^2 - 5)^{1.5}$

Table 3.3. Different fracture widths used by several authors and the correlations (cont.)

Machac and Lecjaks 1995	Spherical Particles	$0.053 \geq d/D_E \geq 0.701$	Linear Gel Glycerol	$\mathbf{F_w} = 1/[1+k_1*(d_p/D_E)+k_2*(d_p/D_E)^2]$ $[0.00014< N_{re} < 0.5]$
Liu and Sharma 2005	Ceramic Walnut hull	0.1 cm 0.15 cm 0.4 cm	Guar gum Water + Glycerin	$\mathbf{V_w} = V_s*1-(f(\mu) * d/w)$
				$\mathbf{V_w} = V_s*g(\mu)*(1-d/w)$

Table 3.4. Different parameters used by several authors and their correlations using water

Author	Proppant	Fluid	Range of Particle Reynolds Number (N_{re})	Correlation
Cheng 1997	Sand	Water	$1<N_{re}<1000$	$\mathbf{C_D} = [(A/N_{re})^{1/n}+B^{1/n}]^n$ $\mathbf{V_s} = \nu/d_p * (\sqrt{25 + 1.2*d_*^2} - 5)^{1.5}$
Wu and Wang 2006	Quartz Sand	Water	Any N_{re}	$\mathbf{V_s} = Mv /Nd* [\sqrt{0.25+((4*N*(D*)^3)/(3*M^2))}^{1/n} - 1/2]^n$
Helbar et al. 2009	0.01 – 100 mm	Water	$D_{gr} <= 10$	$\mathbf{Vs} = 0.033*\nu/d*(d^3*g*(\rho_p/\rho_l - 1)/\nu^2)^{0.963}$
			$D_{gr} > 10$	$\mathbf{Vs} = 0.51*\nu/d*(d^3*g* (\rho_p/\rho_l - 1)/\nu^2)^{0.553}$
Shahi and Kuru 2015	Quartz Sand	Water	-	$\mathbf{Vs} = R_s*\nu/D_c$ [Circular]
				$\mathbf{Vs} = R_{ce}*\nu/D_c$ [Elliptical]

4. EXPERIMENTAL PROCEDURE

4.1. PREPARATION OF THE LINEAR GEL

In order to prepare the linear gel only two components were mixed. One was distilled water and another was guar powder. JAGUAR HP-COS8 was used in different concentration to prepare different solutions of linear gel. Five linear gels with different concentration were prepared adding different amount of guar powder in a required volume of water. Table 4.1 below shows the concentration in field units and amount of water and guar added to prepare that concentration.

Table 4.1. Composition of linear gel with different concentrations

Concentration (pptg)	Water (ml)	Guar (gm)
10	500	0.6
20	500	1.2
30	500	1.8
40	500	2.4
50	500	3.0

In order to prepare linear gel of concentration 10 pptg, stainless steel container was filled with 500 ml of distilled water and stirred for couple of minutes by double spindle overhead mixer (Figure 4.1) at low RPM to allow the water movement to get stabilized inside the container. While stirring the water, 0.6 gram of guar was added continuously very slowly for 5-10 minutes and the mixture was stirred for 10-15 more minutes at low RPM until the vortex disappears. After the mixing process, the same container was covered with aluminium foil and left untouched for 24 hours to allow proper hydration of guar and get the foam settled inside the mixture to avoid erroneous results. The difference between the appearances of the linear gel can be observed from

Figure 4.2 (a) and (b). Then the part of mixture (25 ml) was used for rheological measurements. The same procedure was followed for all the five different concentration of linear gel.

Figure 4.1. Hamilton Beach double spindle overhead mixer

(a) (b)

Figure 4.2. Linear gel condition (a) Immediately after mixing (b) After 24 hours of mixing

4.2. MEASUREMENT OF RHEOLOGICAL PROPERTIES OF THE LINEAR GEL

Two different tests were performed on all the five linear gels with different concentrations to investigate its viscous and viscoelastic properties using Anton Paar MCR 302 Rheometer. Standard concentric cylinder geometry (ID of outer cylinder was 28.915 mm and OD of inner cylinder was 26.670 mm) was used to perform both the tests. The setup of the rheometer and the geometry used is shown in Figure 4.3 below.

Figure 4.3. Anton Paar MCR 302 Rheometer with concentric cylinder geometry

The cylinder at the bottom was filled with the sample and shear sweep test was performed by implementing the shear rate from 0.1 sec^{-1} to 800 sec^{-1} by the upper bob/cylinder to investigate the viscous behaviour of the linear gel. The graph of the shear stress vs shear rate and shear rate vs viscosity was plotted. The fluid was allowed to rest for 5-10 minutes after the first measurement and the test was performed again on the same sample. Shear sweep test was performed thrice on all the samples to ensure the repeatability of the results. Using excel sheet, power law model was fit on the shear stress vs shear rate plot for the range of 10 sec^{-1} – 455 sec^{-1} shear rate to get more accurate K (Fluid consistency index) and n (Fluid behaviour index) parameters within

the range of shear rate caused by the particle during its settling movement inside the stagnant fluid. The results of these tests are discussed in this literature later with details.

Dynamic oscillatory frequency test was performed by implementing the angular frequency from 1.0 rad/sec to 100 rad/sec to investigate the viscoelastic behaviour of the linear gel. The graph of loss modulus (G") and storage modulus (G') vs angular frequency was plotted. After identifying the intersection point of G" and G' on the plot, straight line from that point was stretched to x-axis and value of angular frequency was determined. The inverse of that value was used as the relaxation time of that particular sample. This test takes longer time so it was performed twice to ensure the repeatability of the results. The results of these tests are discussed in this literature later with details.

4.3. MEASUREMENT OF SETTLING VELOCITY IN UNBOUNDED FLUIDS

A transparent cylinder with 43 cm of height and 5.5 cm of diameter was used to perform the experiments in unbounded fluids. As the diameter of the cylinder is more than 50 times than the largest size of the proppant used during experiments, we assumed that there would be negligible wall effects during all the experiments. The setup is shown in the Figure 4.4 and 4.5 below. The foot ruler is placed besides the model to observe the total distance travelled by the proppant while analysing the recorded video in the software.

A single proppant; of different size and different specific gravity, was dropped from the top of the cylinder and allowed to settle in the stagnant fluid. Three different fluids were used which were water, 10 pptg and 20 pptg linear gel. Three different sizes of sand proppant (16/30 mesh = 0.089 cm, 30/40 mesh = 0.051 cm, and 40/50 mesh = 0.036 cm) and two different sizes of ceramic proppant (16/30 mesh = 0.089 cm and

30/50 mesh = 0.042 cm) were used with unbounded fluid. High resolution camera was used to record the video until the proppant settles at the bottom of the cylinder. These

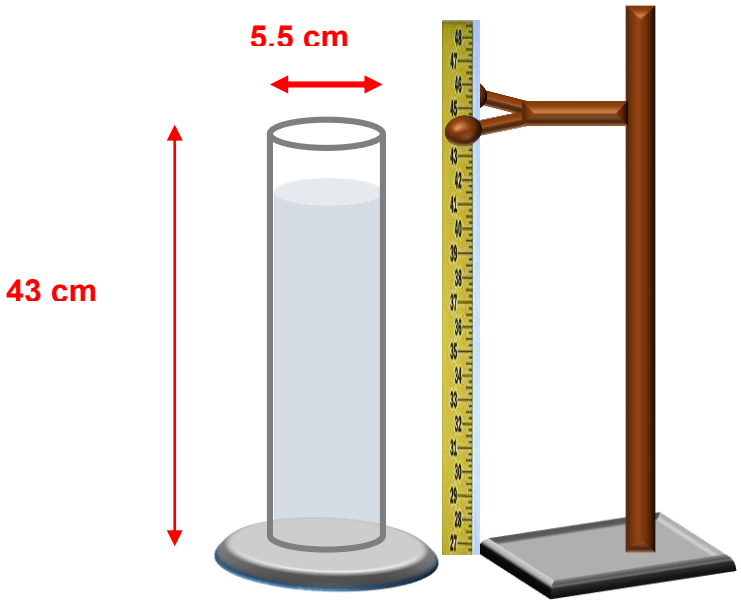

Figure 4.4. Schematic of fracture setup for unbounded fluids

Figure 4.5. Real fracture setup for unbounded fluids

videos were uploaded in the software called “Tracker 4.11.0” to plot the location of the proppant inside the cylinder at different times which can be seen in Figure 4.6.

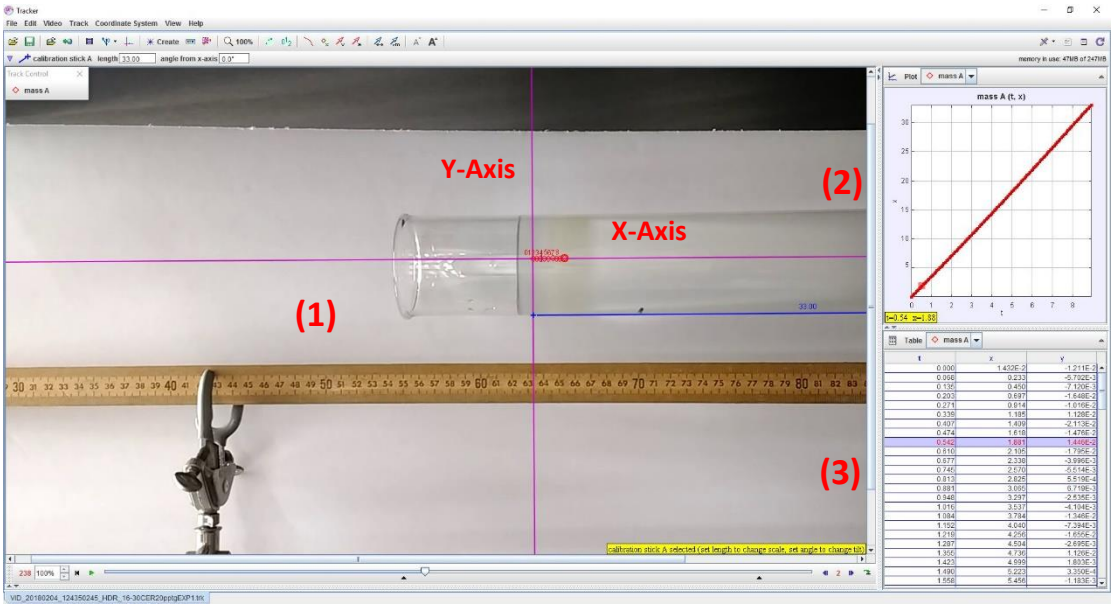

Figure 4.6. Analysis of the video using Tracker 4.11.0

In Figure 4.6 different sections are shown. Section (1) is the window where the motion of the proppant is tracked. Section (2) is the plot between distance and time which is prepared by the software itself as we start tracking the particle. Section (3) shows the table which has x and y coordinates of the proppant at different times. Section (2) and (3) are enlarged and shown in Figure 4.7 and 4.8 respectively. The slope of the plot was calculated which gave the value of terminal settling velocity of the proppant which was then used to validate the correlations. For each single size, fluid and specific gravity of proppant, experiments were performed at least 3 times and average value was considered as final value for terminal settling velocity.

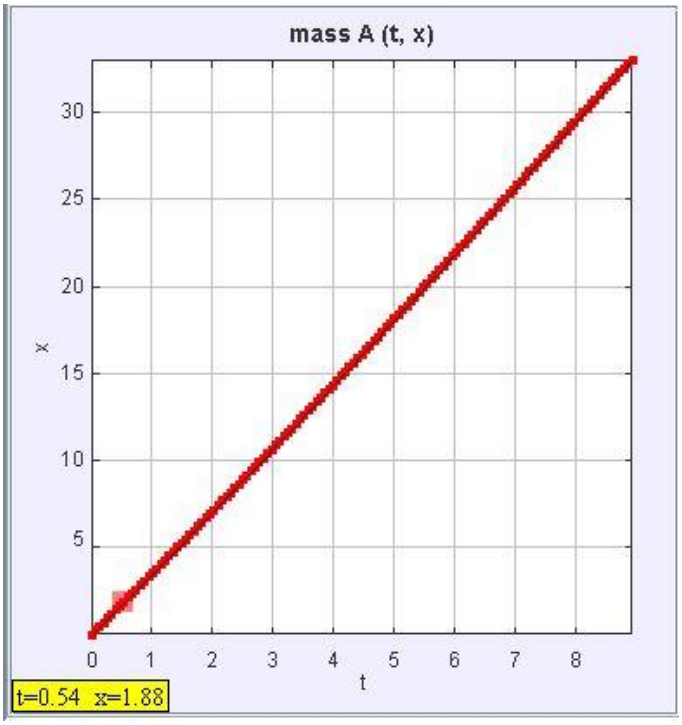

Figure 4.7. Plot between distance travelled by proppant and time taken

Table mass A

t	x	y
0.000	1.432E-2	-1.211E-2
0.068	0.233	-5.702E-3
0.135	0.450	-7.120E-3
0.203	0.697	-1.648E-2
0.271	0.914	-1.016E-2
0.339	1.185	1.128E-2
0.407	1.409	-2.113E-2
0.474	1.618	-1.476E-2
0.542	1.881	1.446E-2
0.610	2.105	-1.795E-2
0.677	2.338	-3.996E-3
0.745	2.570	-5.514E-3
0.813	2.825	5.519E-4
0.881	3.065	6.719E-3
0.948	3.297	-2.535E-3
1.016	3.537	-4.104E-3
1.084	3.784	-1.346E-2
1.152	4.040	-7.394E-3
1.219	4.256	-1.655E-2
1.287	4.504	-2.695E-3
1.355	4.736	1.126E-2
1.423	4.999	1.803E-3
1.490	5.223	3.350E-4
1.558	5.456	-1.183E-3

Figure 4.8. Table with x and y coordinates of the proppant at different times

4.4. MEASUREMENT OF SETTLING VELOCITY IN CONFINED FLUIDS

Two transparent plexiglass plates were connected with each other using rubber sheet of different thicknesses which provided different fracture widths. The height and the length of the fracture model was kept constant throughout all the experiments which was 49 cm and 7 cm respectively. Three different fracture widths were used which were 0.57 cm, 0.27 cm and 0.15 cm according to the availability of the rubber sheet in the laboratory. The holes visible on the front plexiglass plate don't have any significance. The rubber sheets were cut little bit from the top before assembling the whole model to create some space to drop the proppant. The schematic of the setup and the real picture is shown below in the Figure 4.9 and 4.10.

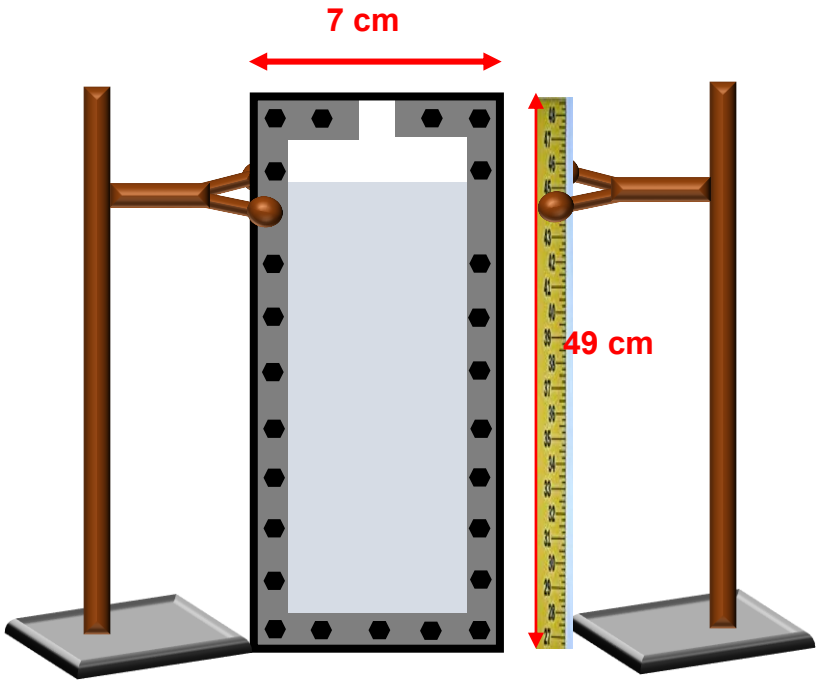

Figure 4.9. Schematic of fracture setup for confined fluids

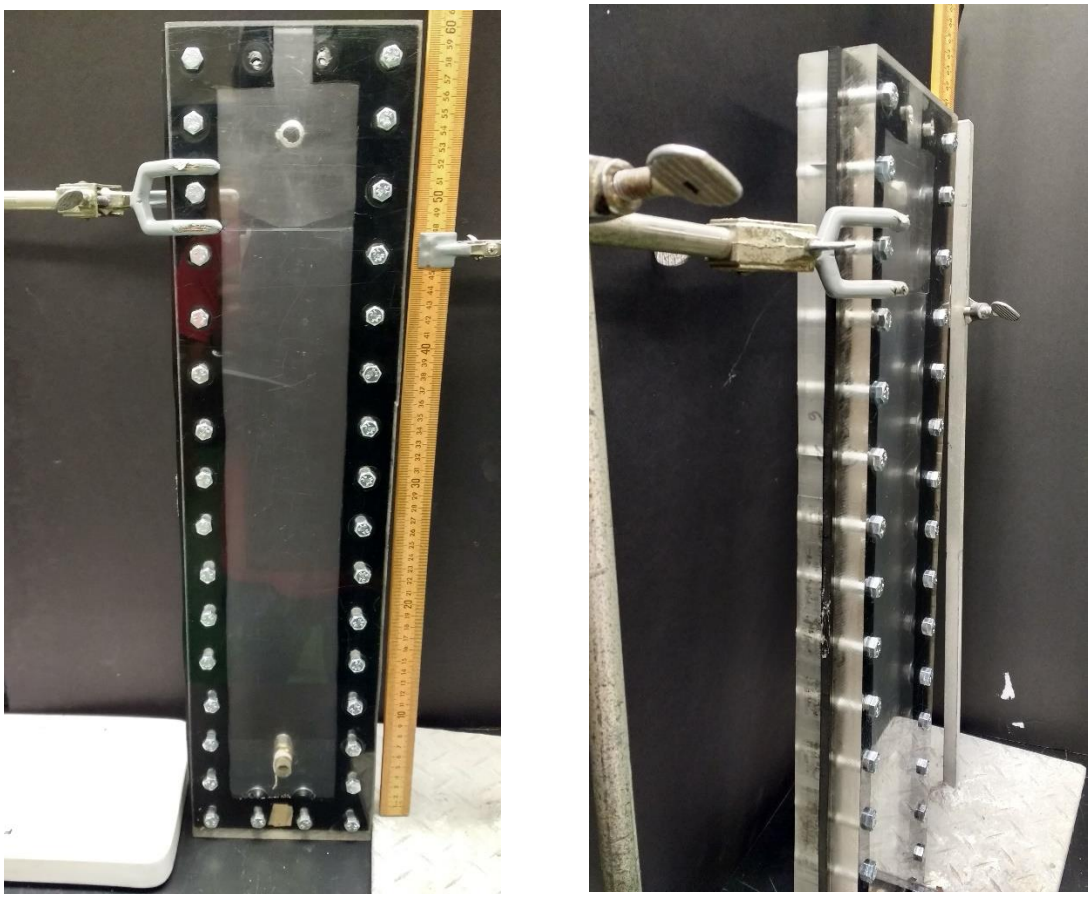

Figure 4.10. Real picture of fracture setup for confined fluids

Same number of experiments were performed with same recording technique and analysis method with this setup and terminal settling velocities were obtained using the same software mentioned in section 4.3 above.

4.5. VALIDATION OF THE PREVIOUSLY ESTABLISHED CORRELATIONS

The values of different parameters like specific gravity of the proppant and fluid, viscosity of the fluid, power law parameters used during our experiments were inserted in the previously established correlations to calculate the value of settling velocity by correlation. Then the calculated values were compared with the values obtained by our experiments. This procedure was followed for both the type of correlations that is correlations for unbounded fluids and correlations for confined

fluids. From the correlations which were compared with the experimental values, one correlation for both the types was identified as best suitable correlation based on least deviated values obtained by correlation from experimental values. The density of the linear gel used for the settling velocity experiments was almost equal to 1.00 which was measured by dividing the weight of the sample with volume of that particular sample.

5. EXPERIMENTAL RESULTS AND ANALYSIS

This section presents the results of the rheological tests performed on five different solutions of HPG linear gel and experiments performed for the settling velocity using two of the linear gel, two different specific gravity of the proppant (Sand = 2.65 and Ceramic = 3.6), four different sizes of the proppants (Sand: 16/30, 30/40, 40/50 and Ceramic: 16/30, 30/50) in unbounded static conditions. The results are also presented for the similar experiments performed with fracture wall effects with three different fracture widths which are 0.57 cm, 0.27 cm and 0.15 cm. The validation of the correlations based on the results are presented in the last subsection with details.

5.1. RHEOLOGICAL PROPERTIES OF THE LINEAR GEL

Power law model was used to characterize the viscosity of the five different linear gels prepared with HPG. Shear sweep test was performed to investigate the behaviour of shear stress vs shear rate for all the five fluids where the shear rate implied was from 0.1 to 800 sec^{-1}. This test was repeated thrice on every fluid to ensure the repeatability of the results and average values of power law parameters were used to characterize the fluid.

5.1.1. Viscosity of the Linear Gel. The power law model was fit for the shear rates between 10 sec^{-1} and 455 sec^{-1}. The average particle shear rate (according to $\gamma = 2V_s/d_p$) encountered during particle settling experiments ranged from 20 sec^{-1} to 450 sec^{-1} and hence the power law model was fit around that range of shear rate. The plot between shear stress vs shear rate and viscosity vs shear rate is shown for 10 pptg to 50 pptg fluid altogether and analysis has been performed by comparing their behaviour.

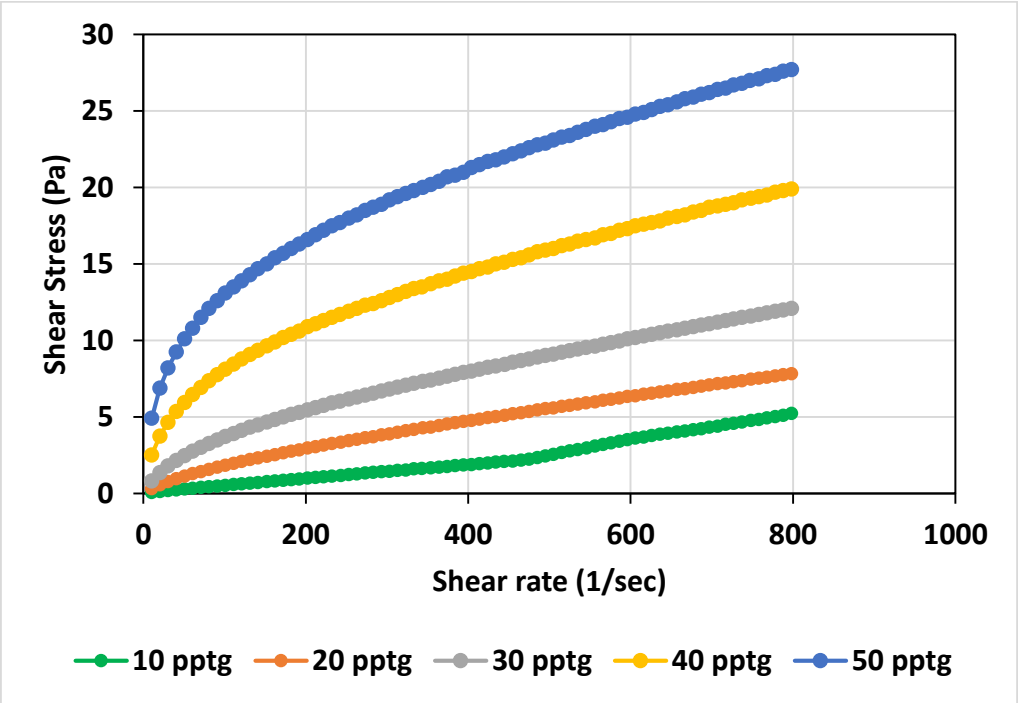

Figure 5.1. Comparison of the shear stress vs shear rate for all linear gels

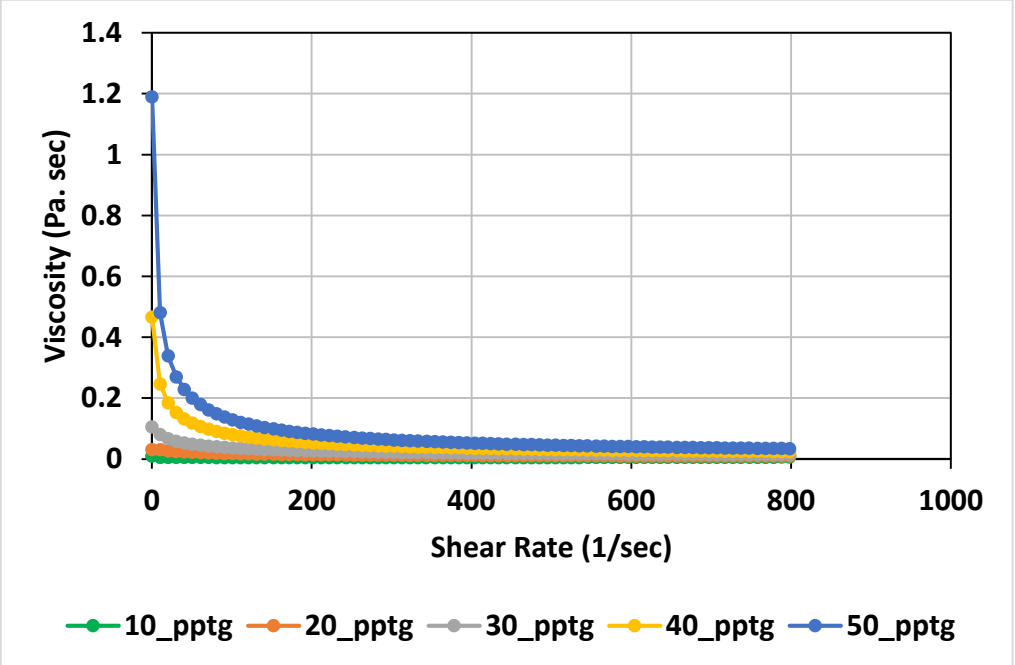

Figure 5.2. Comparison of viscosity vs shear rate plot for all HPG linear gels

From Figure 5.1 and 5.2 it can be observed that the viscosity of the polymer solution increases with the amount of the HPG added. As the concentration of HPG increased from 10 pptg to 50 pptg, the shear thinning behaviour is also increasing. From Figure 5.2 it can be observed that at low shear rates the difference in the viscosities of different solution is very high which is getting lower with the increasing shear rate. So while dealing with the low shear rate it may become important to consider the zero shear viscosity while developing the general correlation to calculate the terminal settling velocity accurately. The observations made from the above figures are quantitatively tabulated in Table 5.1 below. It can be concluded that fluid consistency index (K) increases with increasing concentration of HPG whereas it affects the flow behaviour index in the reverse way.

Table 5.1. Comparison of power law parameters of all the HPG linear gels

Sr. No	Concentration [pptg]	K [Pa.sec^n]	n	Shear Rate [sec^{-1}]
1	10	0.0076	0.9208	10-455
2	20	0.0677	0.7101	10-455
3	30	0.2384	0.5879	10-455
4	40	1.007	0.4446	10-455
5	50	2.3053	0.3701	10-455

When the viscosity vs shear rate are plotted with log-log scale as shown in the Figure 5.3 below, it can be seen that the reduction in the viscosity of the 10 pptg linear gel is very less throughout the range of the shear rate used. Its viscosity goes from 0.01 Pa or 10 cp at 0.1 sec^{-1} shear rate to 0.005 Pa or 5 cp at 500 sec^{-1} which is 50% whereas in the case of 50 pptg linear gel the reduction in the viscosity is found to be 90%

between 0.1 sec^{-1} and 150 sec^{-1} shear rate only that proves the increasing shear thinning behaviour with increasing concentration of HPG. From the same figure it can be observed that as the concentration of HPG increased, the Newtonian plateau (Shear rate up to which the viscosity almost remains constant) at low shear rates decreased. This observation matches with the observation made by (Goel et al. 2002).

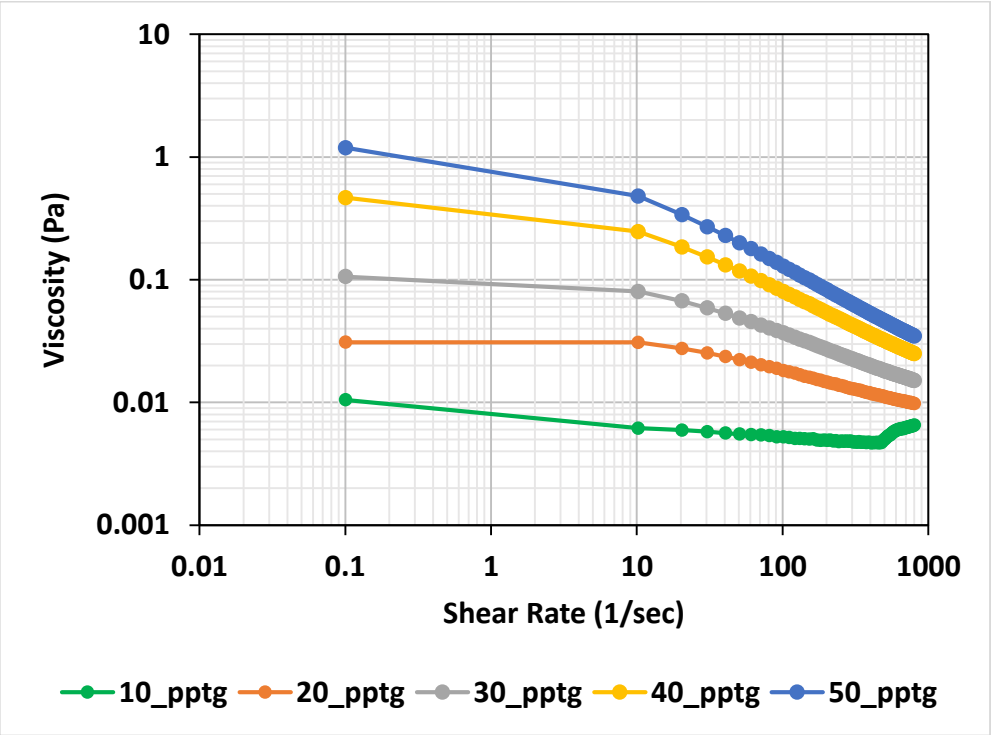

Figure 5.3. Comparison of viscosity vs shear rate log-log plot for all the HPG linear gels

5.1.2. Viscoelasticity of the Linear Gel. Dynamic oscillatory test was performed to investigate the viscoelastic properties of all the five HPG linear gels. The inverse of the frequency at crossover point of loss modulus (G") and storage modulus (G') was considered as relaxation time of the fluid. Higher the relaxation time, more the elasticity of the fluid (Malhotra and Sharma 2011, Arnipally and Kuru 2017). The region on the higher side of the frequency from the crossover point is called elastic dominated region whereas the region on the lower side of the frequency from the

crossover point is called viscosity dominated region. All the viscoelastic measurements were performed at 5% constant shear strain based on the results of (Goel at al. 2002, Gomaa et al. 2015, Hu and Chung 2015).

While carefully observing figures from 5.4 to 5.8 and the values of relaxation time summarized in Table 5.2, it can be seen that the area of elastic dominating region at higher frequencies is almost same and very less compare to the viscous regime and the relaxation time is also same for all the five linear gels. This result indicates that if the molecular weight of the polymer and molecular weight distribution inside the solution is kept constant than the viscoelastic behaviour of the fluid would remain same irrespective of the amount of polymer added (Arnipally and Kuru, 2017).

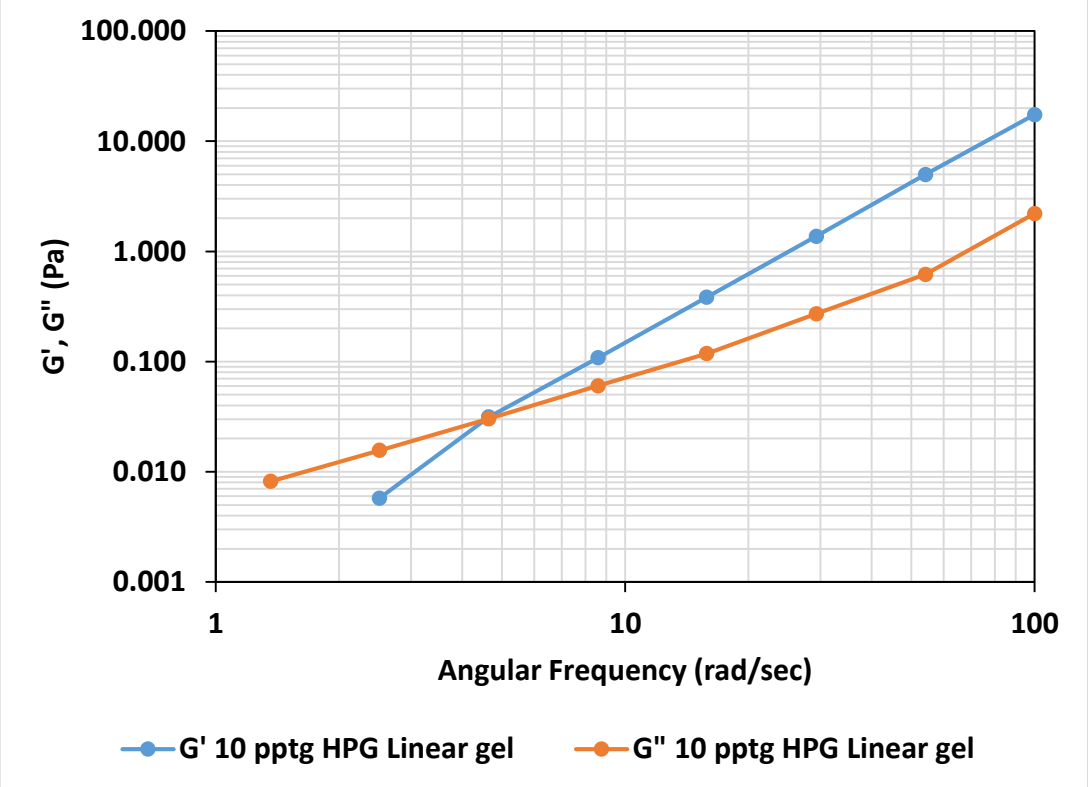

Figure 5.4. Viscoelastic behaviour of 10 pptg HPG linear gel

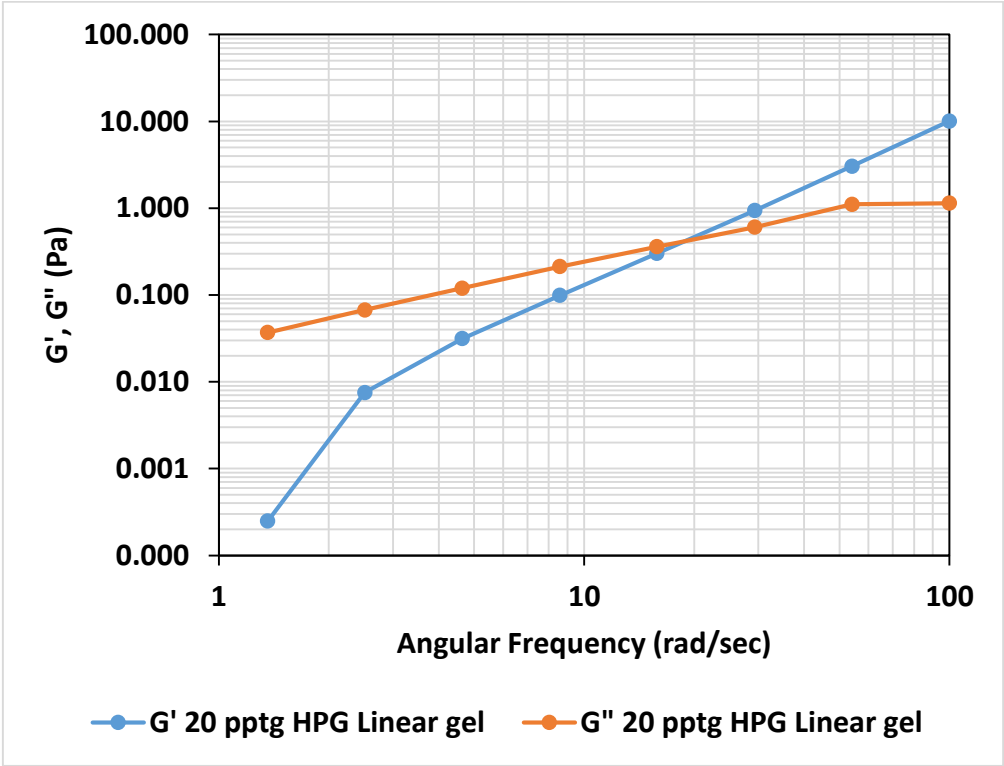

Figure 5.5. Viscoelastic behaviour of 20 pptg HPG linear gel

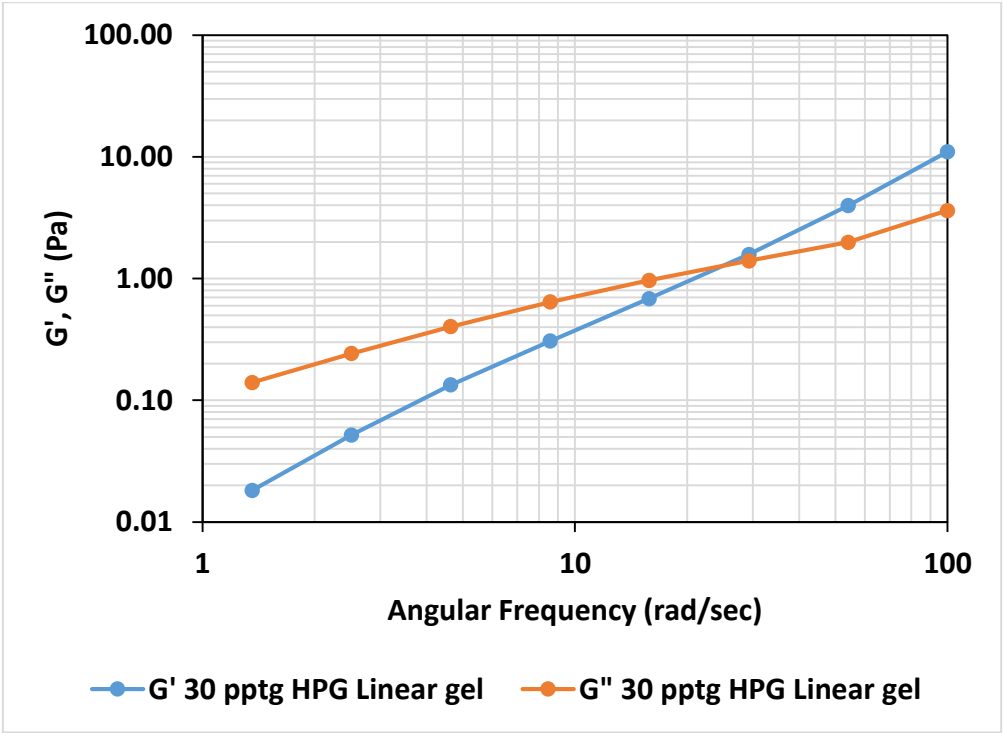

Figure 5.6. Viscoelastic behaviour of 30 pptg HPG linear gel

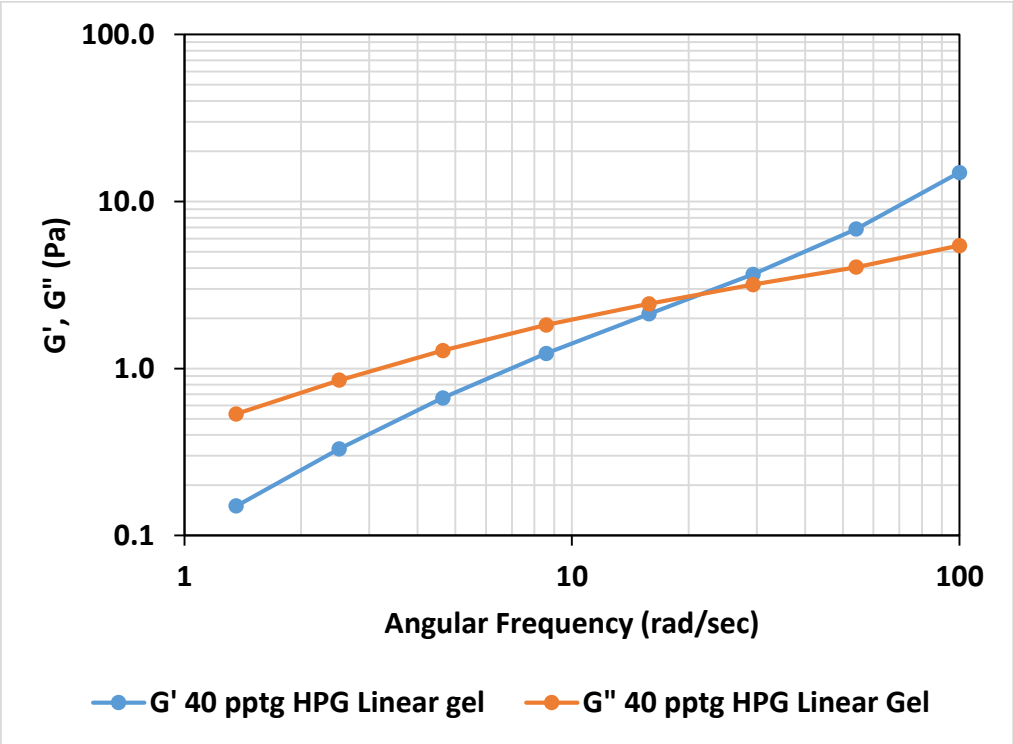

Figure 5.7. Viscoelastic behaviour of 40 pptg HPG linear gel

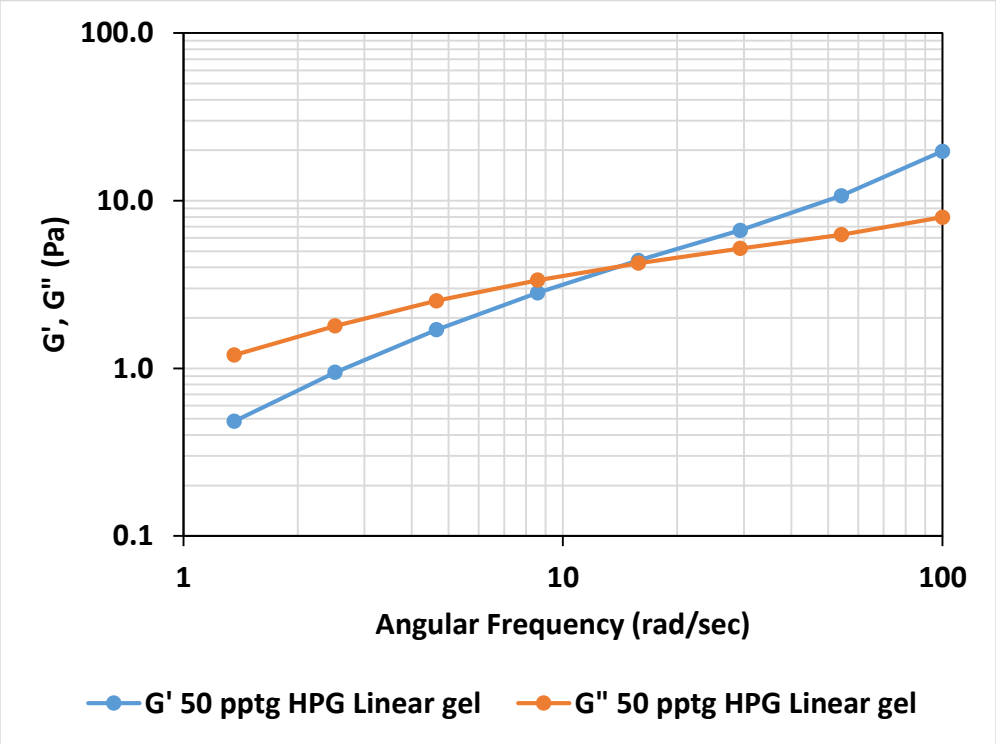

Figure 5.8. Viscoelastic behaviour of 50 pptg HPG linear gel

At low frequencies the breaking and reforming of the intermolecular hydrogen bonds (Zhu and Guo et al., 2017) keep releasing the stress and hence viscous modulus dominates the elastic modulus whereas at higher frequencies the elastic modulus dominates because the polymer bonds do not get sufficient time to relax and regain the original structure. (Moraes and Fasolin, 2011; Hu et al., 2015; Gomaa et al., 2015).

Table 5.2. Comparison of the relaxation time of all the HPG linear gels

Sr. No	Concentration [pptg]	Relaxation Time [sec]	Angular Frequency [rad/sec]
1	10	0.2	1-100
2	20	0.06	1-100
3	30	0.04	1-100
4	40	0.04	1-100
5	50	0.06	1-100

From Table 5.3 and 5.4 shown below it is clear that as the concentration of the HPG increases in the solution, G' and G" both increases at same angular frequency because of the increase in the number of bonds or polymer chains in the solution. Similar observations can be found in other researches as well (Goel et al., 2002; Hu et al., 2015; Gomaa et al., 2015; Arnipally and Kuru, 2017).

The phase angle was also determined to ensure the solutions to be having viscoelastic property. The phase angles were found to be varying from 0^{o} to 90^{o} when going from higher to lower frequencies which proved that all the fluids can be considered as viscoelastic fluids because typical Newtonian fluid has constant phase angle of 90^{o} and pure elastic material has constant phase angle of 0^{o} (Liu and Seright, 2001). The values are provided in Table 5.5.

Table 5.3. Comparison of G' for all the HPG linear gels

Angular Frequency [rad/sec]	G' (Storage Modulus/Elastic Modulus) [Pa]				
	10 [pptg]	20 [pptg]	30 [pptg]	40 [pptg]	50 [pptg]
100	17.4	10.10	11.00	14.90	19.70
54.1	4.98	3.04	3.98	6.84	10.70
29.3	1.37	0.94	1.58	3.66	6.66
15.8	0.38	0.30	0.68	2.12	4.40
8.6	0.11	0.10	0.31	1.23	2.82
4.6	0.03	0.03	0.13	0.67	1.70
2.5	0.01	0.01	0.05	0.33	0.95
1.4	0.00	0.00	0.02	0.15	0.48

Table 5.4. Comparison of G" for all the HPG linear gels

Angular Frequency [rad/sec]	G" (Loss Modulus/Viscous Modulus) [Pa]				
	10 [pptg]	20 [pptg]	30 [pptg]	40 [pptg]	50 [pptg]
100	2.20	1.14	3.62	5.45	7.97
54.1	0.62	1.11	1.99	4.04	6.27
29.3	0.27	0.60	1.40	3.18	5.19
15.8	0.12	0.36	0.97	2.44	4.24
8.6	0.06	0.21	0.64	1.82	3.36
4.6	0.03	0.12	0.40	1.28	2.53
2.5	0.02	0.07	0.24	0.85	1.79
1.4	0.01	0.04	0.14	0.53	1.20

Table 5.5. Phase angle values of all the HPG linear gels

Angular Frequency [rad/sec]	Phase Angle [degree]				
	10 [pptg]	20 [pptg]	30 [pptg]	40 [pptg]	50 [pptg]
100	7.1	8.52	18.1	20.1	22
54.1	7.5	23.1	26.6	30.6	30.5
29.3	11.8	37.4	41.7	41	37.9
15.8	18.1	54.2	54.8	49	43.9
8.6	30.6	67.6	64.4	56	50
4.6	46.0	76.1	71.6	62.6	56.1
2.5	71.2	81.5	77.9	68.8	62.2
1.4	90.0	88	82.6	74.4	68.1

For 10 pptg linear gel the results were slightly differing than the usual trend observed with the other fluids may be because the amount of HPG added was very less (0.6 gram/500 ml) and hence the solution might have got absolutely disturbed during the rheological measurements which eventually lead to erroneous result.

5.2. SETTLING VELOCITY IN UNBOUNDED FLUIDS

In this section the effect of size of the proppant, specific gravity of the proppant and viscosity of the fluid on the settling velocity of the single proppant without fracture wall effects has been analysed with static conditions. The transparent cylinder used had 5.5 cm diameter which is 61 times larger than the largest size of proppant used during this research so the wall effects are assumed not to be affecting the settling velocity of proppant and hence the fluid is considered as unconfined fluid. The average particle size for sand and ceramic proppant was the average value of lower and upper mesh

sizes. The average particle size for different types and sizes for proppant is shown in Table 5.6. Roundness and sphericity of sand proppant was assumed to be 0.7 to validate the correlation according to Cheng (1997)

Table 5.6. Physical properties of proppants used

Proppant Type	Mesh Size	Average Particle Size (cm)	Roundness	Sphericity
Sand (S.G = 2.65)	16/30	0.0893	0.7	0.7
	30/40	0.0508		
	40/50	0.0359		
Ceramic (S.G = 3.6)	16/30	0.0893	0.9	0.9
	30/50	0.0420		

The proppant particle needs to travel some distance before attaining the terminal settling velocity which happens when the drag force + buoyancy force equals the gravity force. Once these forces achieve equilibrium condition, the proppant moves with the constant velocity which is called terminal settling velocity. Figures 5.9, 5.10 and 5.11 shown below prove that all the different type and size of particles reached to their terminal settling velocity during the experiments inside the fracture model used.

It can be observed from the figures that settling velocity increases for very less time in the beginning until the forces achieve equilibrium condition. Then they follow the constant velocity until they get completely settled.

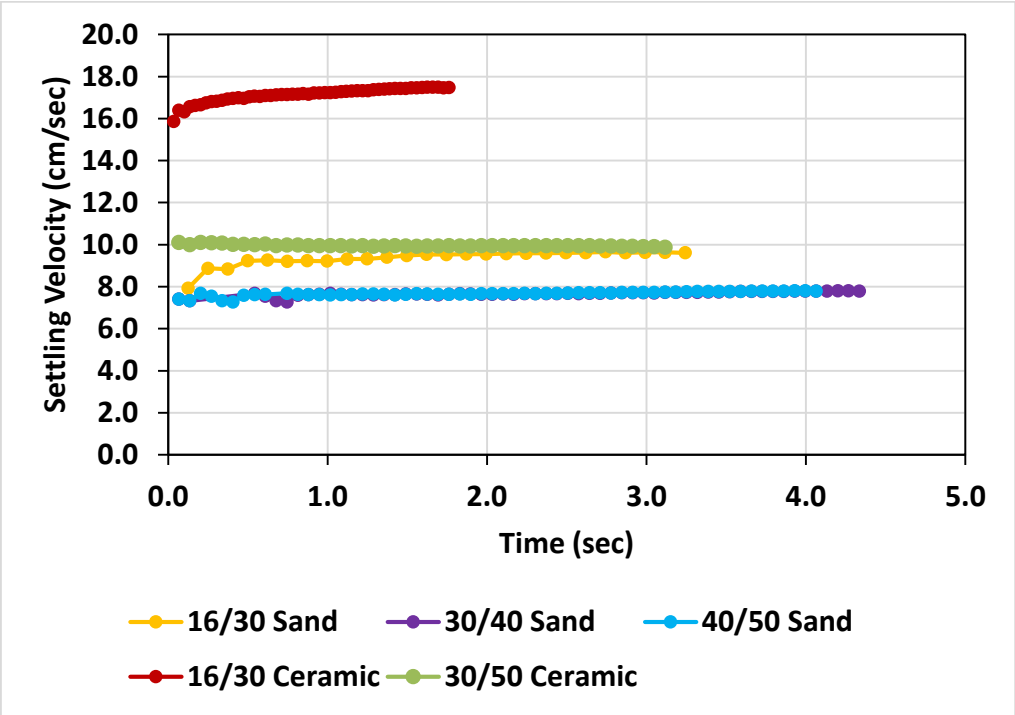

Figure 5.9. Terminal settling velocity of different proppants inside water

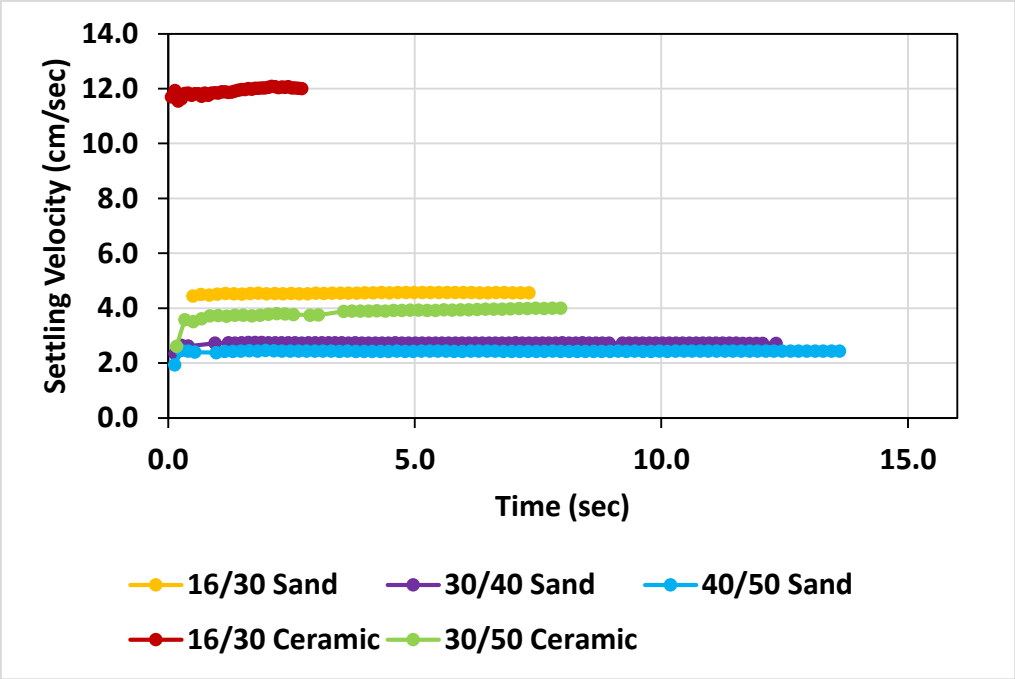

Figure 5.10. Terminal settling velocity of different proppants inside 10 pptg linear gel

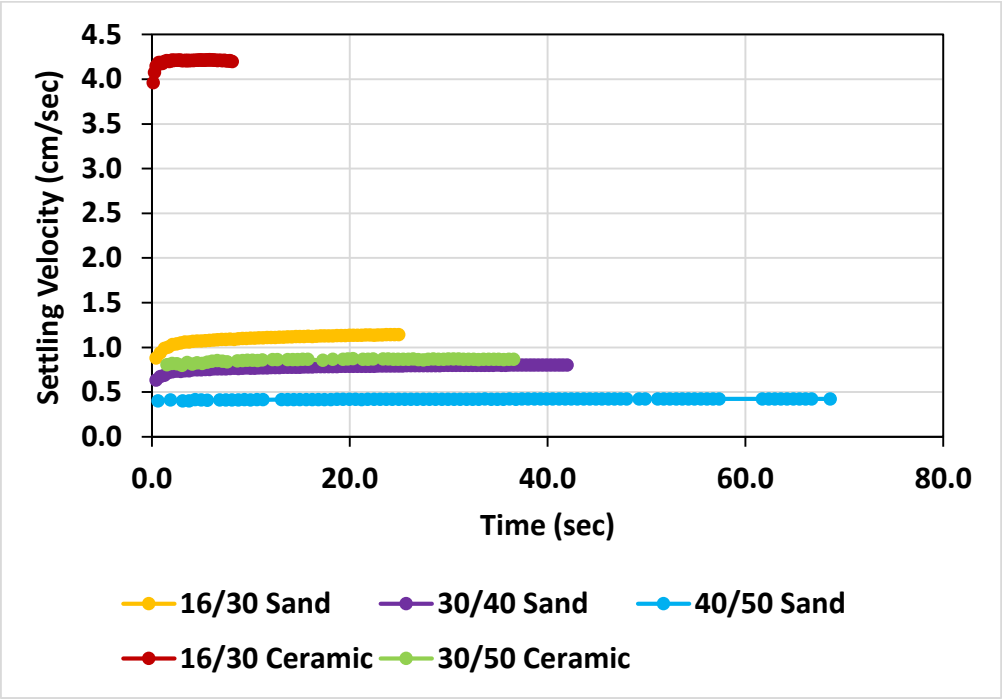

Figure 5.11. Terminal settling velocity of different proppants inside 20 pptg linear gel

5.2.1. Effect of Size of the Proppant and Viscosity of the Fluid on Settling Velocity. Figure 5.12 and 5.13 show the increment in the settling velocity for both the sand and ceramic proppant with increasing the diameter of the proppant for all the three fluids used during experiments as expected. The interesting result to be observed is the increment percentage in the settling velocity which is different for all the three fluids and both the different proppants. It can be observed that as the shear viscosity of the fluid increases or as the shear thinning behaviour of the fluid increases, the effect of increasing diameter on the settling velocity increases as well. Therefore for the field application, changing the viscosity of the fluid might not effectively solve the purpose to control the particle settling in the way it might have anticipated. The same effect was observed by (Arnipally and Kuru, 2017) using glass beads.

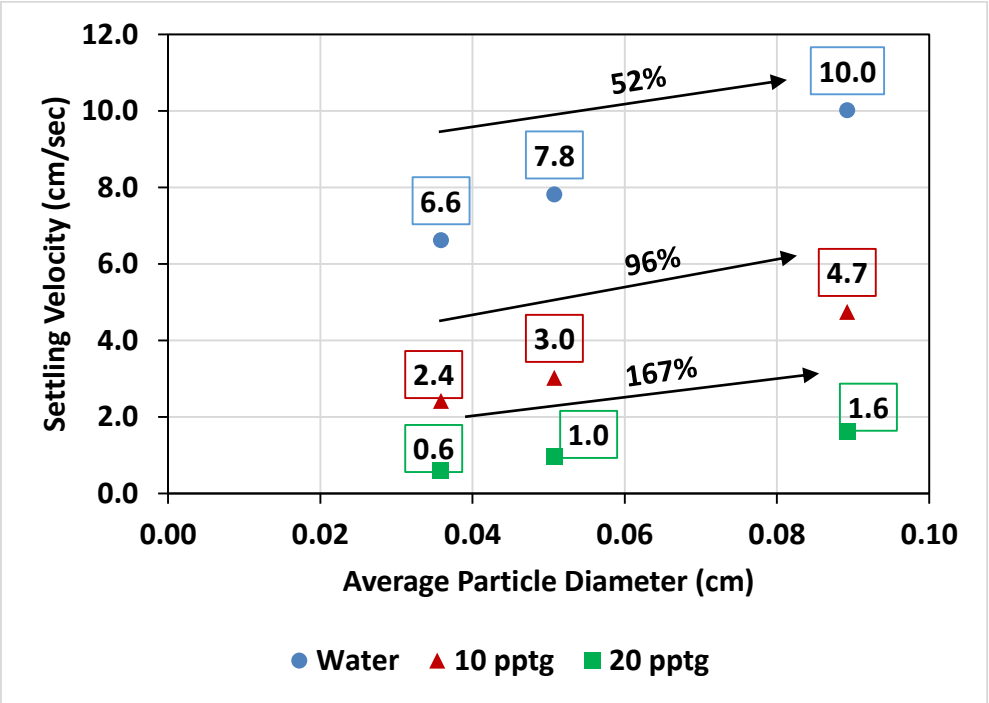

Figure 5.12. Effect of diameter of the sand proppant on the settling velocity

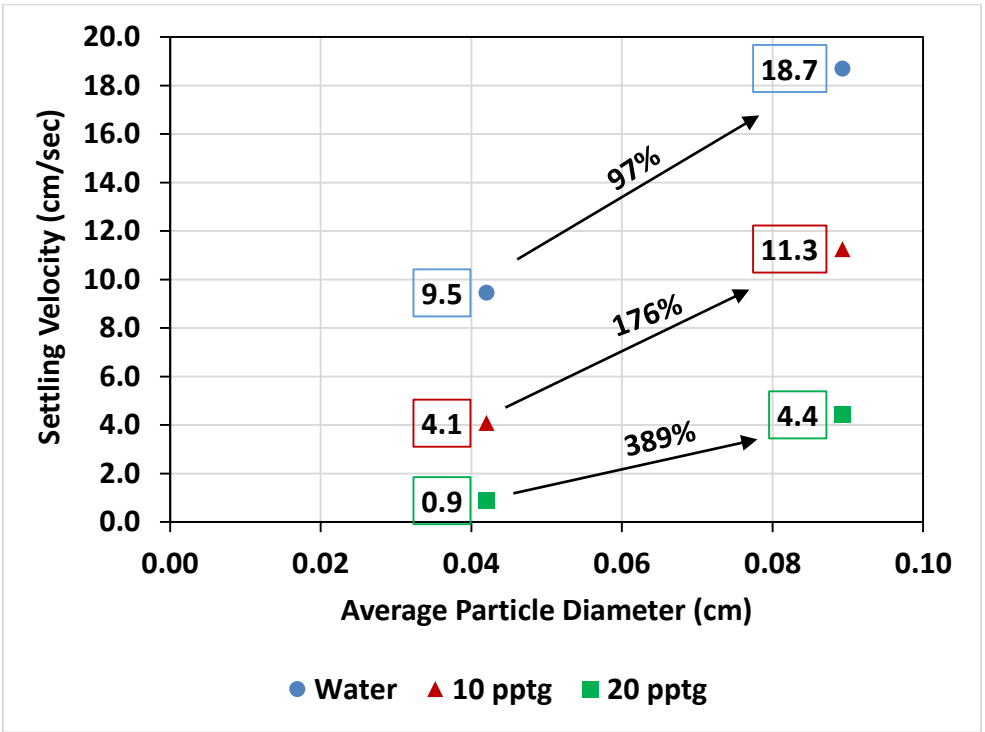

Figure 5.13. Effect of diameter on the settling velocity of ceramic proppant

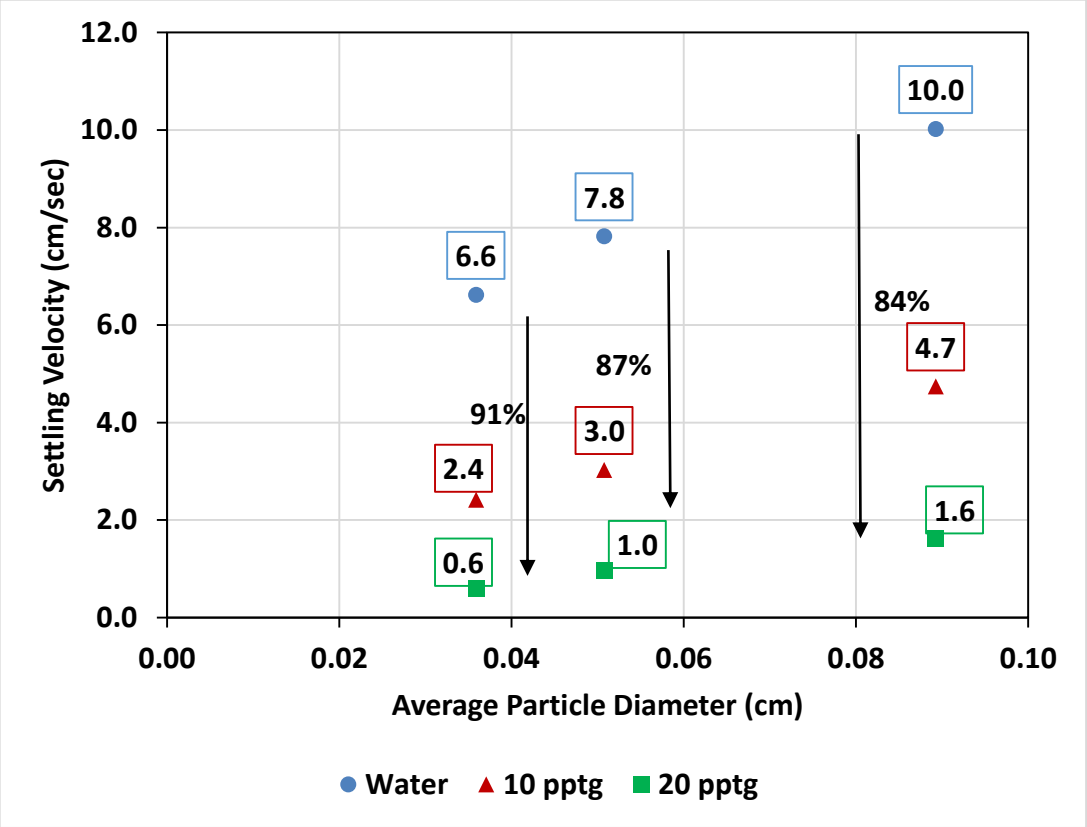

Figure 5.14. Effect of viscosity on the settling velocity of sand proppant

From Figure 5.14 and 5.15 it can be observed that for the same size of proppant particle, the settling velocity decreases with increasing viscosity from 1 cp (water @ any shear rate) to almost 30 cp (20 pptg HPG gel @ 0.1 sec^{-1}) of the linear gel. It is interesting to observe from Figure 5.14 that as the average proppant diameter increased from 0.0359 cm to 0.0893 cm, the effect of increasing viscosity on the settling velocity reduced. In simple words the settling rate of proppant became much faster with increasing diameter of the proppant. This result evidently supports the conclusion made from the Figure 5.12 and 5.13. The same results were obtained by (Arnipally and Kuru, 2017) as well but they were not highlighted in their paper.

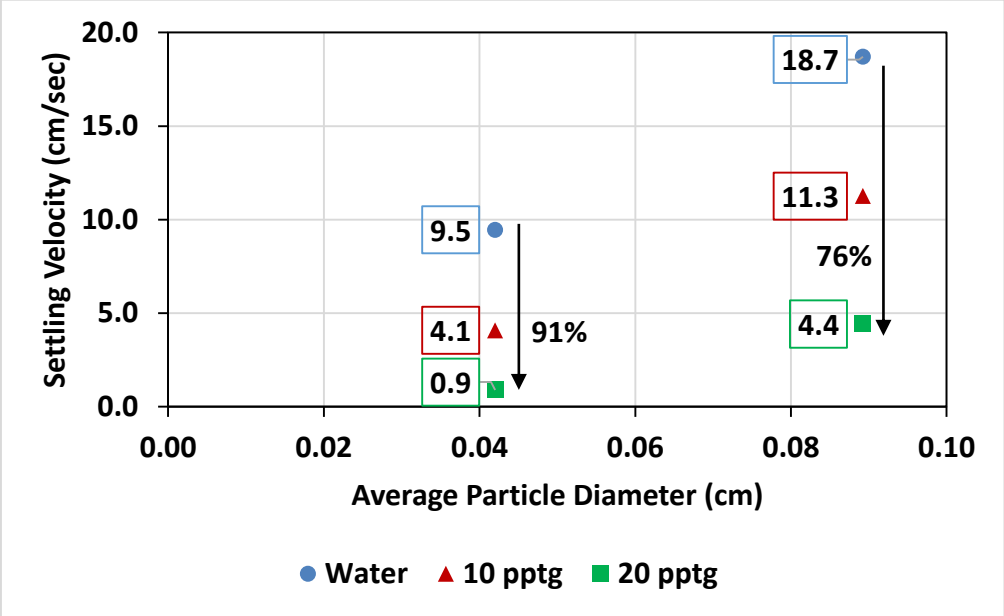

Figure 5.15. Effect of diameter of the ceramic proppant on the settling velocity

5.2.2. Effect of Specific Gravity of Proppant and Viscosity of the Fluid on Settling Velocity. From Figure 5.16 it can be observed that high specific gravity leads to faster settling of proppant particles in all the three fluids. Here the values of viscosities are used for 10 pptg and 20 pptg HPG gel at 0.1 sec^{-1} to portray the results in the effective way. It can be seen from the plot that with increasing viscosity from 1 cp to 30 cp the effect of specific gravity on proppant settling velocity gets pronounced. The reason behind observing the same phenomenon both the times, when increasing proppant diameter and specific gravity may be due to the drag force getting affected by the viscosity of the fluid. In the case of effect of specific gravity on settling velocity, the value of (gravity force – buoyancy force) is going to remain constant for any viscous fluid as these forces are independent of the viscosity. The drag force has two terms; settling velocity and drag coefficient, which are depended on the viscosity. So with different viscosity of the fluid, sand proppant and ceramic proppant will have different drag forces.

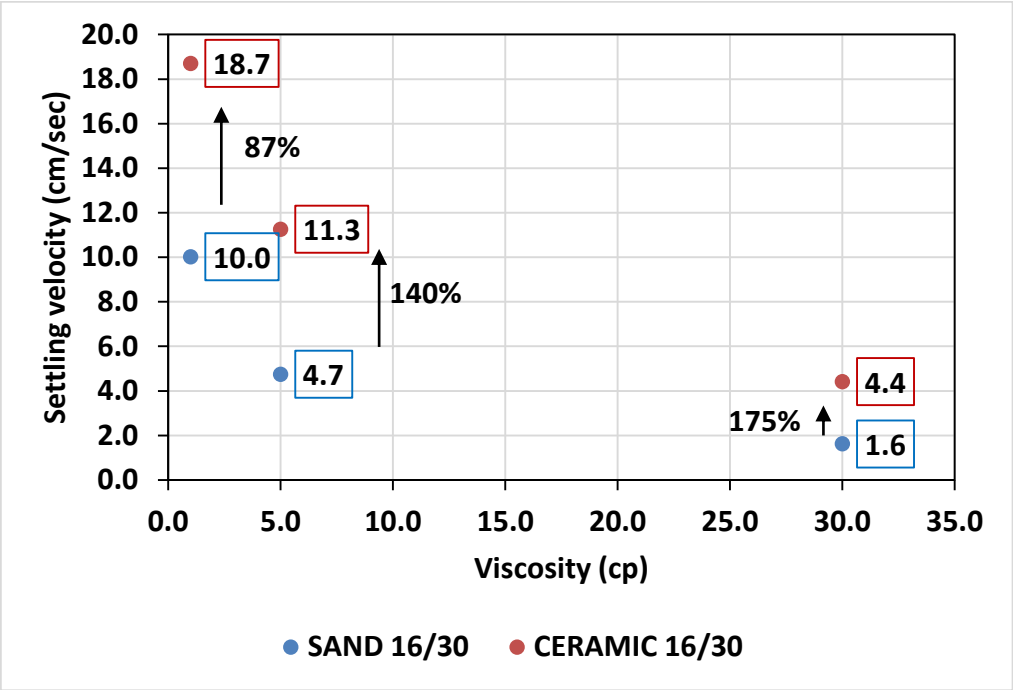

Figure 5.16. Effect of specific gravity of 16/30 proppant on the settling velocity

Adding to that, the drag coefficient also depends on the shape of the particle so the roundness and sphericity of sand might affect the drag forces more than the ceramic proppant. As the velocity decreases with increasing viscosity and drag coefficient increases with increasing viscosity, it is difficult to obtain the perfect correlation for drag force. There are several different correlations established to calculate drag coefficient with different shape factors but that is out of the scope of this research. The reason is same for the results obtained while increasing the size of the proppant. In that case the only parameter which will be varying in the equations of the forces will be diameter of the proppant.

5.3. SETTLING VELOCITY IN CONFINED FLUIDS

In this section the effect of size of the proppant and viscosity of the fluid on the settling velocity of the single proppant with confining fracture walls have been analysed

with static conditions. A fracture model made up of two parallel plexiglass plates was used with different fracture widths like 0.57 cm, 0.27 cm, and 0.15 cm.

5.3.1. Effect of Fracture Walls and Viscosity on the Settling Velocity of Ceramic Proppant. From Figure 5.17 and 5.18 it can be observed that as the fracture width gets narrower, the settling velocity of both the sizes of ceramic proppant decreases because of the particle-wall interaction. From Table 5.7 and 5.9, it can be observed that smaller the proppant, lesser the effect of fracture walls when comparing the effect of diameter of the proppant for the same fracture width. The arrows shown in Figure 5.17 and 5.18 demonstrate how the decrement percentages are calculated in Table 5.7 and 5.9.

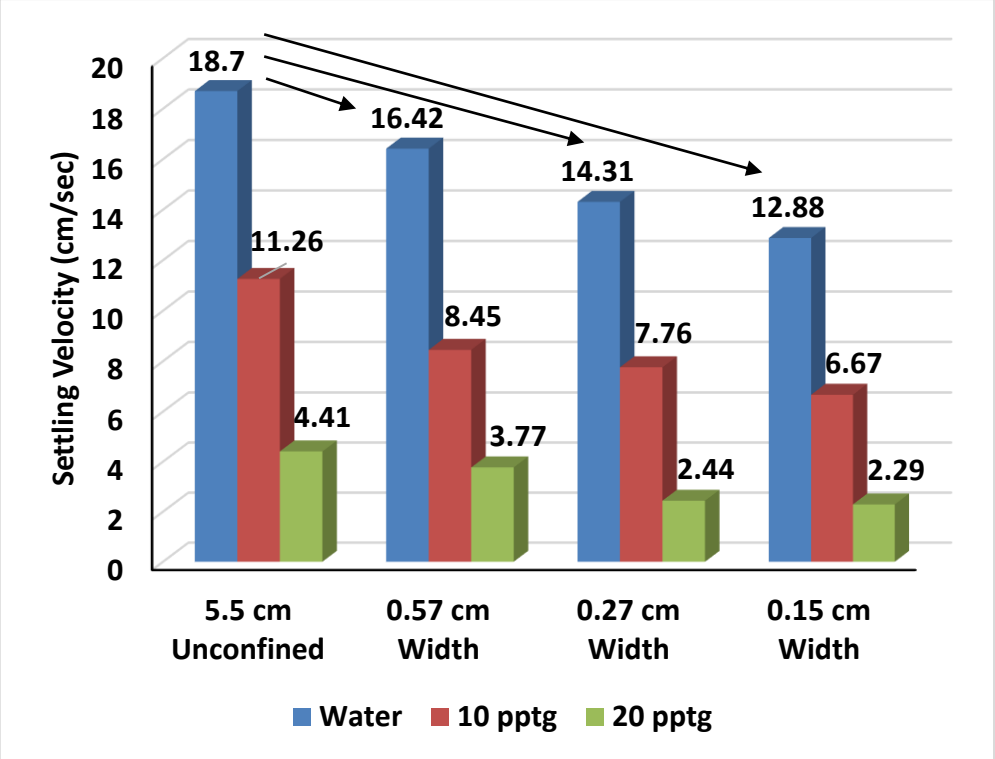

Figure 5.17. Effect of fracture walls and Viscosity on the Vs of 16/30 ceramic proppant

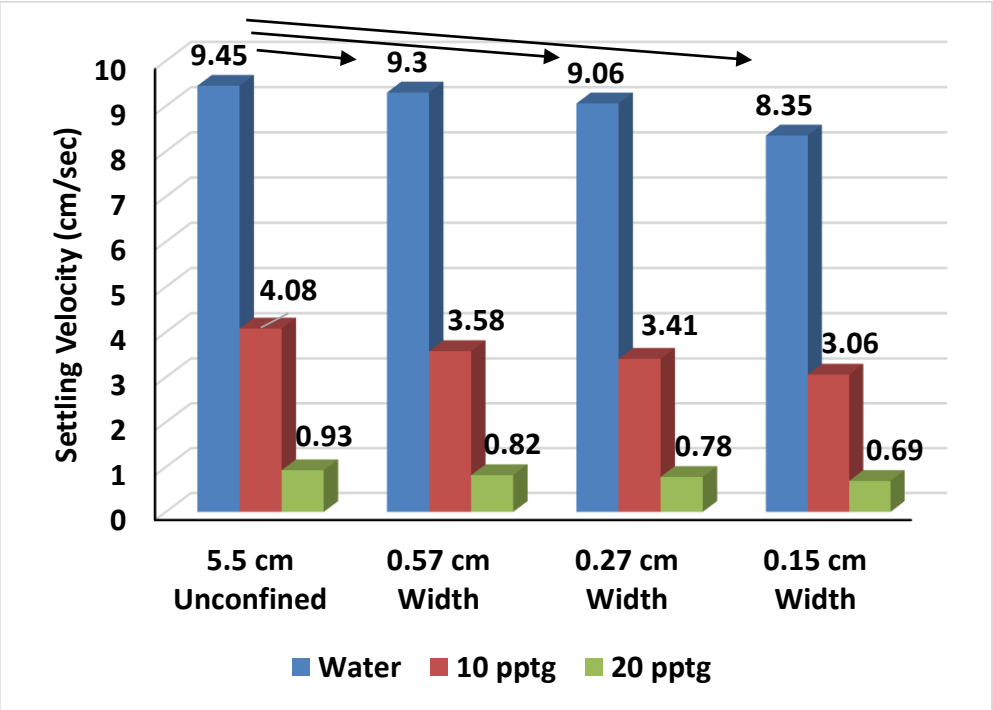

Figure 5.18. Effect of fracture walls and Viscosity on the Vs of 30/50 ceramic proppant

Another thing to be observed from Table 5.7 and 5.9 is that with increasing viscosity of the fluid, effect of fracture walls increase. For an example in Table 5.7 the decrement in the settling velocity inside water is 24% when the fracture width narrows down from 5.5 cm to 0.27 cm whereas in the case of 10 pptg gel the reduction increases to 31% and for 20 pptg the reduction increases more to 45%. Therefore, from the values of decrement percentage in Table 5.7 and Table 5.9 it can be concluded that increasing viscosity of the fluid increases the hydrodynamic interaction between proppant and fracture walls due to which the reduction in the settling velocity increases. The same results were obtained by (Liu and Sharma, 2005) as well using ceramic proppants. This phenomenon was not observed in all the cases may be due to usage of actual proppants in which the size and the specific gravity of the proppant can never be exactly same for every single particle used during experiments.

Table 5.7. Effect of fracture walls on the Vs of 16/30 ceramic proppant

Fracture Width	Percentage Decrement		
	Water	10 pptg	20 pptg
5.5 cm vs. 0.57 cm	12	25	15
5.5 cm vs. 0.27 cm	24	31	45
5.5 cm vs. 0.15 cm	31	41	48

Table 5.8. Effect of viscosity on Vs of 16/30 ceramic proppant

Fracture Width (cm)	Percentage Decrement Water – 10 pptg	Percentage Decrement 10 pptg – 20 pptg
Unconfined	40	61
0.57	49	55
0.27	46	69
0.15	48	66

The values shown in Table 5.8 and 5.10 are used to compare the effect of viscosity on the settling velocity for the fracture widths used and to observe the effect of viscosity separately for any single fracture width as well. The values of Table 5.8 and 5.10 show that when increasing viscosity from 1 cp to 5 cp @ 0.1 sec^{-1} (Water to 10 pptg), the settling velocity decreases for any fracture width. However, the reduction in the settling velocity is more when calculating percentage decrement between 10 pptg and 20 pptg gel because of the higher viscosity difference (5 cp – 30 cp @ 0.1 sec^{-1}).

While comparing percentage decrement of any fracture width (0.57 or 0.27 or 0.15 cm fracture width) with the percentage decrement of unconfined fracture (5.5 cm diameter), it can be observed that the reduction is higher when fracture walls are present. The obvious reason is the fracture walls retard the movement of the proppant

more. However, comparing the percentage reduction only when the fracture walls are present (0.57, 0.27, 0.15 cm fracture width), it can be observed from Table 5.8 that the percentage decrement (49%, 46%, 48%) is almost remaining constant for any fracture width. This observation proves that for the fracture widths and conditions used during this study, the effect of viscosity on the settling velocity remains constant for any fracture widths used.

Table 5.9. Effect of fracture walls on the Vs of 30/50 ceramic proppant

Fracture Width	**Percentage Decrement**		
	Water	**10 pptg**	**20 pptg**
5.5 cm vs. 0.57 cm	2	12	12
5.5 cm vs. 0.27 cm	4	16	16
5.5 cm vs. 0.15 cm	12	25	26

Table 5.10. Effect of viscosity on Vs of 30/50 ceramic proppant

Fracture Width (cm)	**Percentage Decrement Water – 10 pptg**	**Percentage Decrement 10 pptg – 20 pptg**
Unconfined	57	77
0.57	62	77
0.27	62	77
0.15	63	77

5.3.2. Effect of Fracture Walls and Viscosity on the Settling Velocity of Sand Proppant. From Figure 5.19, 5.20, and 5.21 it can be seen that the reduction in the settling velocity is following the same trend as shown previously for ceramic proppant. The reduction in the settling velocity is increasing as the viscosity of the fluid

inside the fracture model increases. Hence it can be concluded that the sand proppant interacts in the same way hydrodynamically with the fracture walls as the ceramic proppant does.

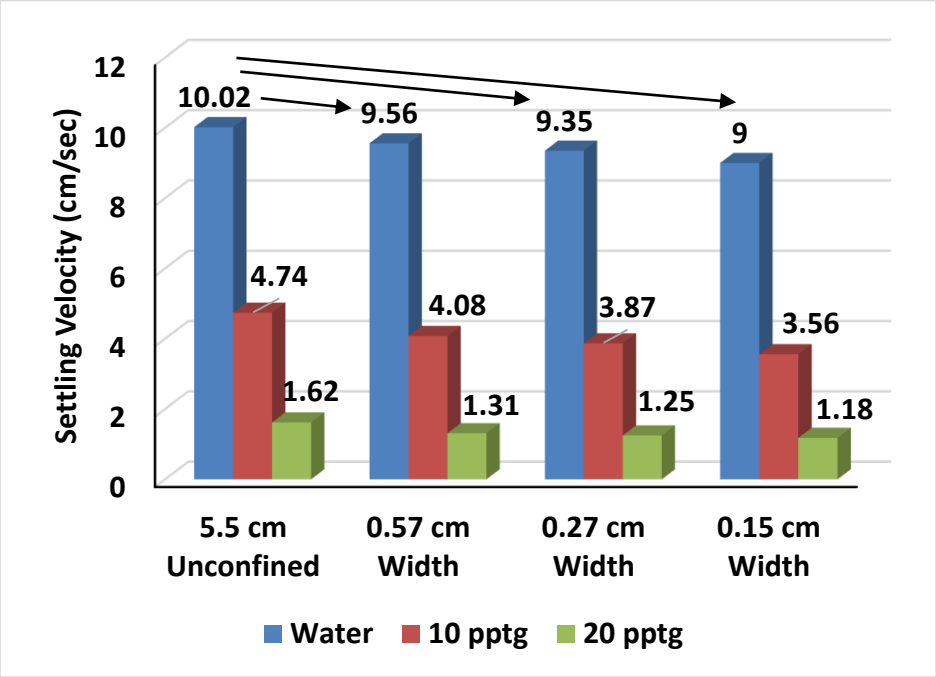

Figure 5.19. Effect of fracture walls and viscosity on Vs of 16/30 sand proppant

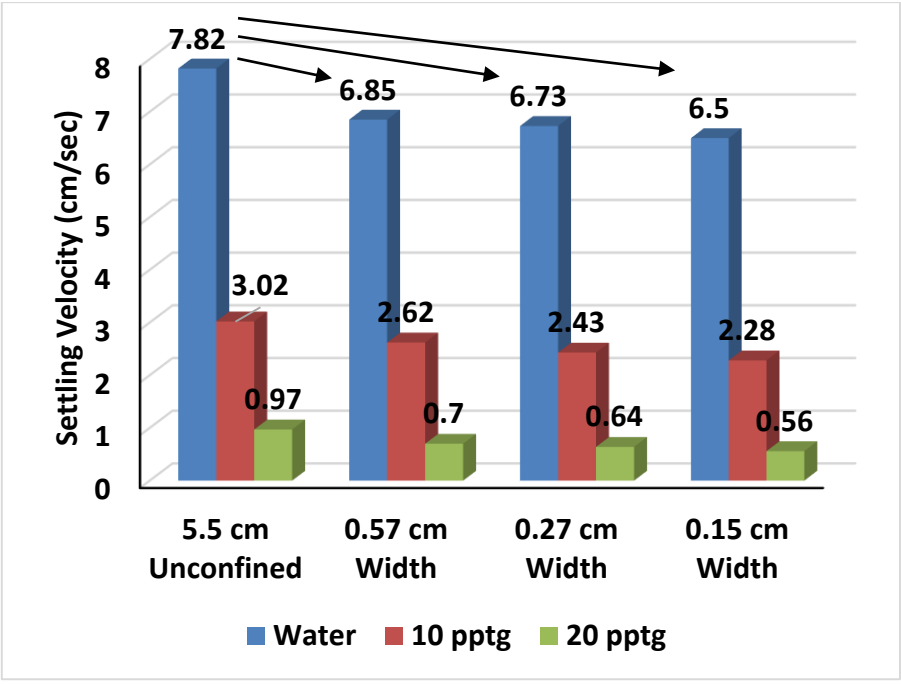

Figure 5.20. Effect of fracture walls and viscosity on Vs of 30/40 sand proppant

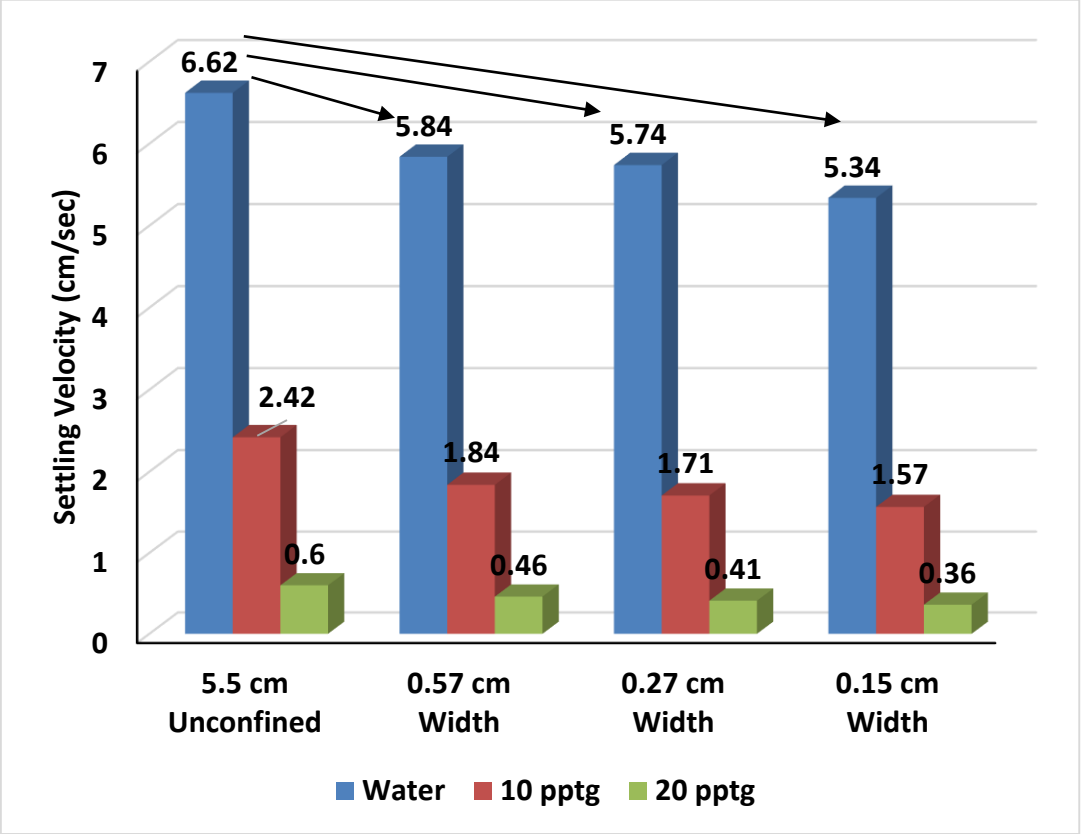

Figure 5.21. Effect of fracture walls and viscosity on Vs of 40/50 sand proppant

Table 5.11, 5.13 and 5.15 show the effect of fracture walls and it was found to be similar as of the case of ceramic proppant. As the viscosity of the fluid increases, the hydrodynamic interaction between fracture walls and proppant increases and hence the settling velocity decreases more.

The values shown in Table 5.12, 5.14, 5.16 are used to compare the effect of viscosity on the settling velocity for the fracture widths used and to observe the effect of viscosity separately for any single fracture width as well. From all the three tables it can be observed that the decrement percentages are remaining almost constant when the fluid is changed inside the fracture model with walls from water (1 cp) to 10 pptg HPG gel (5 cp @ 0.1 sec^{-1}) same as of the case of ceramic proppant. The same results can be observed when the fluid is changed from 10 pptg HPG gel (5 cp @ 0.1 sec^{-1}) to

20 pptg HPG gel (30 cp @ 0.1 sec^{-1}) with increased value of decrement percentage because of the increment in the viscosity. Another result which can be observed is as the average particle diameter decreases, the percentage decrement increases that means the smaller size particles will take more time to settle than the larger particles.

Table 5.11. Effect of fracture walls on the Vs of 16/30 sand proppant

Fracture Width	**Percentage Decrement**		
	Water	**10 pptg**	**20 pptg**
5.5 cm vs. 0.57 cm	5	14	19
5.5 cm vs. 0.27 cm	7	18	23
5.5 cm vs. 0.15 cm	10	25	27

Table 5.12. Effect of viscosity on Vs of 16/30 sand proppant

Fracture Width (cm)	**Percentage Decrement Water – 10 pptg**	**Percentage Decrement 10 pptg – 20 pptg**
Unconfined	53	66
0.57	57	68
0.27	59	68
0.15	60	67

Table 5.13. Effect of fracture walls on the Vs of 30/40 sand proppant

Fracture Width	**Percentage Decrement**		
	Water	**10 pptg**	**20 pptg**
5.5 cm vs. 0.57 cm	12	13	28
5.5 cm vs. 0.27 cm	14	20	34
5.5 cm vs. 0.15 cm	17	25	42

Table 5.14. Effect of viscosity on Vs of 30/40 sand proppant

Fracture Width (cm)	Percentage Decrement Water – 10 pptg	Percentage Decrement 10 pptg – 20 pptg
Unconfined	61	68
0.57	62	73
0.27	64	74
0.15	65	75

Table 5.15. Effect of fracture walls on the Vs of 40/50 sand proppant

Fracture Width	Percentage Decrement		
	Water	10 pptg	20 pptg
5.5 cm vs. 0.57 cm	12	24	23
5.5 cm vs. 0.27 cm	13	29	32
5.5 cm vs. 0.15 cm	19	35	40

Table 5.16. Effect of viscosity on Vs of 40/50 sand proppant

Fracture Width (cm)	Percentage Decrement Water – 10 pptg	Percentage Decrement 10 pptg – 20 pptg
Unconfined	63	75
0.57	68	75
0.27	70	76
0.15	71	77

5.4. VALIDATING THE CORRELATIONS BASED ON EXPERIMENTAL FINDINGS

The correlations to calculate the settling velocity of the proppant particle in the static conditions are related to drag coefficient (C_D) and particle Reynolds number (N_{re}). The correlations developed by different authors using different proppant particles and fracturing fluids are provided in the previous section 3.4 in Table 3.2, 3.3 and 3.4. The correlations are basically divided in three flow regimes based on their particle Reynolds number. If the N_{re} is very low around 2 or lesser than the flow regime is called creepy flow regime or Stokes law region. If N_{re} is between 2 and 500 than the flow regime is called intermediate flow regime and the values more than 500 fall under Newton's law region. In the real field conditions the particle Reynolds number is usually less than 500 and therefore efforts are never made in most of the previous researches to develop accurate correlations to calculate settling velocity in Newton's law region. In this section the experimental settling velocities are compared with the calculated settling velocity from the correlations to validate them. The section is divided in two parts based on particle Reynolds number.

5.4.1. Validating the Correlations for Unconfined Fluid for $N_{re} < 2$. The correlations which are validated with the experimental findings shown in Figure 5.23 and 5.24 are taken from (Swanson, 1967; Novotny, 1977; Daneshy, 1978; Shah, 1986; Acharya, 1988; Kelessidis and Mpandelis, 2004; Shah et al., 2007; and Shahi and Kuru, 2016).

Primarily the experimental values of drag coefficient and particle Reynolds number were plotted with the correlation established by Acharya et al. (1976 (a)) to investigate the effect of elasticity of the fluid on the settling velocity in the creepy flow

regime which is shown in Figure 5.22. Acharya et al. (1976(a)) designed the correlation considering the creepy flow regime at Nre<1.

The blue line shown in Figure 5.22 was established by Acharya et al. 1976(a) using experimental results obtained with different sizes and types of spherical particles with purely viscous fluid. Acharya et al. 1976(a) used Vs/d_p as particle shear rate to obtain particle Reynolds number. The average deviation calculated mathematically using Vs/dp is found to be 63.3% with the highest deviation of 147% for the smallest sand proppant. The least deviation is found to be 1.29% for the large size of the proppant. So it can be concluded that the deviation may be due to the shape factor and elasticity might affect it little bit but can be neglected.

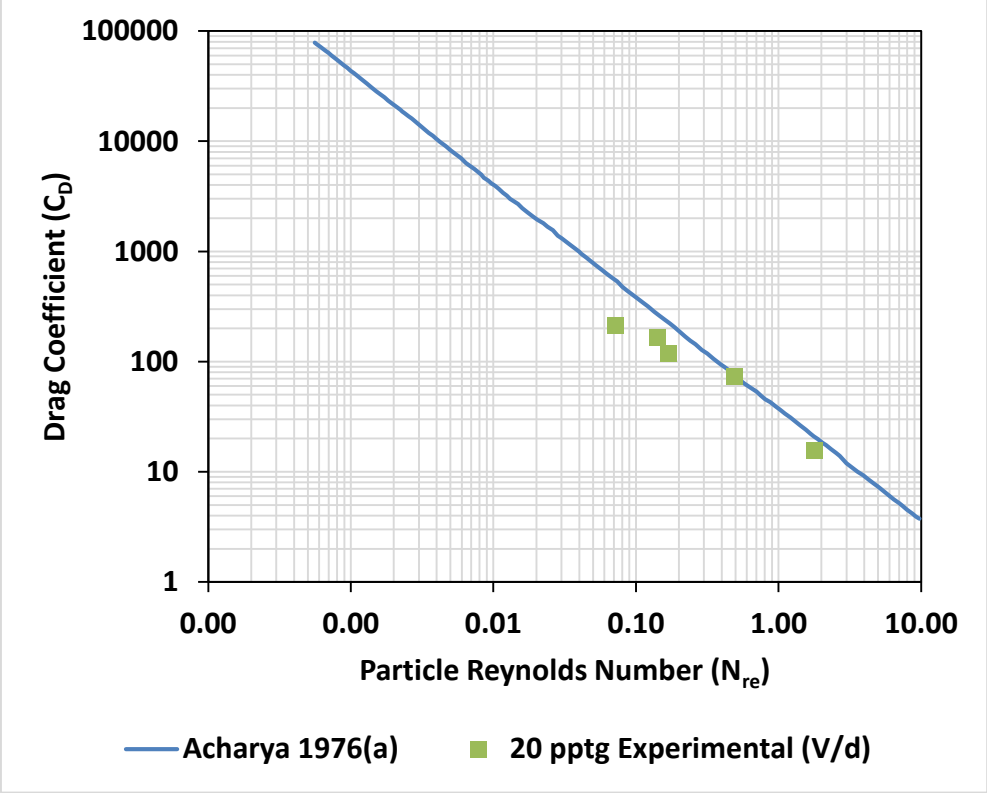

Figure 5.22. Investigation of the effect of elasticity of the 20 pptg linear gel on the settling velocity

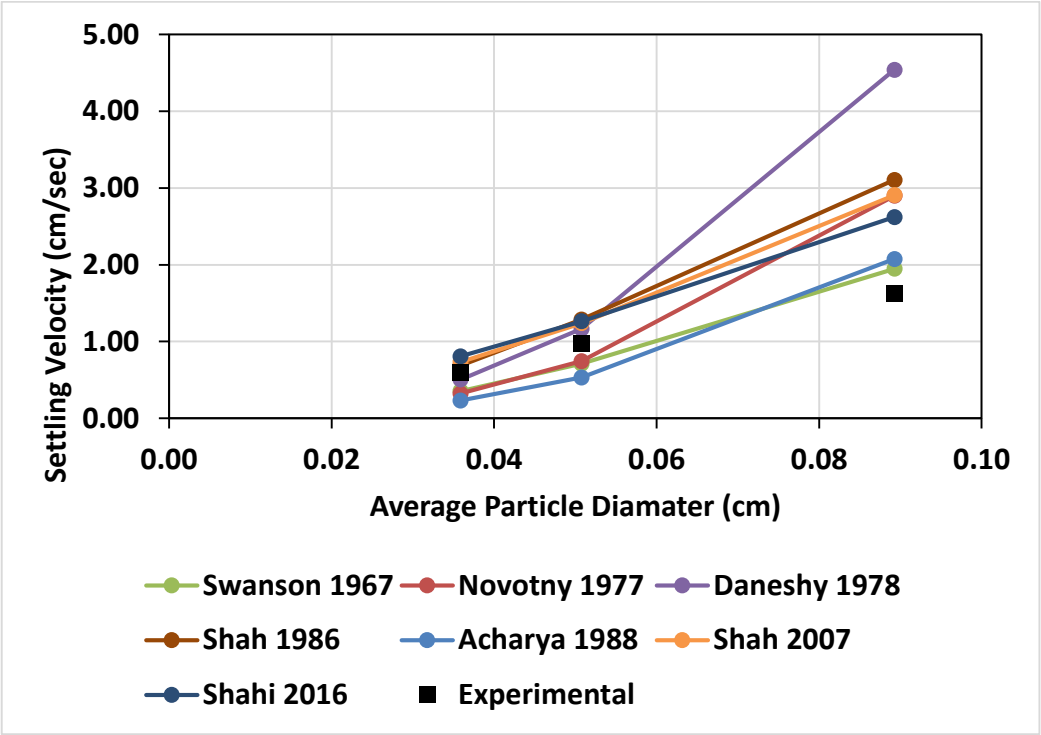

Figure 5.23. Validating different correlations using sand proppant with 20 pptg linear gel

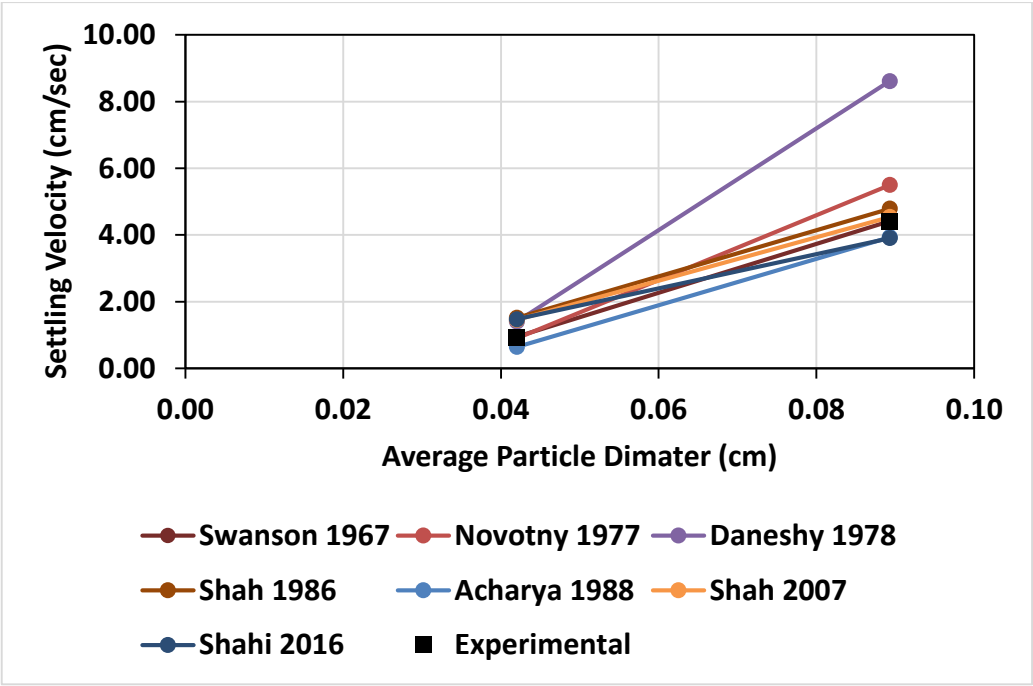

Figure 5.24. Validating different correlations using ceramic proppant with 20 pptg linear gel

From Figure 5.23 it can be observed that as the average diameter of the particle is increasing, the deviation of the experimental values is increasing from the values obtained from the correlations. For the highest particle diameter (0.0893 cm) all the correlations estimate higher values than what is obtained during the experiment may be because of the less sphericity and roundness of the sand proppant used during our experiments. The more the irregularity of the shape of the proppant, higher the drag force during settling and hence lesser settling velocity than the velocity of the equivalent diameter sphere particle.

In the case of ceramic proppant, the values of settling velocities are falling within the range of the values estimated by different correlations. The reason behind underestimation or overestimation of the values by correlation could be due to the usage of flow behaviour index (n) and flow consistency index (K) for different ranges of shear rate and or average particle shear rate (Novotny, 1977; Daneshy, 1978; Shah, 1982; Shah, 1986; Acharya, 1988) and usage of artificial spherical particles which have smoother surfaces which helps to reduce the drag force than the actual proppant particle encounters (Novotny, 1977; Shah, 1982; Shah, 1986; Acharya, 1988; Shahi and Kuru, 2016). Elasticity would not be playing an important role in the creepy flow regime as indicated by the results of this study and previous studies as well by (Acharya et al., 1976(a); Acharya, 1986; Acharya, 1988; and Hu et al., 2015)

Table 5.17 below shows the average deviation for settling velocities of sand and ceramic proppant from the calculated values by the correlation. The positive deviations (overestimation) and negative deviations (underestimation) both were taken as positive values to calculate total average deviation to understand the actual difference between the calculated values and experimental values by percentage. Almost in all the cases it can be seen that the deviation is lesser for ceramic proppant than sand proppant.

Different sphericity and roundness cause the deviation to be higher in case of sand proppant. For the calculation of the particle Reynolds number different authors have used different particle shear rate such as Vs/dp (Novotny, 1977; Acharya, 1988), 2Vs/dp (Shah et al., 2007; Shahi and Kuru, 2016) and 3Vs/dp (Daneshy, 1978; Shah, 1986) to determine the effective viscosity.

Table 5.17. Total average deviation of correlations for unbounded 20 pptg linear gel

Author	Average Deviation (%) For 20 pptg	
	Sand	Ceramic
Swanson 1967	29.21	0.7
Novotny 1977	49.4	15.17
Daneshy 1978	72.22	73
Shah 1986	46.42	35.83
Acharya 1988	44.85	21
Shah 2007	43.29	29.68
Shahi 2016	42.24	35.02

5.4.2. Validating the Correlations for Unconfined Fluid for $500 < N_{re} < 2$.

The correlations validated with the experimental findings which are shown from Figure 5.26 to 5.29 are taken from (Swanson, 1967; Novotny, 1977; Shah, 1986; Acharya, 1988; Kelessidis and Mpandelis, 2004; Shah et al., 2007; and Shahi and Kuru, 2016).

Primarily the experimental values of drag coefficient and particle Reynolds number were plotted with the correlation established by Acharya et al. 1976 (a) to investigate the effect of elasticity of the fluid on the settling velocity in the intermediate flow regime which can be seen in Figure 5.25. The applicability of this correlation is 1000<Nre<0.001.

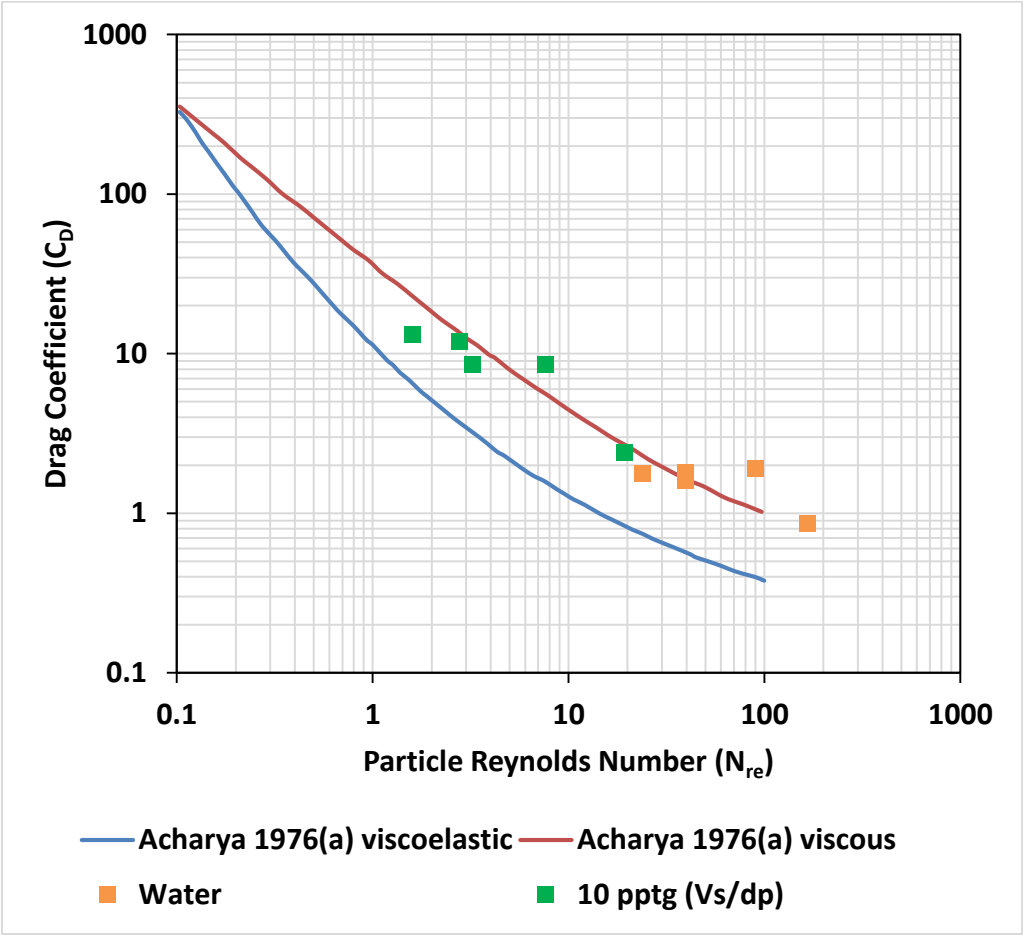

Figure 5.25. Investigation of the effect of elasticity of the 10 pptg linear gel on the settling velocity of proppant using correlation

The red curve shown above in Figure 5.25 was established by Acharya et al. 1976(a) using different sizes and types of spherical particles with purely viscous fluid. The blue curve shows their experimental results using one of the viscoelastic fluids which values lie way below than the curve of viscous inelastic fluid. From Figure 5.25 it is clear that the values are very far from the curve of viscoelastic region and hence the elasticity of the fluid is not impacting the settling velocity in this regime as well. Acharya et al. 1976(a) used Vs/dp as particle shear rate to obtain particle Reynolds number. The average deviation was calculated mathematically using Vs/dp for 10 pptg

linear gel which is around 34.1%. For water only 4 data points were used to match the results and the total average deviation is found to be 20.9%.

From the analysis of Figures 5.22 and 5.25 it can be concluded that with decreasing viscosity, the total average deviation from the correlation decreased. Elasticity is not found to be playing any role in both the flow regime for this study because of its low values so it can be neglected for all the other analysis.

The same phenomenon can be observed in Figure. 5.26 and 5.27 which was explained in the previous section that increasing the diameter of the proppant increases the deviation of the calculated values of settling velocities than the values obtained by experiments because of additional drag caused by the irregular shape of the sand proppant as well as the effective viscosity during particle's settling.

As shown by the previous researches elasticity might be playing some role in the intermediate flow regime, but as the values of relaxation time are very low and as there is no other pure viscous or elastic fluid to compare the results with, the elasticity factor was neglected during this study based on comparison with the correlations and results of previous studies. Table 5.18 below shows the deviation of the calculated values by different correlations from the values obtained by the experiments.

Table 5.18. Total average deviation of correlations for unbounded 10 pptg linear gel

Author	**Average Deviation (%) For 10 pptg**	
	Sand	**Ceramic**
Swanson 1967	22.4	7.32
Novotny 1977	18.13	13.05
Shah 1986	21.13	15.74
Acharya 1988	31.85	20.48
Shah 2007	21.63	13.27
Shahi 2014	20.61	8.95

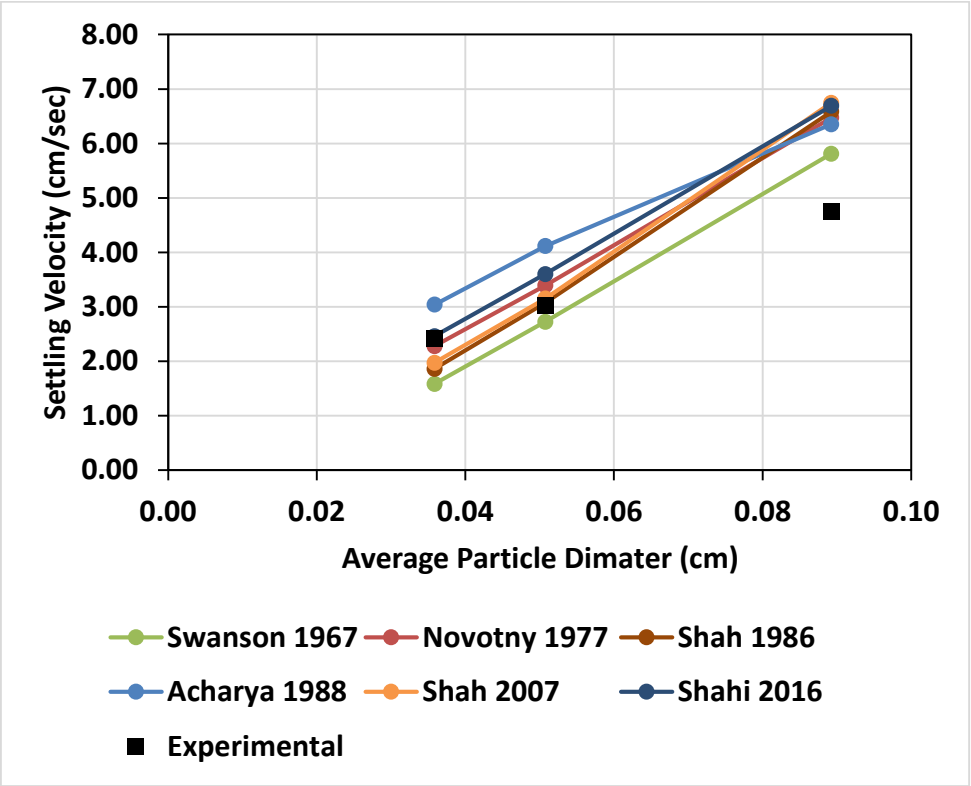

Figure 5.26. Validating different correlations using sand proppant with 10 pptg linear gel

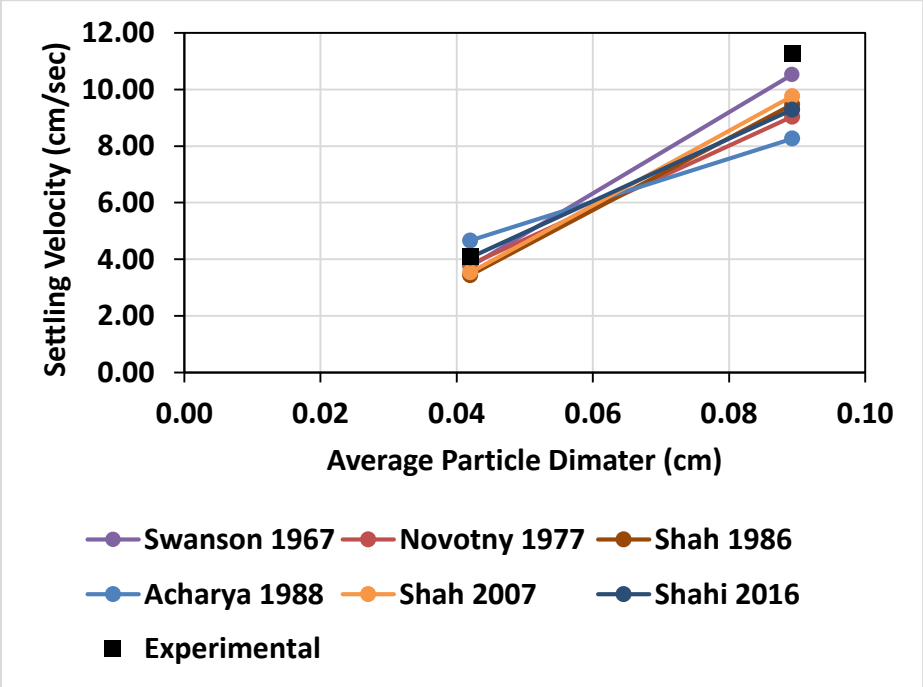

Figure 5.27. Validating different correlations using ceramic proppant with 10 pptg linear gel

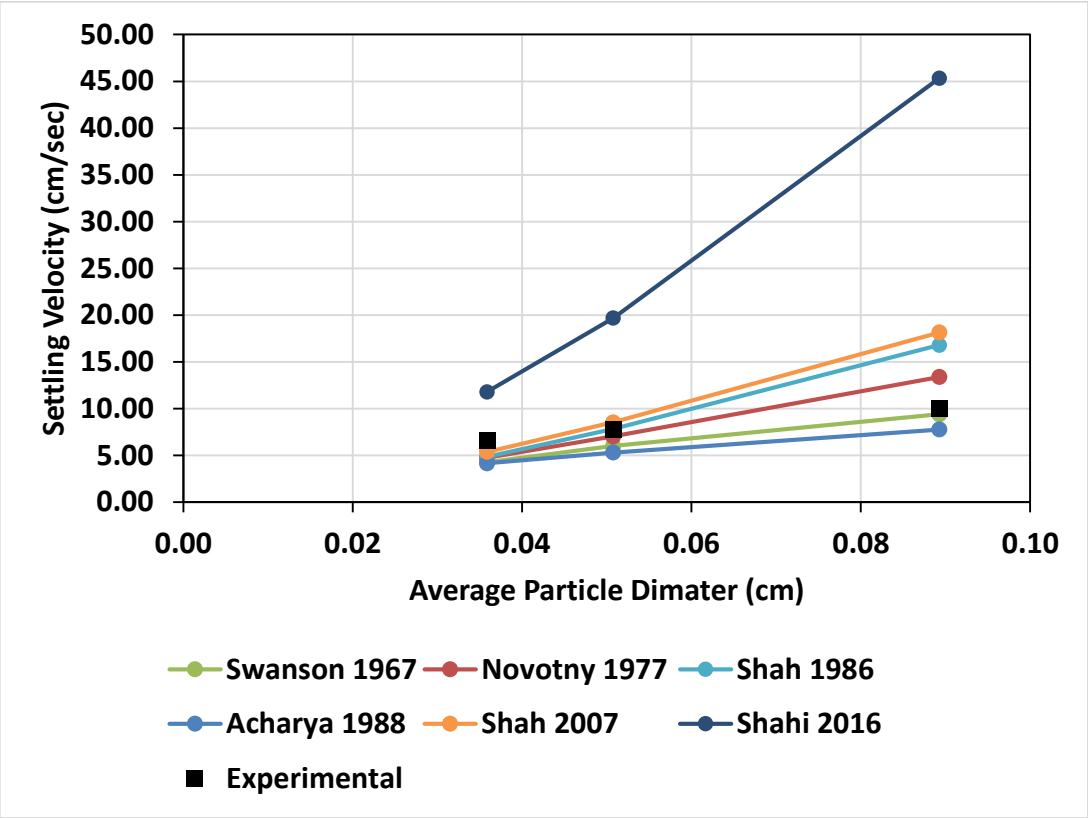

Figure 5.28. Validating different correlations using sand proppant and water

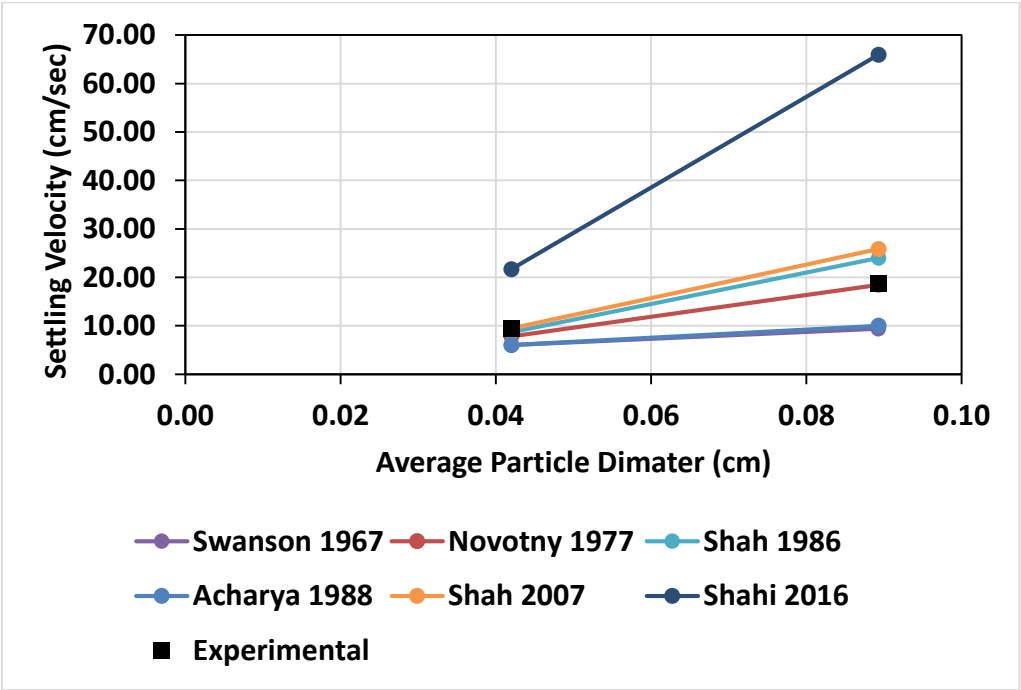

Figure 5.29. Validating different correlations using ceramic proppant with water

In the case of water similar results are observed which can be seen in Figures 5.28 and 5.29. Table 5.18 and 5.19 show that the correlation provided by (Swanson, 1967) still provides best estimation overall for both the proppants.

Table 5.19. Total average deviation of correlations for unbounded water

Author	**Average Deviation (%) For Water**	
	Sand	**Ceramic**
Swanson 1967	21.72	10.65
Novotny 1977	24.05	9.19
Shah 1986	31.43	18.42
Acharya 1988	30.74	41.55
Shah 2007	36.36	19.12
Shahi 2014	193.97	190.98

The value of particle Reynolds number obtained using experimental settling velocity was inserted in two different correlation to calculate the value of drag coefficient which can be seen from Figure 5.30 and then compare it with the drag coefficient calculated according to the actual definition using experimental settling velocities. The correlations (30) and (31) were used to compare the results. The average deviation when using correlation (31) is found to be 20.5% and for the correlation (30) it was 20% considering Vs/dp as the particle shear rate. As suggested by the authors, it is better to use the correlation (31) even though the average deviation percentage is less for (30) because of the usage of wider range of data while establishing correlation (31) using Newtonian fluids.

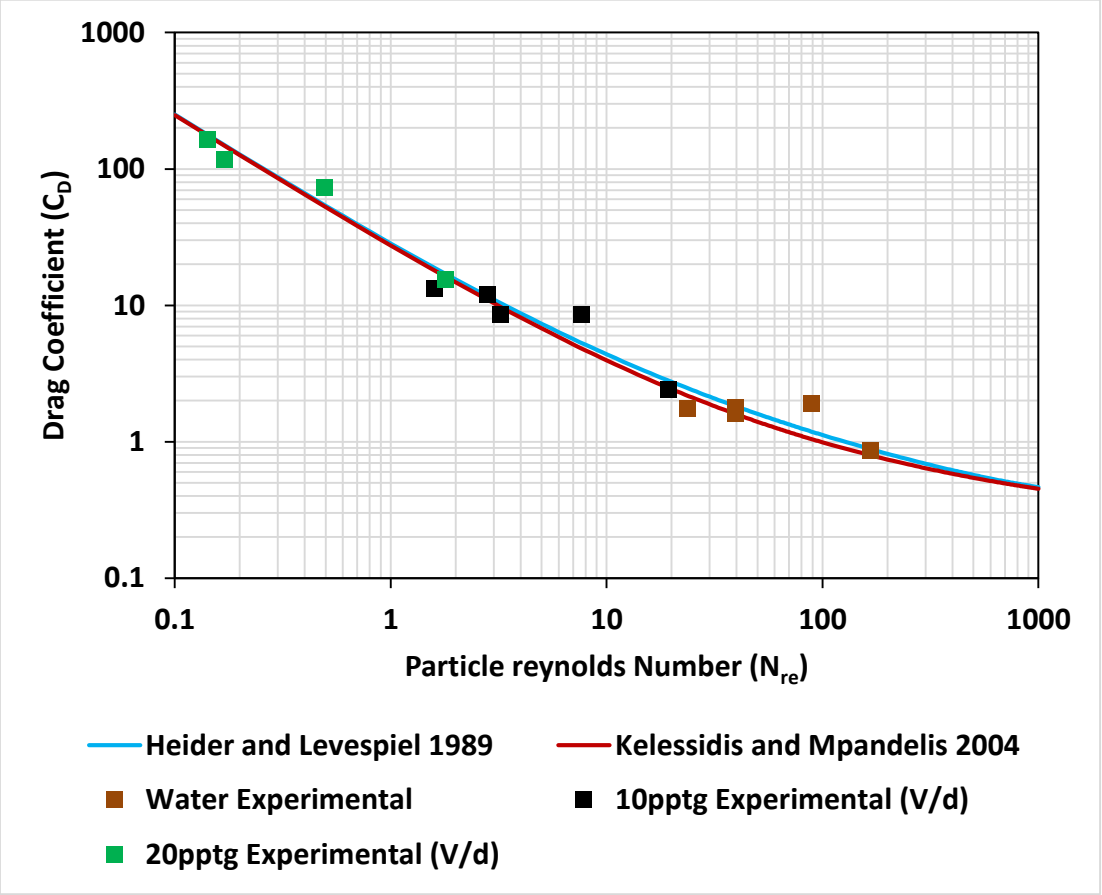

Figure 5.30. Investigating the applicability of correlation for Newtonian fluids

So it can also be concluded that the relationship between C_D-N_{re} for Newtonian fluids can also be used by merely replacing the viscosity term with effective viscosity as the average deviation is within 20%.

5.4.3. Validating the Correlations for Confined Fluid. The correlations validated with the experimental findings are taken from (Machac and Lecjaks, 1995) and (Liu and Sharma, 2005).

Machac and Lecjaks (1995) used different correlations to compare their results using different linear gels. Then the generalized equation was provided based on the conclusion that the retardation of settling velocity by fracture walls decreases as the shear thinning behaviour of the fluid increases. Here the comparison is made between

the wall factors from the correlation given by them and the experimental results of only 30/40 sand and 30/50 ceramic proppant because of the limitation of the applicability of the correlation which is described in the literature review section.

From the data points used in Figure 5.31 and 5.32 some of the data points fall outside the range for which their results were obtained but it is clear from both the figures that the results obtained during our experiments are completely contrasting. We found that with the increasing shear thinning behaviour of the fluid, the wall retardation effect on the settling velocity increases.

As our results are in complete agreement with Liu and Sharma 2005, critical analysis has been performed with the correlations established by them from Figure 5.33 to 5.38.

From Figures 5.33 to 5.38 it can be observed that some of the values from correlations are matching very well with the experimental data but most of the experimental values are lying below the values which are calculated using correlations.

In the case of sand proppant, the settling velocity of the larger size of proppant matches well with the correlation while the case is exactly opposite for the ceramic proppant. No clear trend for increasing viscosity can be observed from the plots. Therefore, the deviation is calculated for each value and tabulated in Tables 5.20, 5.21, and 5.22.

From Table 5.20 to 5.22 it can be observed that there is no evident trend which can explain the deviation on the values based on size of the proppant. But it can be clearly seen that as the viscosity of the fluid increases, the deviation percentages also increase in sand and ceramic both the cases.

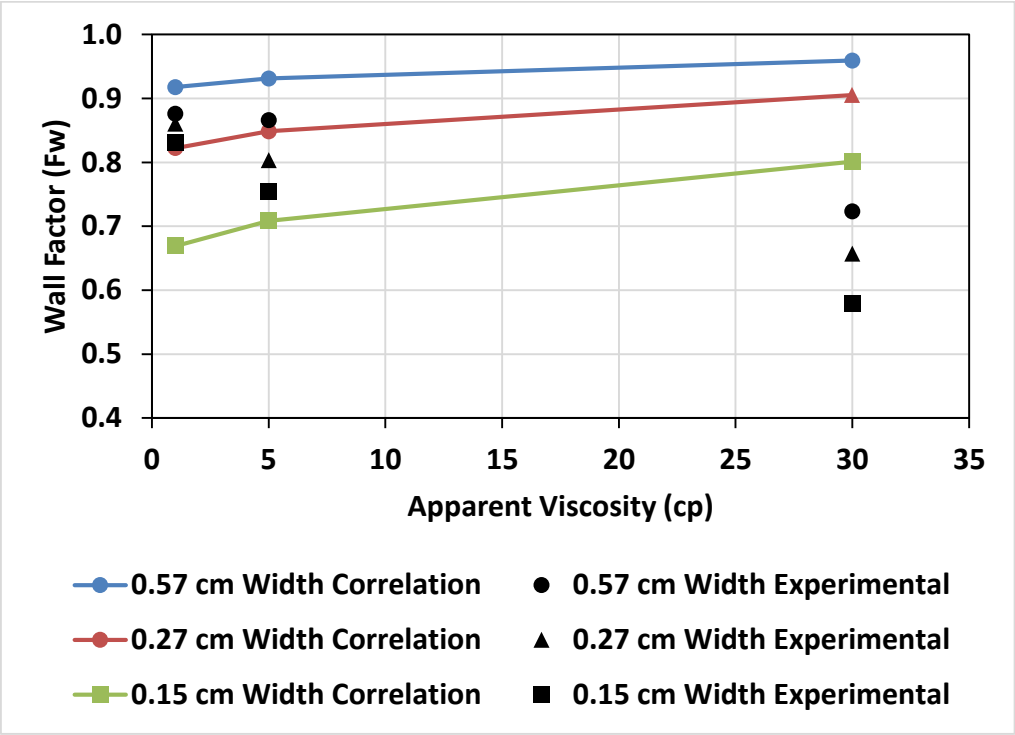

Figure 5.31. Validation of the correlations with 30/40 sand proppant for different fracture widths

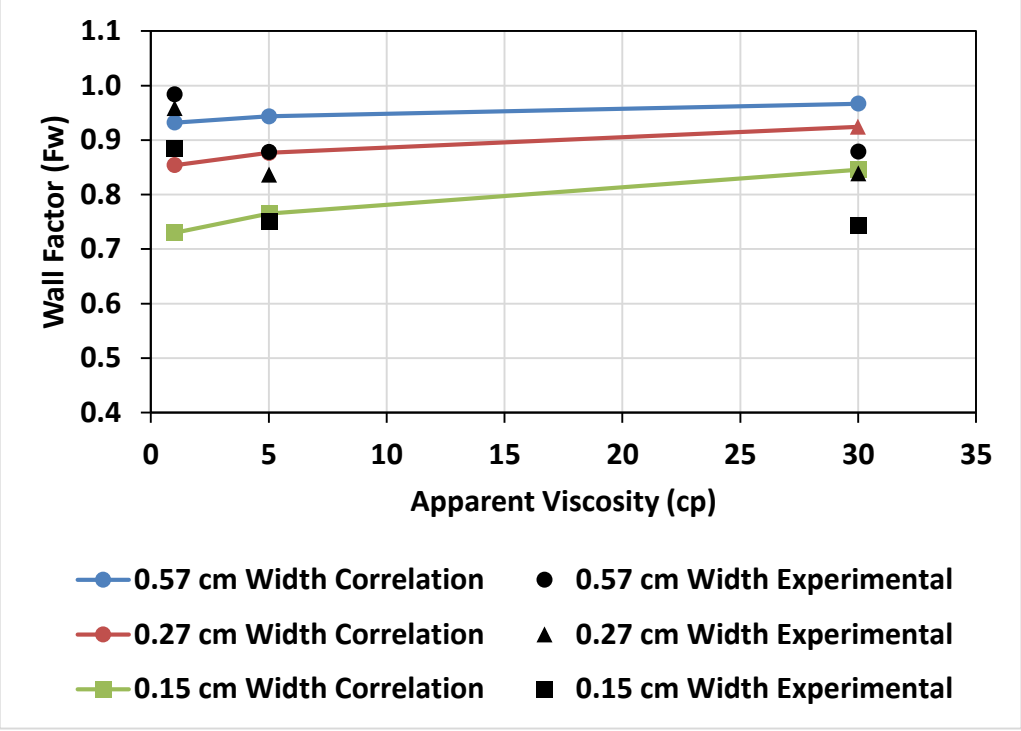

Figure 5.32. Validation of the correlations with 30/50 ceramic proppant for different fracture Widths

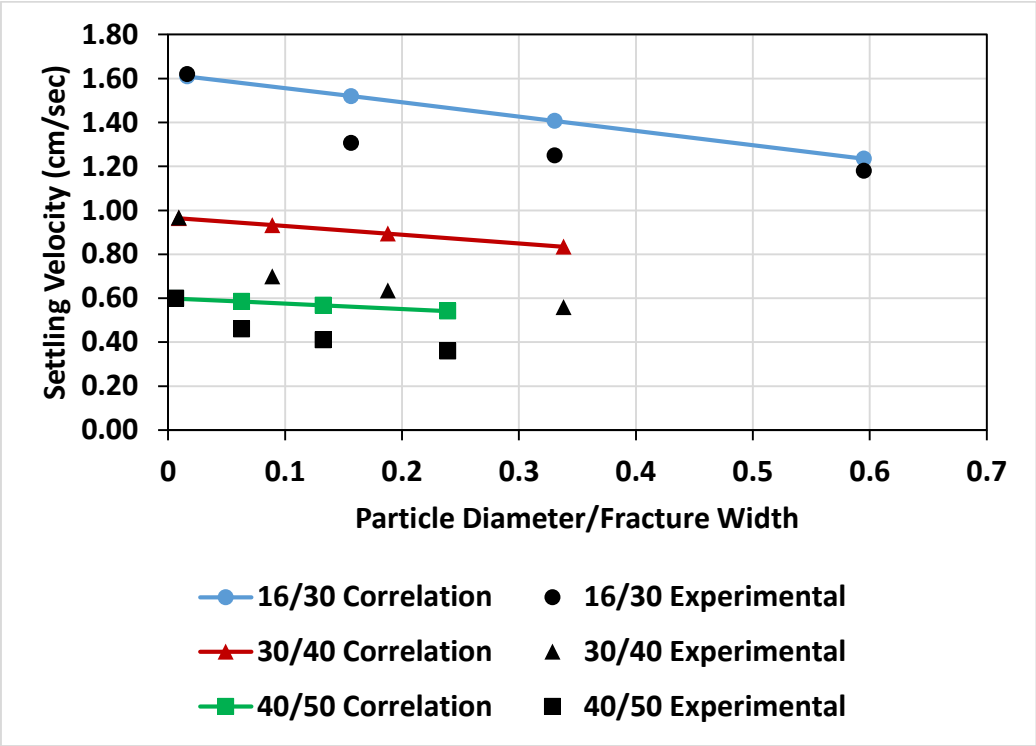

Figure 5.33. Validation of the correlation using different sized sand proppant with 20 pptg linear gel

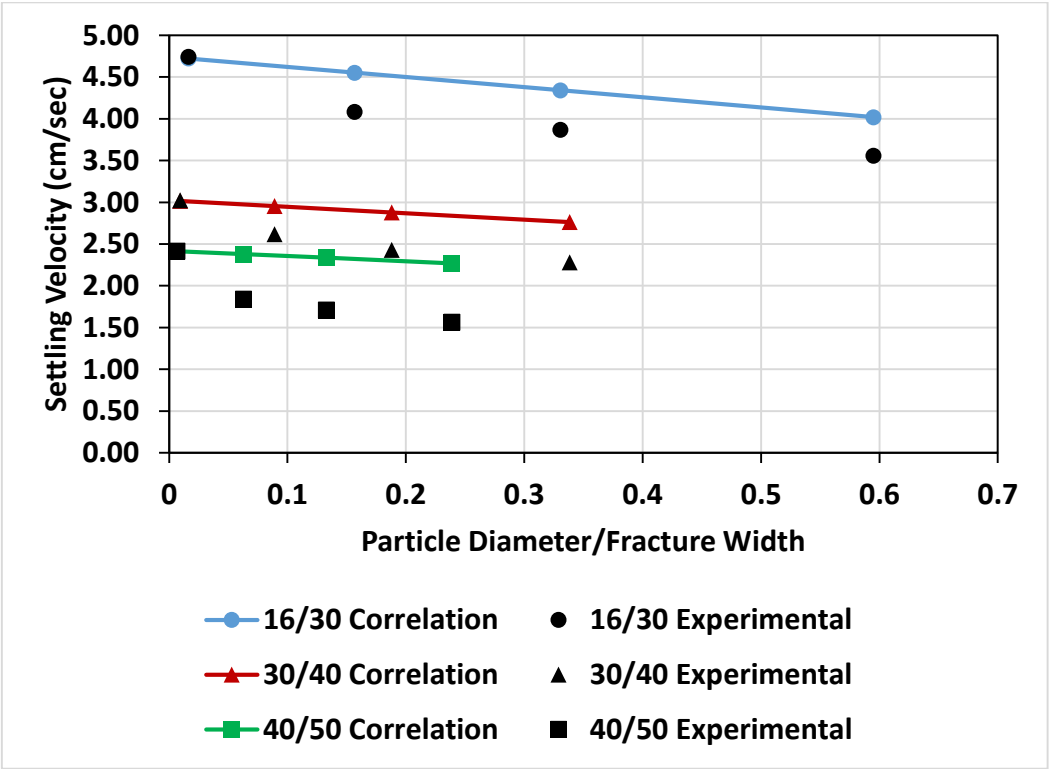

Figure 5.34. Validation of the correlation using different sized sand proppant with 10 pptg gel

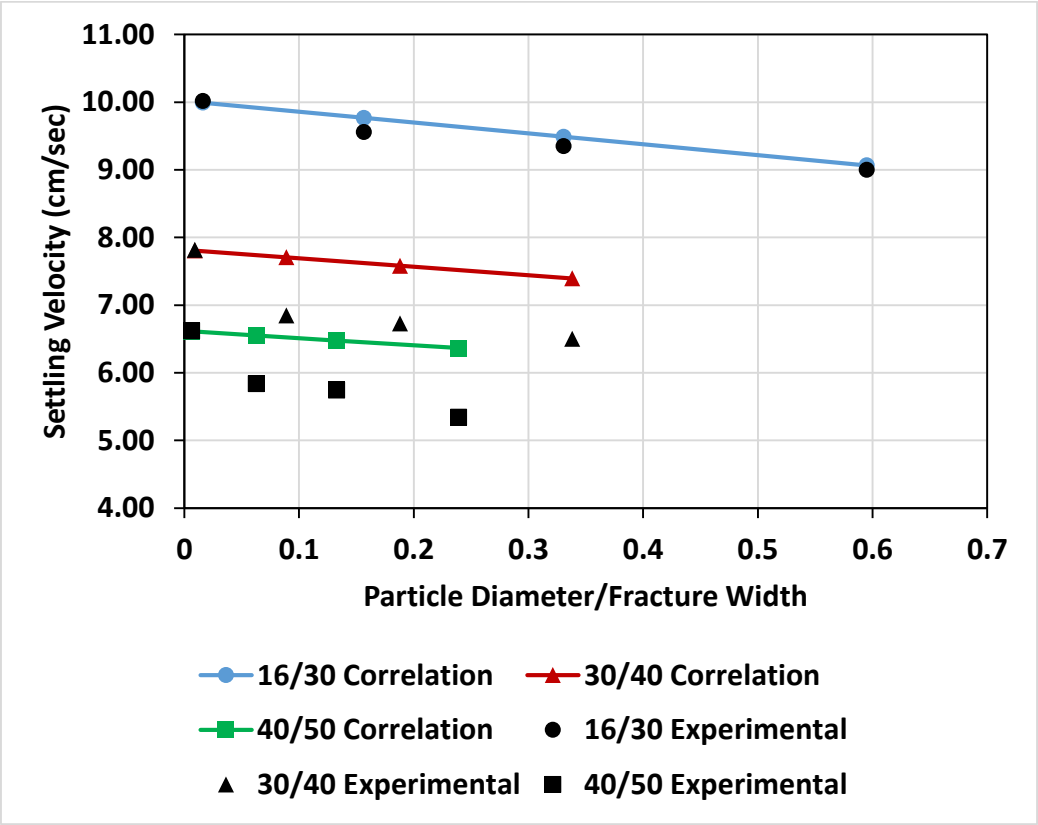

Figure 5.35. Validation of the correlation using different sized sand proppant with water

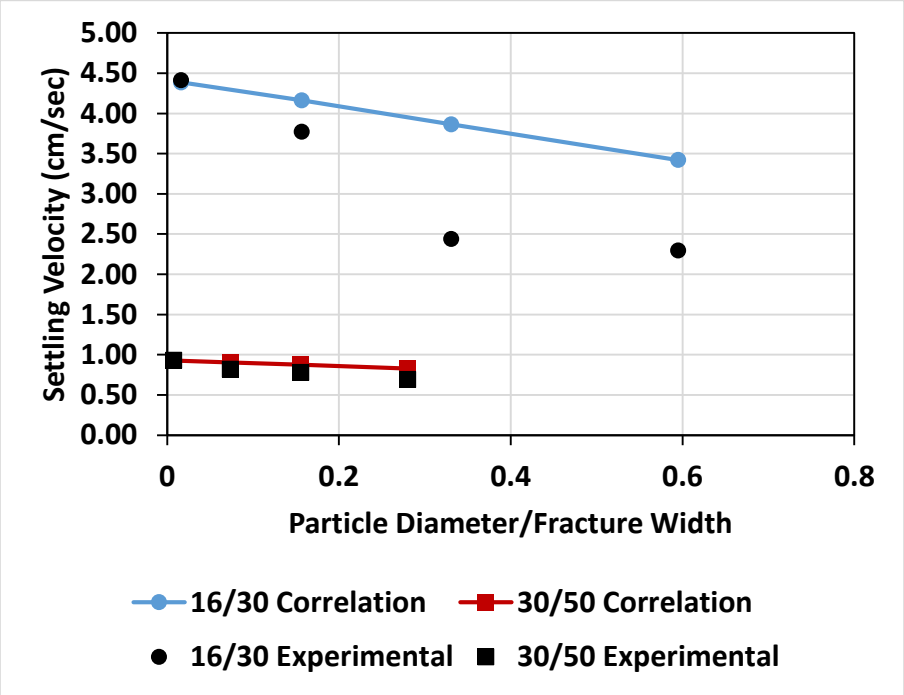

Figure 5.36. Validation of the correlation using different sized ceramic proppant with 20 pptg linear gel

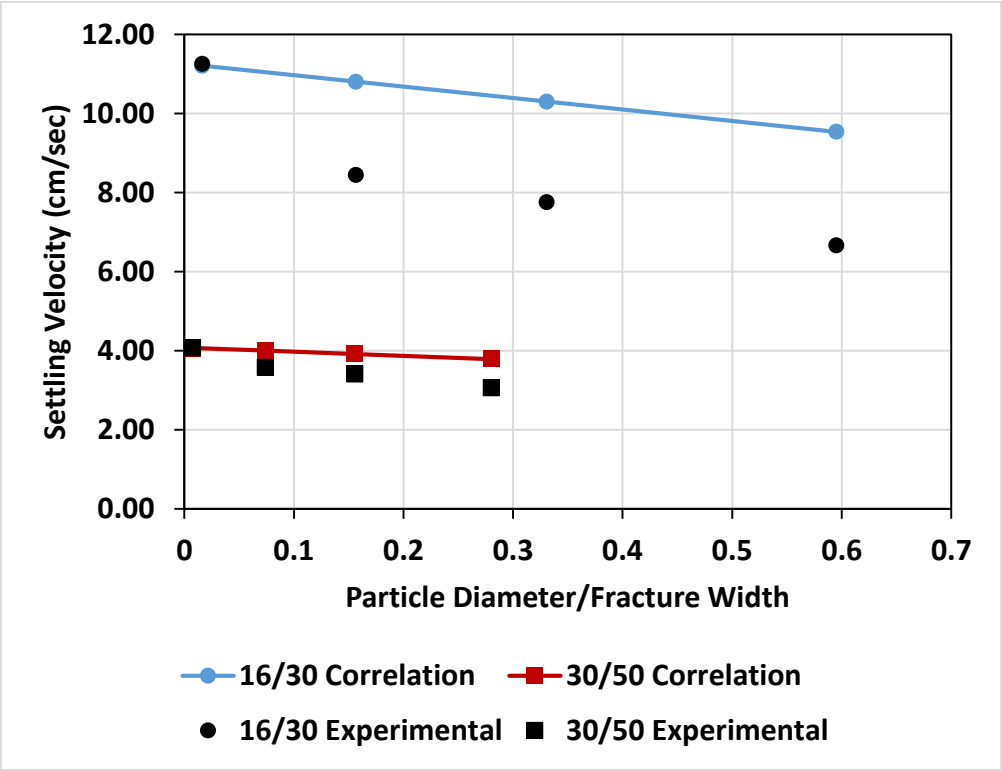

Figure 5.37. Validation of the correlation using different sized ceramic proppant with 10 pptg linear gel

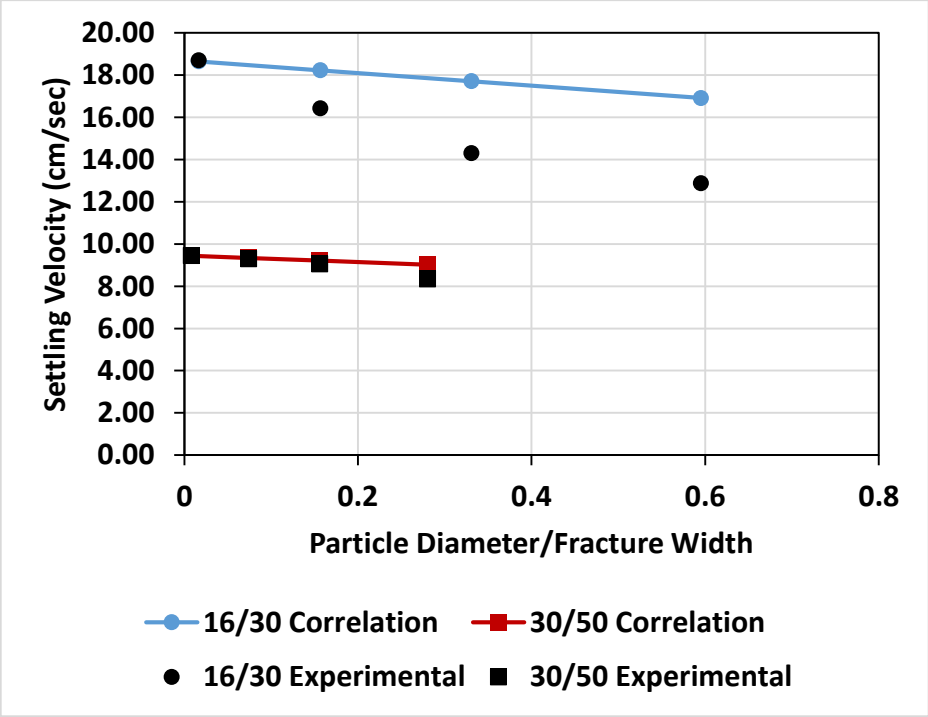

Figure 5.38. Validation of the correlation using different sized ceramic proppant with water

Not only viscosity but also with decreasing the fracture width the deviation from the correlation increased. That proves that as the shear thinning behaviour of the fluid increases, the effect of fracture walls on the settling velocity increases more and therefore it may be important to include the flow behaviour index (n) in the correlation to get accurate results.

The only major difference in the experiments performed by Liu and Sharma (2005) and our experiments is the value of power law parameters. In the case of water it can be seen from Table 5.20 that there are lot of values which exactly match with the values calculated by correlation whereas the values start deviating more than 30% as the viscosity of the fluid increases which supports the fact that the power law parameters has important role to play when the fracture walls are present.

Table 5.20. Deviation of correlations for confined water

Fracture Width (cm)	**Average Deviation (%) For Water**				
	Sand			**Ceramic**	
	16/30	30/40	40/50	16/30	30/50
Unconfined	-0.26	-0.15	-0.10	-0.26	-0.12
0.57	2.19	12.53	12.19	11.02	0.41
0.27	1.50	12.69	12.78	23.78	1.70
0.15	0.73	13.77	19.16	31.36	8.09

Table 5.21. Deviation of correlations for confined 10 pptg linear gel

Fracture Width (cm)	**Average Deviation (%) For 10 pptg**				
	Sand			**Ceramic**	
	16/30	30/40	40/50	16/30	30/50
Unconfined	-0.41	-0.23	-0.17	-0.41	-0.19
0.57	11.47	12.82	29.33	27.92	11.75
0.27	12.18	18.50	36.57	32.80	14.84
0.15	12.90	21.18	44.91	43.08	23.77

Table 5.22. Deviation of correlations for confined 20 pptg HPG gel

Fracture Width (cm)	Average Deviation (%) For 20 pptg				
	Sand			Ceramic	
	16/30	30/40	40/50	16/30	30/50
Unconfined	-0.63	-0.36	-0.26	-0.63	-0.29
0.57	16.24	33.35	27.10	10.41	10.59
0.27	12.58	40.67	38.49	58.43	12.03
0.15	4.68	49.06	50.78	49.15	19.81

5.4.4. Validating the Correlations for Irregularly Shaped Proppant. This analysis is performed to put emphasis on the effect of roundness and sphericity of the proppant on the settling velocity as the researches which are used here were specially performed to show the impact of roundness and sphericity of the solid particle on their settling behaviour. All the correlations which are validated here were established using natural sand and other different shaped particles such as disc and plates with water. These correlations are taken from (Cheng, 1997; Wu and Wang, 2006; Helbar et al., 2009; and Shahi and Kuru, 2015). All the experimental parameters and results fall within the range of all these correlations. The analysis is also performed using shear thinning non-Newtonian fluid which is actually out of the range of applicability of these correlations but still in order to provide an idea whether the range could be widen or not.

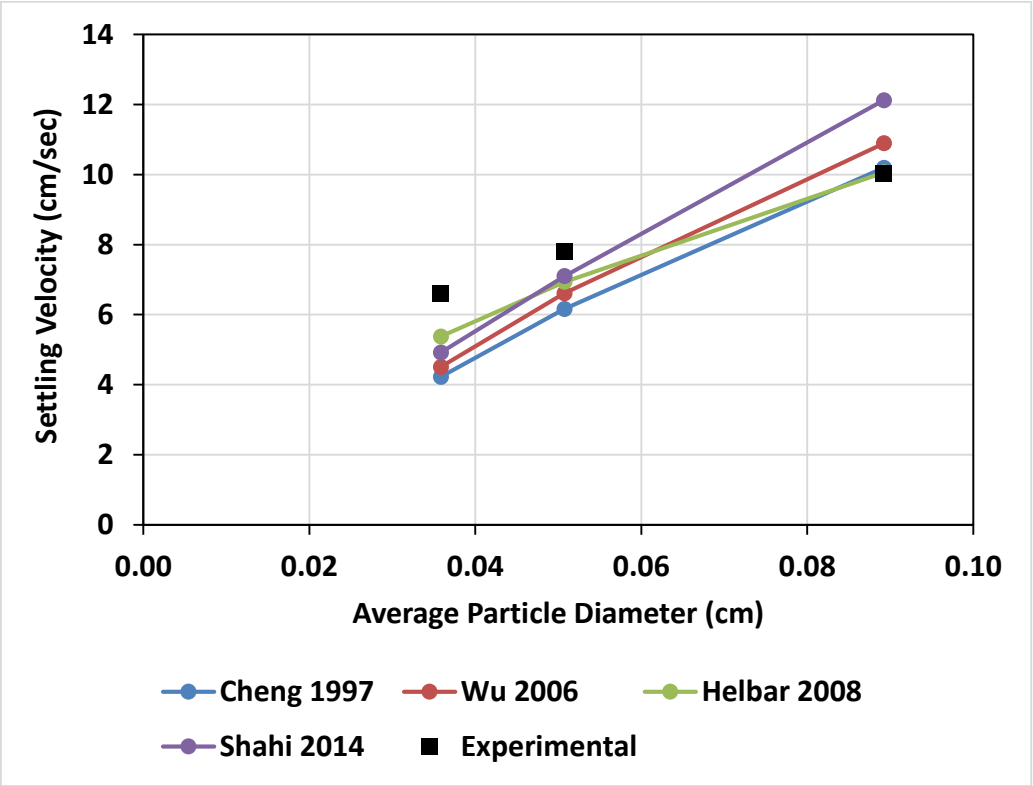

Figure 5.39. Validation of the correlations for irregularly shaped proppant using different sized sand proppant and water

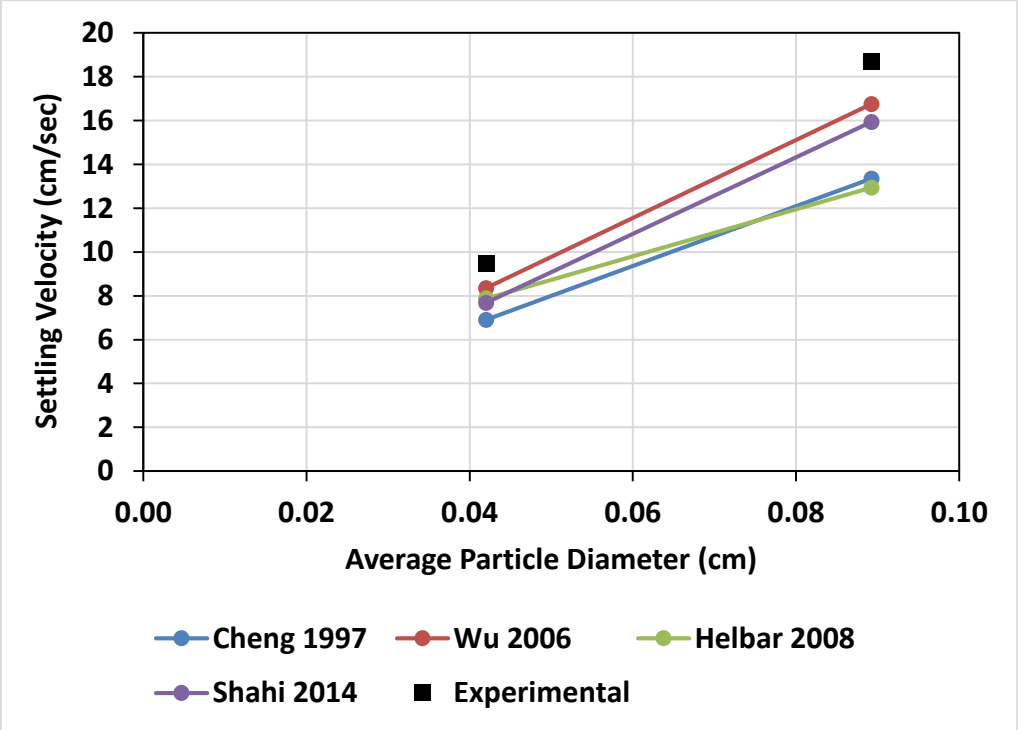

Figure 5.40. Validation of the correlations for irregularly shaped proppant using different sized ceramic proppant and water

As it can be seen from Figure 5.39, 5.40 and Table 5.23 that the average deviation is not exceeding more than 30% in any case. For irregularly shaped sand proppant the average deviation is found to be within 20%. Though having higher roundness and sphericity, the values of settling velocity of ceramic proppant is deviating more may be because these correlations were established solely using irregularly shaped proppant and the drag in case of spherical particles would be less compare to irregularly shaped particle.

Therefore the conclusion is that the consideration of roundness and sphericity is very important while establishing correlations to calculate the settling velocity explicitly because the experimental results are still deviating at least by 10% in all the cases when all the parameters of experiments and correlations are similar except roundness and sphericity of the particles.

Table 5.23. Total average deviation of correlations for irregularly shaped proppant with water

Author	**Average Deviation (%) For Water**	
	Sand	**Ceramic**
Cheng 1997	19.71	27.79
Wu 2006	18.68	11
Helbar 2008	10.16	23.75
Shahi 2014	18.61	16.76

Although these correlations are not meant to predict the settling velocity using shear thinning non-Newtonian fluid, the validation was performed to investigate whether their range of applicability can be made wider or not (Figure 5.41 to 5.44). It can be seen from the tabulated values in Table 5.24 and 5.25 below that with the increasing shear thinning behaviour of the fluid the deviation percentage increased in almost all the cases for both the types of proppant. Still the average deviations are almost within 35% for the correlations provided by Cheng et al. (1997), Wu and Wang

(2006) and Helbar et al. (2008). By correlating the power law parameters with these correlations may reduce the average deviation and can provide the values within acceptable range.

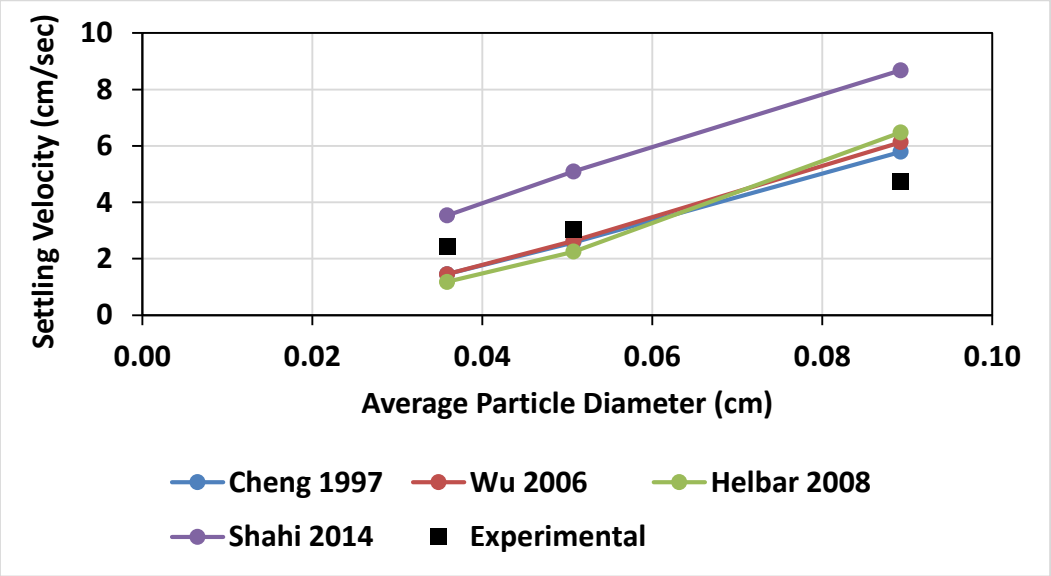

Figure 5.41. Validation of the correlations for irregularly shaped proppant using different sized sand proppant and 10 pptg linear gel

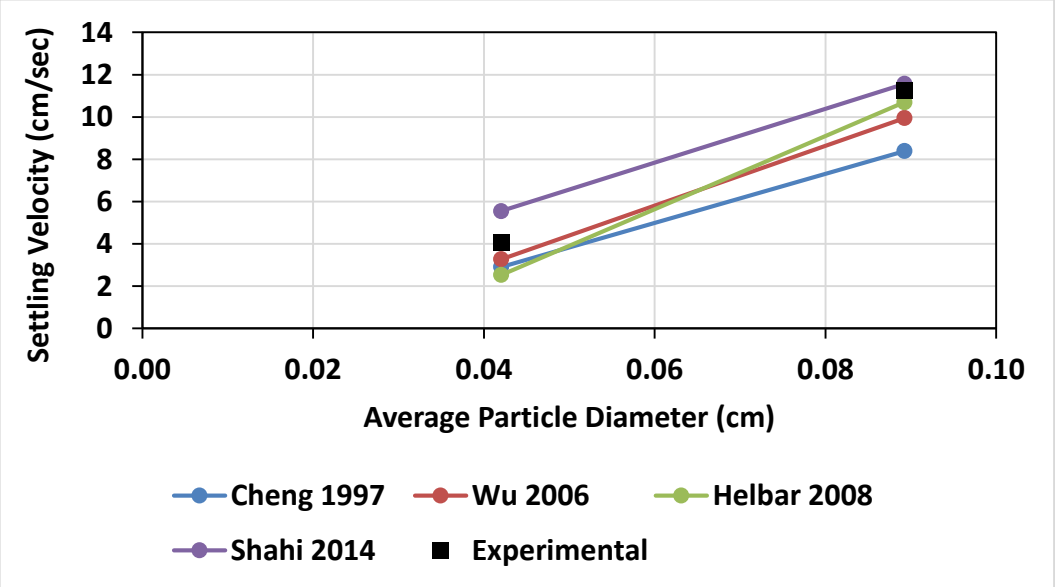

Figure 5.42. Validation of the correlations for irregularly shaped proppant using different sized ceramic proppant with 10 pptg linear gel

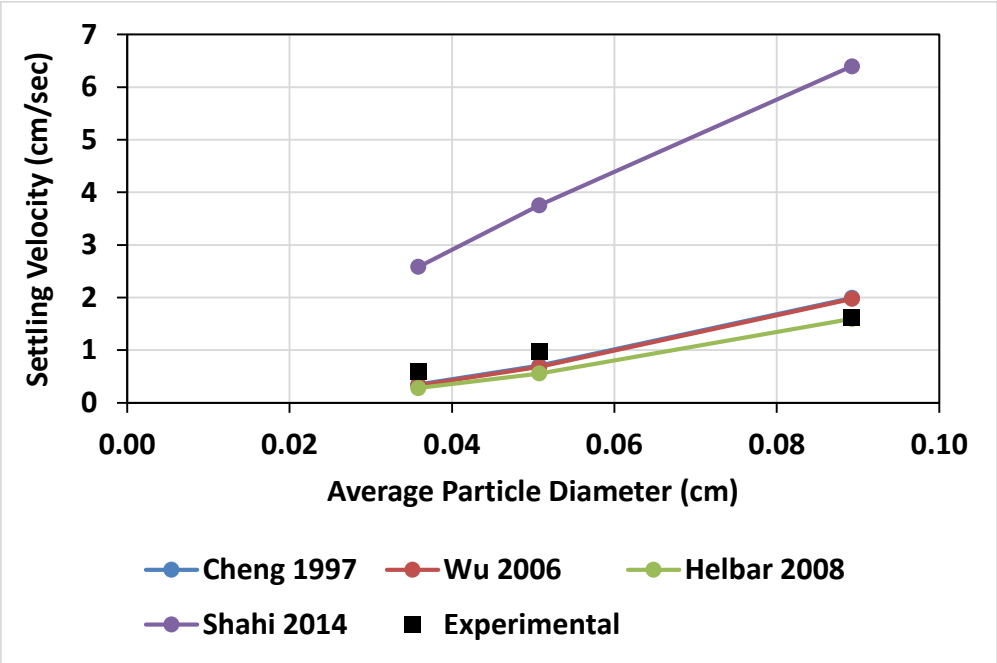

Figure 5.43. Validation of the correlations for irregularly shaped proppant using different sized sand proppant with 20 pptg linear gel

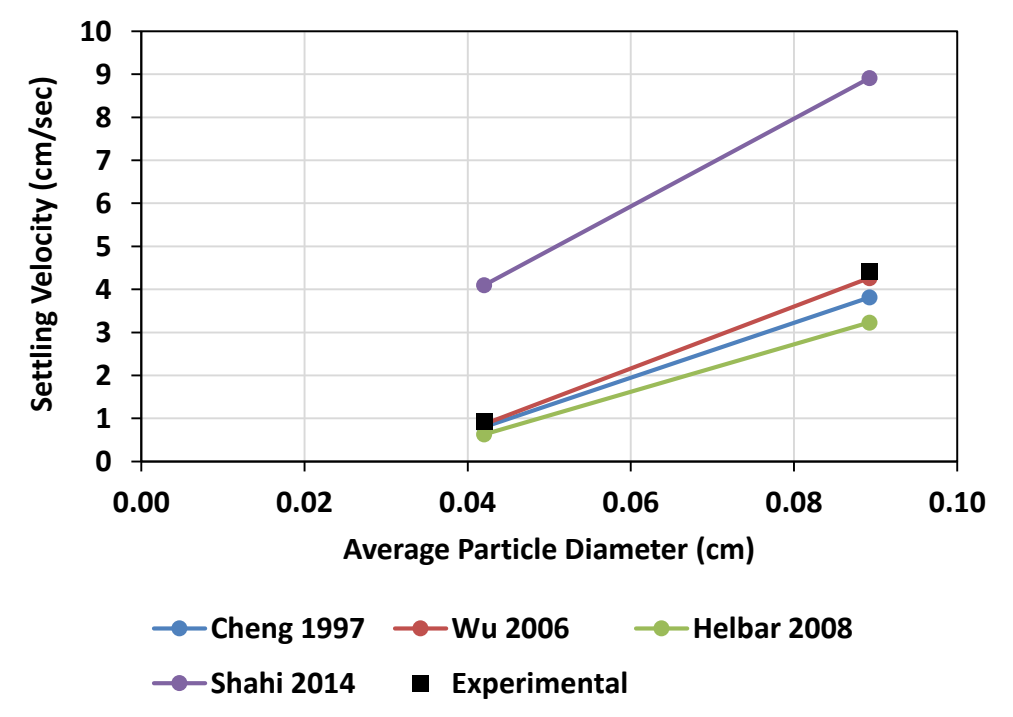

Figure 5.44. Validation of the correlations for irregularly shaped proppant using different sized ceramic proppant with 20 pptg gel

Table 5.24. Total average deviation of correlations for irregularly shaped proppant with 10 pptg HPG gel

Author	Average Deviation (%) For 10 pptg Gel	
	Sand	Ceramic
Cheng et al. 1997	25.55	27.06
Wu 2006	27.37	15.69
Helbar 2008	37.86	21.48
Shahi 2014	65.88	19.46

Table 5.25. Total average deviation of correlations for irregularly shaped proppant with 20 pptg HPG gel

Author	Average Deviation (%) For 20 pptg Gel	
	Sand	Ceramic
Cheng et al. 1997	30.79	14.03
Wu 2006	32.11	5.29
Helbar 2008	32.61	29.70
Shahi 2014	304.47	221.26

6. CONCLUSION & FUTURE WORK

6.1. CONCLUSION

1. HPG linear gels show little elasticity which can be neglected during the analysis of settling behaviour of the proppant in static conditions
2. With the increasing shear thinning behaviour of the fluid, the effect of increasing diameter and specific gravity of the proppant and fracture wall get more pronounced
3. With increasing diameter and specific gravity of the proppant, the effect of viscosity of the fluid on the settling velocity decreases
4. For the fracture widths used during this study, the effect of viscosity of the fluid on the settling velocity remained almost constant
5. Correlation provided by Swanson 1967 was found to be best suitable correlation according to this study
6. Correlation provided by Liu and Sharma 2005 has acceptable range of deviation for water but with increasing viscosity and narrower fracture width, the deviation increases
7. Correlations used for irregularly shaped proppant give deviation within acceptable range which proves that inclusion of shape factor of the proppant can reduce the error in the calculated settling velocity from the correlations
8. Based on comparison with the correlation of Heider and Levespiel (1989) for Newtonian fluid it was found that the correlation can be used for non-Newtonian fluids as well by using the value of effective viscosity

6.2. FUTURE WORK

1. Effect of elasticity on the static settling velocity should be investigated separately by using one set of fluid with similar viscosity and different elasticity and other set of fluid with similar elasticity and different elasticity using real proppants.
2. Effect of roundness and sphericity and specific gravity have been shown affecting the settling velocity but the effects are not quantified separately.
3. Effect of smooth fracture walls have been shown but the usage of rough fracture walls might replicate the field condition better.
4. The analysis and validation of the correlation was based on the settling behaviour of single proppant whereas usage of concentration of the proppant will be more replicable to the field conditions.
5. Investigation of the effect of shape of shape of the proppant using real proppants and the smooth glass spheres.

REFERENCES

Acharya, A. R. 1986. Particle Transport in Viscous and Viscoelastic Fracturing Fluids. Society of Petroleum Engineers. doi:10.2118/13179 PA.

Acharya, A. R. 1988. Viscoelasticity of Crosslinked Fracturing Fluids and Proppant Transport. Society of Petroleum Engineers. doi:10.2118/15937-PA.

Acharya, A., Mashelkar, R.A. and Ulbrecht, J. 1976a. Flow of Inelastic and Viscoelastic Fluids Past a Sphere. Part 1: Drag Coefficient in Creeping and Boundary-Layer Flows. Rheologica Acta 15 (9): 454–470. http://dx.doi.org/10.1007/bf01530348.

Alcocer, C. F., Ghalambor, A., & Sweet, L. H. 1992. A Study Of Rheological Properties Of Non-Newtonian Fluids And Settling Behavior Of Ceramic Proppants Manufactured In Louisiana, USA. Society of Petroleum Engineers. doi:10.2118/23727-MS.

Al-Muntasheri, G. A. 2014. A Critical Review of Hydraulic Fracturing Fluids over the Last Decade. Society of Petroleum Engineers. doi:10.2118/169552-MS.

Alotaibi, M. A., & Miskimins, J. L. 2015. Slickwater Proppant Transport in Complex Fractures: New Experimental Findings and Scalable Correlation. Society of Petroleum Engineers. doi:10.2118/174828-MS.

Arnipally, S. K., & Kuru, E. 2017. Settling Velocity of Particles in Viscoelastic Fluids: A Comparison of the Shear Viscosity vs Elasticity Effect. Society of Petroleum Engineers. doi:10.2118/187255-MS.

Asadi, M., Shah, S. N., & Lord, D. L. 1999. Static/Dynamic Settling of Proppant in Non-Newtonian Hydraulic Fracturing Fluids. Society of Petroleum Engineers. doi:10.2118/52217-MS.

Asadi, M., Conway, M. W., & Barree, R. D. 2002. Zero Shear Viscosity Determination of Fracturing Fluids: An Essential Parameter In Proppant Transport Characterizations. Society of Petroleum Engineers. doi:10.2118/73755-MS.

Asmolov, E. S. "The inertial lift on a small particle in weak-shear parabolic flow", Physics of Fluids, v. 14, No. 1, pp. 15, 2002.

Barati, R. and Liang, J. T. 2014. A Review of Fracturing Fluid Systems Used for Hydraulic Fracturing of Oil and Gas Wells. Article in Journal of Applied Polymer Science. doi: 10.1002/app.40735.

Cheng, N. S. (1997). "A simplified settling velocity formula for sediment particle. "Journal of Hydraulic Engineering, ASCE, 123(2), 149-152.

Chhabra, R.P. 2007. Bubbles, Drops and Particles in Non-Newtonian Fluids, second edition, Boca Raton, Florida: Taylor & Francis.

Chien, S. F. 1994. Settling Velocity of Irregularly Shaped Particles. Society of Petroleum Engineers. doi:10.2118/26121-PA.

Choi, S.K. 2008. pH Sensitive Polymers for Novel Conformance Control and Polymer Flooding Applications. PhD Thesis, University of Texas, Austin, USA.

Clark, P. E., Manning, F. S., Quadir, J. A., & Guler, N. 1981. Prop Transport in Vertical Fractures. Society of Petroleum Engineers. doi:10.2118/10261-MS.

Daneshy, A. A. 1978. Numerical Solution of Sand Transport in Hydraulic Fracturing. Society of Petroleum Engineers. doi:10.2118/5636 PA

Economides, M.; Nolte, K. Reservoir Stimulation, NY and Chichester, 3rd ed. Wiley, 2000.

Ely, J.W. 1989. Fracturing Fluids and Additives. Vol. 12 of Recent Advances in Hydraulic Fracturing (SPE Henry L Doherty Monograph Series). SPE, Richardson, Texas.

EPA, U. (2004). Evaluation of Impacts to Underground Sources of Drinking Water by Hydraulic Fracturing of Coalbed Methane Reservoirs.

Ferry, J. D. 1970. Viscoelastic Properties of Polymers, second edition, John Wiley & Sons Inc., USA.

Gandossi, L. 2013. An Overview of Hydraulic Fracturing and Other Formation Stimulation Technologies for Shale Gas Production. Report by the Joint Research Centre of the European Commision. doi: 10.2790/99937.

Goel, N., Shah, S. N. and Grady, B. P. 2002. Correlating Viscoelastic Measurements of Fracturing Fluid to Particle Suspension and Solids Transport. J. Pet. Sci. Eng.35: 59-81.

Gomaa, A. M., Gupta, D. V. S., & Carman, P. 2015. Viscoelastic Behavior and Proppant Transport Properties of a New High-Temperature Viscoelastic Surfactant Based Fracturing Fluid. Society of Petroleum Engineers. doi:10.2118/173745-MS.

Gracssley, W. W. The Entanglement Concept in Polymer Rheology, Advanced Polymer Science, 16, 1974.

Gupta, D. V. S. 2009. Unconventional Fracturing Fluids for Tight Gas Reservoirs. Society of Petroleum Engineers. doi:10.2118/119424-MS.

Halliburton 2011. Fracturing Fluid Systems.

Hannah, R. R., & Harrington, L. J. 1981. Measurement of Dynamic Proppant Fall Rates in Fracturing Gels Using a Concentric Cylinder Tester (includes associated paper 9970). Society of Petroleum Engineers. doi:10.2118/7571-PA.

Harrington, L. J., Hannah, R. R., & Williams, D. 1979. Dynamic Experiments On Proppant Settling In Crosslinked Fracturing Fluids. Society of Petroleum Engineers. doi:10.2118/8342-MS.

Harris, P. C., Morgan, R. G., & Heath, S. J. 2005. Measurement of Proppant Transport of Frac Fluids. Society of Petroleum Engineers. doi:10.2118/95287-MS.

Heider, A., and Levespiel, O. Drag coefficient and terminal velocity of spherical and nonspherical particles, Powder Tech. 58 (1989) 63– 70.

Helbar, S. M. S., Tokaldany, E. A., Darby, S., and Shafaie, A. Fall velocity of sediment particles, IASME/WSEAS Int. Conf. on Water Resources, Hydraulics and Hydrology 2009, pp. 39–45.

Hölzer, A., and Sommerfeld, M. New simple correlation formula for the drag coefficient of non-spherical particles, Powder Technology, Volume 184, Issue 3, 2008, pages 361-365, ISSN 0032-5910, https://doi.org/10.1016/j.powtec.2007.08.021.

Horton, R., Moran, L., Ochs, R., Rawn, J., and Scrimgeour, K. Principles of Biochemistry, 2nd, Ed., Prentice Hall, New Jersey, 1996.

Hu, K., Sun, J., Wong, J., & Hall, B. E. 2014. Proppants Selection Based on Field Case Studies of Well Production Performance in the Bakken Shale Play. Society of Petroleum Engineers. doi:10.2118/169566-MS.

Hu, Y. T., Chung, H., & Maxey, J. E. (2015, February 3). What is More Important for Proppant Transport, Viscosity or Elasticity? Society of Petroleum Engineers. doi:10.2118/173339-MS.

Hu, Y. T., Kishore, T., Maxey, J., & Loveless, D. (2015, April 13). Effects of Crosslinking Chemistry on Proppant Suspension in Guar Networks. Society of Petroleum Engineers. doi:10.2118/173726-MS.

Hurst, W. 1953. Establishment of the Skin Effect and its Impediment to Fluid Flow into a Well Bore. The Petroleum Engineer. Petroleum Engineering, Dallas. 25 (Oct.): 36-38, B6 through B16.

ISO 13503-2: 2006/Amd.1:2009(E), Petroleum and Natural Gas Industries Completion Fluids and Materials Part 2: Measurement of Properties of Proppants Used in Hydraulic Fracturing and Gravel-packing Operations, ISO, Geneva, Switzerland, 2009.

Jennings, A.R. 1996. Fracturing Fluids - Then and Now. Journal of Petroleum Technology 48 (7): 604-610.

Kaufman, P., Penny, G.S., and Paktinant, J. 2008. Critical Evaluations of Additives Used in Shale Slickwater Fracs. Paper SPE 119900 presented at the SPE Shale Gas Production Conference held in ForthWorth, Texas, USA, 16-18 November.

Kelessidis, V.C. and Mpandelis, G. 2004. Measurements and Prediction of Terminal Velocity of Solid Spheres Falling through Stagnant Pseudoplastic Liquids. Powder Technology 147 (1–3): 117–125. http://dx.doi.org/10.1016/j.powtec.2004.09.034.

Kirkby, L. L., & Rockefeller, H. A. 1985. Proppant Settling Velocities in Nonflowing Slurries. Society of Petroleum Engineers. doi:10.2118/13906-MS.

Krumbein, W. C., and Sloss, L. L. Stratigraphy and Sedimentation, second ed., W.H. Freeman and Company, San Francisco, 1963, p. 660.

Liang, F., Sayed, M., Al-Muntasheri, G. A., Chang, F. F., and Li, L. A comprehensive review on proppant technologies, Petroleum,Volume 2, Issue 1, 2016, Pages 26-39, ISSN 2405-6561, https://doi.org/10.1016/j.petlm.2015.11.001.

Liu, Y., Fonseca, E. R., Hackbarth, C., Hulseman, R., and Tackett, K. 2015. A New Generation High-Drag Proppant: Prototype Development, Laboratory Testing, and Hydraulic Fracturing Modeling. Society of Petroleum Engineers. doi:10.2118/173338-MS.

Liu, J., & Seright, R. S. 2001. Rheology of Gels Used for Conformance Control in Fractures. Society of Petroleum Engineers. doi:10.2118/70810-PA.

Liu, Y., & Sharma, M. M. 2005. Effect of Fracture Width and Fluid Rheology on Proppant Settling and Retardation: An Experimental Study. Society of Petroleum Engineers. doi:10.2118/96208-MS.

Machac, I. and Lecjaks, Z. 1995. Wall Effect for a Sphere Falling Through a Non Newtonian Fluid in a Rectangular Duct. Chem. Eng. Sci. 50 (1): 143-148.

Malhotra, S., & Sharma, M. M. 2011. A General Correlation for Proppant Settling in VES Fluids. Society of Petroleum Engineers. doi:10.2118/139581-MS.

Malhotra, S. and Sharma, M.M. 2012. Settling of Spherical Particles in Unbounded and Confined Surfactant-Based Shear Thinning Viscoelastic Fluids: An Experimental Study. Chemical Engineering Science 84: 646-655. http://dx.doi.org/10.1016/j.ces.2012.09.010.

McCabe, W. L. and Smith, J. C.: Unit Operations of Chemical Engineering, McGraw Hill Book Co., Inc., New York (1956), Ch. 7.

McDaniel, G. A., Abbott, J., Mueller, F. A., Anwar, A. M., Pavlova, S., Nevvonen, O., and Alary, J. 2010. Changing the Shape of Fracturing: New Proppant Improves Fracture Conductivity. Society of Petroleum Engineers. doi:10.2118/135360-MS.

McMechan, D. E., & Shah, S. N. 1991. Static Proppant-Settling Characteristics of Non-Newtonian Fracturing Fluids in a Large-Scale Test Model. Society of Petroleum Engineers. doi:10.2118/19735-PA.

Mohanty, K. K., and Ming Gu, A. G. 2012. "Improvement of Fracturing for Gas Shales. "Report for RPSEA (Research Partnership to Secure Energy for America).

Moraes, I. C. F., Fasolin, L. H., Cunha, R. L., & Menegalli, F. C. 2011. Dynamic and steady: shear rheological properties of xanthan and guar gums dispersed in yellow passion fruit pulp (Passiflora edulisf.flavicarpa). Brazilian Journal of Chemical Engineering, 28(3), 483-494. https://dx.doi.org/10.1590/S0104-66322011000300014.

Novotny, E. J. 1977. Proppant Transport. Society of Petroleum Engineers. doi:10.2118/6813-MS.

Ozden, S., Li, L., Al-Muntasheri, G. A., & Liang, F. 2017. Nanomaterials Enhanced High-Temperature Viscoelastic Surfactant VES Well Treatment Fluids. Society of Petroleum Engineers. doi:10.2118/184551-MS.

Palisch, T., Duenckel, R., Bazan, L., Heidt, H., and Turk, G. Determining Realistic Fracture Conductivity and Understanding Its Impact on Well Performance—Theory and Field Examples, in Hydraulic Fracturing Technology Conference, College Station, 2007.

Palisch, T. T., Vincent, M., & Handren, P. J. 2010. Slickwater Fracturing: Food for Thought. Society of Petroleum Engineers. doi:10.2118/115766-PA.

Peden, J. M., and Luo, Y. 1987. Settling Velocity of Variously Shaped Particles in Drilling and Fracturing Fluids. Society of Petroleum Engineers. doi:10.2118/16243-PA.

Rae, P., and Lullo, G. Fracturing Fluids and Breaker Systems—A Review of the State-of-the-Art, in SPE Eastern Regional Meeting, Columbus, 1996.

Robert, M., and Pin, T. J. Enzyme Breaker for Galactomannan Based Fracturing Fluid. USA Patent 5201370, 13 April 1993.

Roodhart, L. P. 1985. Proppant Settling in Non-Newtonian Fracturing Fluids. Society of Petroleum Engineers. doi:10.2118/13905-MS.

Schein, G. 2005. The Application and Technology of Slickwater Fracturing. Society of Petroleum Engineers.

Schmidt, D., Rankin, P.E., Williams, B., Palisch, T., and Kullman, J. Performance of Mixed Proppant Sizes, 2014. SPE 168629.

Shah, S. N. 1982. Proppant Settling Correlations for Non Newtonian Fluids Under Static and Dynamic Conditions. Society of Petroleum Engineers. doi:10.2118/9330-PA.

Shah, S.N, El Fadili, Y., Chhabra, R.P., 2007. New model for single spherical particle settling velocity in power law (visco-inelastic) fluids. Int. J. Multiphase Flow 33 (1), 51-66.

Shahi, S. and Kuru, E. 2015. An Experimental Investigation of Settling Velocity of Natural Sands in Water Using Particle Image Shadowgraph. Powder Technology 281: 184–192. http://dx.doi.org/10.1016/j.powtec.2015.04.065.

Shahi, S. and Kuru, E. 2016. Experimental Investigation of the Settling Velocity of Spherical Particles in Power-Law Fluids Using Particle Image Shadowgraph Technique. International Journal of Mineral Processing 153: 60–65. http://dx.doi.org/10.1016/j.minpro.2016.06.002.

Weaver, J., Schmelzl, E., Jamieson, M., and Schiffner, G. New Fluid Technology Allows Fracturing without Internal Breakers, in SPE Gas Technology Symposium, Calgary, 2002.

Wu, W. and Wang, S. S. Y. Formulas for sediment porosity and settling velocity, J. Hydraul. Eng. (2006) 858–862.

Yu, W., Luo, Z., Javadpour, F., Varavei, A., and Sepehrnoori, K. 2014. Sensitivity analysis of hydraulic fracture geometry in shale gas reservoirs, Journal of Petroleum Science and Engineering, Volume 113, Pages 1-7, ISSN 0920-4105, https://doi.org/10.1016/j.petrol.2013.12.005.

Yu, W., Xu, Y., Weijermars, R., Wu, K., and Sepehrnoori, K. 2017. Impact of Well Interference on Shale Oil Production Performance: A Numerical Model for Analyzing Pressure Response of Fracture Hits with Complex Geometries. Society of Petroleum Engineers. doi:10.2118/184825-MS

Zhu, J., Guo, P., Chen, D., Xu, K., Wang, P., & Guan, S. 2017. Fast and excellent healing of hydroxypropyl guar gum/poly (N,N – dimethylacrylamide) hydrogels. Journal of Polymer Science Part B: Polymer Physics. 56. 10.1002/polb.24514.

VITA

Vismay Manishbhai Shah was born in Gujarat, India. He received his bachelor's degree in Petroleum Engineering from Pandit Deendayal Petroleum University in June 2016. He joined Missouri University of Science and Technology in August 2016. He joined hydraulic fracturing research group under direct supervision of Dr. Abdulmohsin Imqam. He received his Master of Science in Petroleum Engineering in December 2018 from Missouri University of Science and Technology.